Norwegian University
of Life Sciences

Master's Thesis 2022   60 ECTS
Faculty of Environmental Sciences and Natural Resource Management

Biochars from contaminated sewage sludge as sustainable PFAS-sorbents for water and soil clean-up

Katinka Muri Krahn

Environment and Natural Resources, soil chemistry specialization

[This page has been left blank intentionally]

Abstract

Due to the considerable persistence, mobility, and toxicity of per- and polyfluoroalkyl substances (PFAS), techniques for the remediation of soil and water contaminated with PFAS are urgently needed. The potential for using various lightly contaminated organic waste materials in the production of biochar sorbents for PFAS has sparked great interest among researchers. Biochar also represents one of the most promising technologies for carbon sequestration.

This study sought to test if biochar produced from sewage sludge can function equally effectively in sorbing PFAS as biochar produced from a clean wood-based feedstock (CWC) and activated carbons tested in earlier studies. The sewage sludge feedstocks tested were Ullensaker sludge (ULS) which contains PFAS-enriched wastewater, and digested sludge (DSL), the fraction remaining from anaerobic digestion of waste organic matter. A series of batch tests were prepared for each biochar. These were spiked with six perfluorinated carboxylic acids (PFCA) with 5 to 10 perfluorinated carbons at different concentrations. To measure sorption attenuation–the sorption suppression effect that occurs in more complex systems where natural organic matter found in soil can block biochar pores, and where other compounds compete for a limited number of sorption sites—both single-compound experiments and a cocktail of different PFCAs added to sandy soil (1.3% TOC) with and without biochar, were tested. Biochar-water and soil-biochar-water isotherms were generated from the batch tests. Using pore size distributions determined by CO_2 and N_2 sorptometry for pores 0.4-1.5 nm and larger than 1.5 nm respectively, surface area and pore volumes were evaluated in terms of their effects on PFCA sorption. The effects of carbon, calcium and iron content on PFCA sorption were also evaluated.

In all batch tests, the sewage sludge biochars turned out to be stronger sorbents for PFCA than CWC biochar. Differences in sorption between the CWC, DSL, and ULS biochars were explained by three main findings: 1) the majority of pores in CWC were too small (<0.6 nm) to accommodate PFCAs, whose maximum molecular dimensions range from 0.96-1.54 nm, 2) CWC had a much lower pore volume for pore sizes above 1.5 nm than DSL and ULS, limiting the pores' filling capacity, and 3) ULS biochar had higher pore volume, surface area, and carbon-content than DSL biochar. Freundlich partition coefficients (log K_F) in $(\mu g/kg)/(\mu g/L)^n$ were highest for the batch tests with biochar and singly spiked PFCAs. For PFDA, log K_Fs were 6.00 ± 0.04, 5.61 ± 0.02, and 5.22 ± 0.07 for ULS, DSL, and CWC biochars respectively. Sorption was positively correlated with increasing perfluorinated chain length. Chain length dependency on sorption indicated that hydrophobic interactions are likely the dominant sorption mechanisms over electrostatic interactions between biochar and PFAS. Sorption was attenuated by factors of 6-140 in the presence of a PFCA cocktail, 8-138 in the presence of soil and a PFCA cocktail for PFOA, PFNA, and PFDA, and 3-10 for PFOA in the presence of soil.

One of this study's limitations is that its conclusions were drawn based on no more than three biochar samples. To corroborate the findings in this study, further research based on testing a larger sample size is needed.

The high sorption strength of sewage sludge biochars found in this study shows great promise for developing new, sustainable, and cost-effective toxic waste management methods. Converting contaminated wastes that are costly to dispose of properly into commercial sorbents is an important contribution to a circular economy, and one that simultaneously addresses the urgent need for increased carbon sequestration.

Sammendrag

Grunnet per- og polyfluoralkylsubstansers (PFAS) betydelige persistens, mobilitet og toksisitet, er teknikker for remediering av jord og vann forurenset med PFAS høyst nødvendig. Potensialet for å bruke ulike lettforurensede organiske avfallsmaterialer til produksjon av biokullsorbenter for PFAS har vakt stor interesse blant forskere. Biokull representerer også en av de mest lovende teknologiene for karbonbinding.

Denne studien forsøkte å teste om biokull produsert fra kloakkslam kan fungere like effektivt til sorpsjon av PFAS som biokull produsert fra et rent, trebasert materiale (CWC), og aktivert karbon som har blitt testet i tidligere studier. Avløpsslammene som ble testet var Ullensaker-slam (ULS) som inneholder avløpsvann anriket med PFAS, og slam fra biorest (DSL), fraksjonen som gjenstår fra anaerob nedbryting av organisk avfall. En serie med ristetester ble utført for hvert biokull. Disse ble tilsatt seks perfluorerte karboksylsyrer (PFCA) med 5 til 10 perfluorerte karboner ved økende konsentrasjoner. Demping er den sorpsjonsdempende effekten som oppstår i mer komplekse systemer der naturlig organisk materiale som finnes i jord kan blokkere porene til biokull, og hvor andre forbindelser konkurrerer om et begrenset antall sorpsjonsseter. For å måle demping ble både forsøk med enkeltforbindelser og en cocktail av forskjellige PFCA tilsatt sandig jord (1,3% TOC) med og uten biokull utført. Biokull-vann og jord-biokull-vann-isotermer ble generert fra ristetestene. Ved å bruke porestørrelsesfordelingene bestemt av CO_2- og N_2-sorptometri for henholdsvis porer mellom 0,4-1,5 nm og porer større enn 1,5 nm, ble sammenhengen mellom størrelsen på overflatearealene og porevolumene, og biokullenes evne til sorpsjon av PFCA vurdert mot hverandre. Effektene av karboninnhold, kalsium og jern for PFCA-sorpsjon ble også evaluert.

I alle risteforsøkene viste avløpsslambiokullene seg å være sterkere sorbenter for PFCA enn CWC-biokull. Forskjellene i sorpsjon mellom biokull fra CWC, DSL og ULS kunne forklares basert på tre hovedfunn: 1) flertallet av porene i CWC var for små (<0,6 nm) til å romme PFCA, hvorav de maksimale molekylære dimensjonene varierer fra 0,96-1,54 nm, 2) CWC-biokull hadde et mye lavere porevolum for porestørrelser over 1,5 nm enn DSL- og ULS-biokull, noe som begrenser porenes fyllingskapasitet, og 3) ULS-biokull hadde høyere porevolum, overflateareal og karboninnhold enn DSL-biokull. Freundlich partisjonskoeffisienter (log K_F) i $(\mu g/kg)/(\mu g/L)^n$ var høyest for ristetestene med biokull og enkelt-spikede PFCAer. For PFDA var log K_Fs 6,00 ± 0,04, 5,61 ± 0,02 og 5,22 ± 0,07 for henholdsvis ULS-, DSL- og CWC-biokull. Sterkere sorpsjon var positivt korrelert med økende perfluorert kjedelengde. Kjedelendeavhengigheten ga indikasjoner på at hydrofobe interaksjoner sannsynligvis dominerer sorpsjonsmekanismene over elektrostatiske interaksjoner mellom biokull og PFAS. Dempingsfaktorer var mellom 6-140 i en PFCA-cocktail, 8-138 i jord og en PFCA-cocktail for PFOA, PFNA og PFDA, og 3-10 for PFOA i jord.

En av hovedbegrensningene for denne studien var at konklusjonene som ble trukket er basert på kun tre biokullprøver. For å bekrefte funnene i denne studien vil det derfor være nødvendig med ytterligere forskning basert på testing av et høyere antall biokullprøver.

Den høye sorpsjonsstyrken til biokull fra kloakkslam funnet i denne studien lover svært godt for videre utvikling av nye, bærekraftige og kostnadseffektive metoder for håndtering av giftig avfall. Å konvertere forurenset avfall som er kostbart å deponere på riktig måte, til kommersielle sorbenter er et viktig bidrag til en sirkulær økonomi, et bidrag som samtidig imøtekommer nåtidens tidskritiske behov for økt karbonbinding.

[This page has been left blank intentionally]

Preface

This thesis concludes my master's degree in Environment and Natural Resources at the Norwegian University of Life Sciences (NMBU). The work presented here was carried out in the fall and spring of 2021/22 in collaboration with the Norwegian Geotechnical Institute (NGI), and was part of the Valorization of Organic Waste into Sustainable Products for Clean-up of Contaminated Water, Soil, and Air (VOW) project funded by The Research Council of Norway (NFR 299070). It is a continuation of MSc work done by Nora Bjerkli (NMBU, May 2021), and a part of the ongoing research within the VOW project being done by Erlend Sørmo, my main thesis advisor.

Sørmo is working on generating a database on the mass balance of contaminants in the pyrolysis of organic wastes, and looking into ways of optimizing this process with respect to handling contaminants and producing good sorbents for various contaminants present in soil and water. He will also gather data necessary for a life cycle analysis (LCA). Sørmo's work is examining a range of feedstocks, including wood chips, garden waste, digested sludge, raw sewage sludge, food waste reject, and residual wood waste. The two sewage sludge biochars selected for the current study are part of Sørmo's set of waste substrates. One contaminant class of great interest is per- and polyfluoroalkyl substances (PFAS) whose sorption affinity to sewage sludge biochar I have tested. The VOW-project is scheduled to be completed in 2023.

The VOW-project is a joint industry sustainability (BIA-X) project led by Gerard Cornelissen, my co-supervisor from NGI, in collaboration with Lindum, Vesar and VEAS (waste/sewage-related management), Scanship (technology supplier), Lindum, Mivanor and Clairs (respectively stakeholders in product application to soil, water and air), and SINTEF (pyrolysis optimization developer). My work has also received important contributions from Hans Peter Arp, a leading expert in PFAS pollution. He is the project coordinator for the SLUDGEFFECT project (NFR 302371), a research and development program that investigates the potentials for reuse of sewage sludge and e-waste plastic by mitigating the harmful presences of organic pollutants.

My interest in writing this thesis has not only been to fulfill the requirements for an MSc degree, but to be able to publish the results of my research together with the VOW-team. With financial support from NGI, and the guidance from Gabriela Castro Varela, PhD in analytical chemistry, I was given the opportunity to spend the month of January 2022 at the Norwegian University of Science and Technology (NTNU) in Trondheim to conduct my own sample analysis. Although challenging, being introduced to advanced analytical chemistry has been rewarding, and work that I am very proud to have been able to complete successfully. The process of writing my Master's thesis has sparked an interest to continue in academia as an organic chemistry researcher. For this reason, I expressed an interest in presenting my findings at a scientific conference. My work was accepted as a poster which was presented at SETAC Europe's 32nd annual meeting in Copenhagen, Denmark in May 2022, the same day this Master's thesis was submitted. The poster is added to Appendix H.

[This page has been left blank intentionally]

Acknowledgments

[This page has been left blank intentionally]

Abbreviations

AC activated carbon.

BC biochar.

CO₂-eq carbon dioxide (CO_2) equivalents.
CWC clean wood chips.

DOC dissolved organic carbon.
DSL digested sludge Lindum.

ESI electrospray ionization.

GHG greenhouse gas.

HOC hydrophobic organic compound.

IS internal standard.

LCA life cycle assessment.
LC-MS/MS liquid chromatography coupled with tandem mass spectrometry.
LOQ limit of quantification.

MeOH methanol.
MQ milli-Q water.

NGI Norwegian Geotechnical Institute.

OM organic matter.

PAHs polycyclic aromatic hydrocarbons.

PFAS perfluorinated alkyl substances.
PFCA perfluorinated carboxylic acid.
PFDA perfluorodecanoic acid.
PFHpA perfluoroheptanoic acid.
PFHxA perfluorohexanoic acid.
PFNA perfluorononaoic acid.
PFOA perfluorooctanoic acid.
PFPeA perfluoropentanoic acid.
PFSA perfluorinated sulfonic acid.
PMT persistent mobile and toxic.
POPs persistent organic pollutants.
PP polypropylene.
PV pore volume.

SA surface area.
SC spike concentration (ref. SP).
SDGs sustainable development goals.
SPE solid phase extraction.
SS-BCs sewage sludge-based biochars.

TA target analyte.
TOC total organic carbon.

ULS Ullensaker sludge.

VOW Valorization of Organic Waste.
vPvM very persistent very mobile.

WWTP wastewater treatment plant.

Symbols

AF	attenuation factor, predicted/measured K_{BC}
AF	attenuation factor
AR	absolute recovery
C_i	initial concentration
C_s	sorbed equilibrium concentration
C_w	aqueous equilibrium concentration
D_{eff}	effective cross-sectional diameter of a molecule
D_{max}	maximum diameter of a molecule
K_d	solid/liquid distribution coefficient
K_F	Freundlich distribution coefficient
K_{AW}	air/water distribution coefficient
K_{BC}	biochar/water partition coefficient
K_{OC}	organic carbon/water distribution coefficient
K_{OW}	octanol/water partition coefficient
ME	matrix effect
n_F	Freundlich coefficient of non-linearity (< 1)
n_F	Freundlich coefficient of non-linearity
pK_a	acid dissociation constant
RR	relative recovery

Contents

Chapter 1

Introduction

1.1 PFAS

Per- and polyfluorinated alkyl substances (PFAS) are a large group of synthetic compounds that are used in numerous industrial and consumer products. After decades of use, PFAS are ubiquitous in soils, groundwater, and surface water (Rankin et al., 2016). PFAS are both oil and water repellent, making them ideal as foaming agents and flame retardants. They are also used as a coating for waterproof Gore-Tex® textiles, and non-stick, frictionless Teflon™, used as a coating for cooking utensils (Du et al., 2014). Despite having many desirable properties, the widespread production and distribution of PFAS into waterways has led to its accumulation in soil, crops, wildlife, and higher trophic levels, including humans (Bhhatarai and Gramatica, 2011; Lau et al., 2007).

The synthetic structure of PFAS, and the strength of the C-F bonds, makes these chemicals resistant to natural degradation (Krafft and Riess, 2015). And although the mechanisms of PFAS-toxicity are not well understood, they are also suspected to be bioaccumulative and toxic (Ding and Peijnenburg, 2013; Lau et al., 2007). Today, PFAS are recognized as emerging persistent organic pollutants (POPs) (ECHA, 2020), and legislation that regulates the manufacture, sale, and use of several PFASs has been introduced in most parts of the Western World (EPA, 2014; European Commission, 2020). Two of the most widely used and distributed compounds, PFOA and PFOS, are listed under the Stockholm Convention as POPs. Consideration is currently being given to adding other PFAS compounds to this convention (European Commission, 2020). An important example is efforts by the German Environment Agency to identify a new class of compounds as PMT (persistent, mobile, and toxic) and vPvM (very persistent, very mobile), and to include these under REACH, the EU chemicals regulation (Registration, Evaluation, Authorization and Restriction of Chemicals), and ECHA (the European Chemicals Agency) (Hale et al., 2020). PMT/vPvM substances have properties that are not covered by the Stockholm Convention, but represent an equally great threat to the environment, and to maintaining the purity of the world's drinking water.

1.1.1 Overarching research concept

A great deal of research has been done to develop effective ways of remediating PFAS-contaminated soil and water. One of these is the overarching focus of this thesis. The aim of the research

presented here is to study whether biochar from various lightly contaminated organic waste materials can be used as a sorbent in the remediation of PFAS-contaminated soil and water. A sorbent is a porous, carbonaceous material with the ability to remove contamination (adsorbate molecules) from water by strongly binding the contaminants to its internal structure (Lehmann and Joseph, 2015). This process is called sorption. Sorption is a collective term used to describe removal of molecules from the water phase by *ab*sorption, the dissolution-like partitioning *into* the sorbent, while *ad*sorption is bonding *onto* the surface of the sorbent. These processes immobilize the contaminants, making them unavailable for biological uptake (CRCCARE, 2017).

The degree to which molecules sorb to solid surfaces depends on both the physicochemical properties of the sorbent and the adsorbate, as in "like attracts like" (Ball, 2012). In order to achieve the desired decontamination result, it is therefore necessary to identify sorbents that match the exact chemical properties of the target adsorbate. The present study is based on information concerning the physicochemical properties of two biochars produced from two lightly contaminated feedstocks, and one biochar produced from a clean, wood-based feedstock, to evaluate the suitability of these biochars as sorbents for PFAS.

1.1.2 PFAS in industrial runoff and wastewater

The sources of PFAS contamination are typically local industrial point sources such as paper mills (Lee et al., 2020; Langberg et al., 2021), leaching from landfills (Masoner et al., 2020), firefighting training facilities (Filipovic et al., 2015), and discharge from fluorochemical plants into the wastewater system (Gebbink et al., 2017). This puts wastewater treatment plants (WWTP) under additional pressure to adequately treat wastewater so as to avoid further release of PFAS chemicals into the environment (Morin et al., 2017). By restricting many long-chain PFASs, new challenges have emerged. These are related to controlling the spread, and the resulting effects, of the increased use of short-chain replacements (Knutsen et al., 2019). Short-chain PFAS have higher mobility and tend to slip through existing water treatment processes, thereby contaminating food and drinking water (Hale et al., 2020; Brendel et al., 2018). Although short-chain PFAS are less bioaccumulative, persistence and toxicity are expected to be equivalent to the substances they replace (European Commission, 2020).

1.1.3 Physicochemical and sorption properties of PFAS

PFAS are synthetic organic compounds that consist of a polar head, most commonly a carboxyl or sulfate functional group, and a non-polar chain of alkyl moieties that are either fully substituted (per-), or partly substituted (poly-), with fluorine (Wang et al., 2011). PFAS are divided into compound classes based on functional group and the degree of carbon-chain fluorination, of which perfluorinated carboxylic acids (PFCAs) and perfluorinated sulfonic acids (PFSAs) are the most common. Since fluorine is the most electronegative atom identified, the C-F covalent bonds make up one of the strongest known bonds in organic chemistry (BDE=485 kJ mol^{-1}) (Lau et al., 2007). The nature of these bonds is significant for two main reasons: 1) C-F bonds are not found naturally in the environment which means that no natural enzymes can degrade them. This accounts for why PFAS is persistent in the environment (Hale et al., 2020; Krafft and Riess, 2015). 2) The chain of repeating CF_2 units consists of highly polar bonds with a symmetric structure, causing the entire surface area of the PFAS tail to carry a net negative charge. This in turn minimizes the ability of PFAS to undergo either van der Waals interac-

tions with other molecules, or hydrogen bonding due to the lack of a positive dipole (Arp et al., 2006). The combined properties of low van der Waals and non-polarity make the tail neither hydrophobic nor lipophobic. The result is a new compound class that is "everything-phobic". This everything-phobic-ness causes PFAS to behave uniquely in the environment. They are more mobile than other organic pollutants that are often are hydrophobic (Hale et al., 2020).

Sorption of PFAS is often discussed interchangeably with sorption of hydrophobic compounds that have strong affinities to hydrophobic surfaces. Sorption of PFAS should, more correctly, be discussed in terms of their capacity to directly push water molecules onto hydrophobic surfaces (Arp et al., 2006). The cavity formation energy barrier rises for every CF_2 moiety present, making dissolution increasingly difficult at longer chain lengths (Bhhatarai and Gramatica, 2011; Arp et al., 2006). This is the primary mechanism that reduces the mobility of PFAS, and leads to its accumulation in soils and biota. The role different mechanisms of attraction and repulsion play, as well as the effect of chain length on PFAS interaction with sorbents, are two of the main topics that will be discussed in further detail throughout this thesis.

In contrast to the everything-phobic chain, the hydrophilic head of PFAS can hydrogen-bond to other polar compounds such as water, and interact electrostatically with positively charged species (Sigmund et al., 2022). Since the head groups of PFAS are acids, knowledge of its protonation state is key to further understand solubility and volatility, which in turn affect the mobility and long range transport potential of these chemicals. Determining the acid dissociation constants (pK_a) of PFAS has been the subject of much debate in the scientific community (Goss and Arp, 2009). This debate is linked to the complexity of how PFAS behaves at different concentrations, and on the surface of water. However, most researchers agree that pK_a values are below 1 and decrease with increasing chain length (Wang et al., 2011; Reemtsma et al., 2016). PFAS are thus expected to be negatively charged at environmentally relevant pH levels, enhancing their ability to dissolve in water by charge-assisted H-bonds (Reemtsma et al., 2016). For example, PFOA has a water solubility of 3.4 g L^{-1} (Merck, 2022b), whereas its structural analog, perfluorooctane (PFO) (Merck, 2022a), which has no polar functional group, exhibits a far lower solubility (1 mg/L). Furthermore, hydrophobic organic compounds (HOCs) are much more insoluble. Hexachlorobenzene (HCB), for example, has a solubility of $0.005 mg/L$ (McPhedran et al., 2013).

1.1.4 Mobility and accumulation of PFAS in the environment

The combination of an everything-phobic tail and an ionizable hydrophilic head makes understanding the mobility of PFAS in the environment more complex than that of legacy POPs (Cabrerizo et al., 2018; Arp et al., 2006). Since PFAS are not very volatile—having a low vapor pressure and air-water partition coefficient (K_{aw})—aqueous solubility and uptake in migrating biota play primary roles in mobilizing PFAS in the environment (Arp et al., 2006). Schlabach et al. (2018) reported that a diverse group of PFAS congeners are present in Arctic biota such as fish, polar bears and mink. Sorption mechanisms are also slightly different for PFAS compared to hydrophobic and lipophilic legacy POPs like polychlorinated biphenyls (PCBs), hexacholorocyclohexanes (HCHs), and polycyclic aromatic hydrocarbons (PAHs) which have higher volatility, lower solubility, and higher lipophilicity than PFAS (Cabrerizo et al., 2018; Cornelissen et al., 2005; Li et al., 2018). The latter property is often expressed as the octanol water partition coefficient ($K_{ow} = C_o/C_w$). This coefficient is used to represent partitioning of adsorbate molecules between particulate organic matter in the water phase (numerator) and

water (denominator) (Reemtsma et al., 2016). Due to the unique properties of PFAS described above, PFAS has a lower K_{ow} value as compared to HOCs. Therefore, K_{OW} can be used to explain why PFAS more readily leaches from soils to groundwater (Cornelissen et al., 2005; Du et al., 2014)). A more environmentally relevant parameter than K_{ow} is K_{oc}, the organic carbon-water partition coefficient. Determining K_{oc} is tedious, costly and time-consuming. Hence models have been found to estimate K_{oc} from water solubility and K_{ow} (Pandey and Roy, 2021). This coefficient also represents the higher tendency of PFAS to leach from soils to groundwater, and is a more dynamic parameter because it accounts for the fraction of organic matter present in soil. PFAS has a lower K_{oc} than hydrophobic organic contaminants like PAHs and PCBs that sorb more strongly to organic matter (Cornelissen et al., 2005). The influence of soil organic matter on sorption of PFAS to biochar will be discussed in Section 1.4.

1.2 Biochar—from traditional soil amendment to sorbents for emerging contaminants

Biochar (BC) is a common term for the carbon-enriched product produced from the pyrolysis of biomass (Lehmann and Joseph, 2015). Common feedstocks used to produce BC are various crop residues, poultry litter, wood shavings, and grain straw (Ahmad et al., 2014). Pyrolysis is a thermal treatment method that burns organic matter in the absence of oxygen, a process which forms fused aromatic ring structures that have high porosity and large surface areas, and low residual functional groups (Lehmann and Joseph, 2015). BC improves soil health by increasing water retention and carbon content. It also increases the pH of acidic soils, and secures a more steady nutrient release (Das et al., 2020). In addition, ash co-products of pyrolysis enrich biochar with macro- and micro nutrients that are beneficial in agriculture.

The use of biochar as a soil amendment dates back 2,500 years to the pre-Columbian Amazonian peoples (Tindall et al., 2017). They used slash-and-char techniques to produce biochar which they spread onto their fields. The result was *terra preta*, a soil that was much more fertile compared to adjacent soils (Ahmad et al., 2014). Notably, the biochar that was added during this period is still present in the soil today. The recalcitrance of this carbon fraction becomes significant for biochar's potential to function as a carbon sequestration technology. This will be described in greater detail in the next section. Today, biochar has numerous multidisciplinary applications, such as soil fertility improvement, waste recycling, carbon sequestration, and sorbents for remediation of contaminated sites (Beesley et al., 2011).

1.2.1 Biochar as sorbents

The application of biochar as a sorbent for soil and water remediation, is relatively new (Beesley et al., 2011). Historically, activated carbon (AC) from fossil coal sources has been the only product used for soil remediation (Hagemann et al., 2018). The term "activation" is used to describe the thermal treatment ($< 800°C$) of a carbonaceous material by using steam (H_2O) or carbon dioxide (CO_2). These treatments expand the surface area of carbonaceous material by creating new nanopores (<2nm), thereby increasing sorption capacity (Lehmann and Joseph, 2015). Simultaneously, surface functional groups are oxidized to create a smoother, aromatic surface that improves sorption affinity to organic molecules (Sajjadi et al., 2019). This process makes biochar an ideal sorbent for organic pollutants (Ahmad et al., 2014). Current challenges

connected to the production of AC include high operating costs and energy inputs, the use of a non-renewable fossil fuel (coal) as raw material (Li et al., 2019), and the fact that the activation process of char is associated with higher carbon losses and lower yields. All of these challenges result in reduced carbon sequestration (Sørmo et al., 2021). Biochar is often termed a universal sorbent because its surface has regions of hydrophilic or charged functional groups that make it ideal for electrostatically binding cationic organic and inorganic species such as heavy metals (Silvani et al., 2019; Zhang et al., 2013). Biochar also has other regions of more condensed, aromatic surfaces which are better suited to sorb hydrophobic molecules (Cornelissen et al., 2005).

Researchers have been successful in using activation technology on biochar instead of fossil coal as a sorbent for organic contaminants (Sørmo et al., 2021). Commercial production is increasing internationally, and activated biochar is now widely used for soil remediation (Hagemann et al., 2018). In recent years, there has been increasing interest in studying whether non-activated biochars can also be effective sorbents for use in contaminant remediation and water purification (Hagemann et al., 2018). Two of biochar's main advantage over AC is its potential for carbon sequestration (Smith, 2016), and reduced reliance on Chinese coal mines (Zheng et al., 2019). If engineered correctly, biochar is expected to be at least as effective as AC in sorption of organic pollutants (Sørmo et al., 2021).

Another important area of investigation has been to study how different feedstocks, pyrolysis temperature, and residence time affect biochar properties (Hale et al., 2016). Since feedstocks used to produce biochars often have a heterogeneous composition of elements other than carbon, they need to be pyrolyzed at higher temperatures to gain sufficient surface area and porosity for sorption (Beesley et al., 2011). By adjusting pyrolysis temperature, biochar can be tailored to match the physicochemical properties of the contaminants of interest (Hale et al., 2016). The oxygen to carbon ration (O/C) is used as a proxy for the polarity and hydrophobicity of a sorbent's surface, where a high ratio indicates a more oxidized surface, one that is high in oxygen-containing functional groups. Likewise, the hydrogen/carbon (H/C) ratio is used as a proxy for aromaticity, where a lower ratio indicates a higher degree of fused aromatic ring structures that form a more porous biochar material (Ahmad et al., 2014). O/C and H/C ratios have been found to decrease with increasing pyrolysis temperature (Hale et al., 2016). Therefore, biochars produced at high temperatures (700-900 °C) are the ones that are most suitable for sorbing organic contaminants (Figueiredo et al., 2018).

One of the main challenges posed by the application of non-activated biochar to natural systems is its lower porosity than AC (Leng et al., 2021). High porosity becomes particularly important when carbonaceous sorbents are applied to organic matter (OM)-rich soils. Small pores are vulnerable to pore blockage by large organic molecules (Sorengard et al., 2019). However, application of biochar to soil with low OM content has proved to be equally effective as the application of non-activated biochar (Alhashimi and Aktas, 2017). In this way, biochar contributes to reducing the demand for AC in a range of remedial uses, thereby limiting the future need for AC for the treatment of OM-rich soils, and ultra-fine water cleansing.

The latest research on biochar has studied the potential for producing biochar sorbents from various lightly contaminated organic waste materials such as papermill waste (Van Zwieten et al., 2010), sewage sludge (Fathianpour et al., 2018), biosolids (Wang and Shih, 2011), and palm oil mill sludge (Lam et al., 2017). Using these waste materials represents a better waste-management alternative to the use of landfill sites and incineration. This would result in a net

reduction in energy use and a reduction in the emission of GHGs, and the leaching of harmful chemicals into the environment (Alhashimi and Aktas, 2017). Ongoing research, including the present study, is investigating the effectiveness of non-activated biochar, produced from waste feedstocks, as a sorbent for PFAS.

1.2.2 Sorption mechanisms

Sorption to BC involves several factors such as biochar morphology, contaminant concentration, competing contaminants, sorbate physicochemical properties, and molecular size (Li et al., 2019; Du et al., 2014). Sorption to porous carbonaceous materials occurs via chemisorption (covalent sorbent-sorbate bonding), and physisorption, the encapsulation of the adsorbent into the biochar's maze of pores and electrostatic attraction (Li et al., 2019).

Researchers have postulated that sorption of PFAS occurs primarily via direct (specific) polar interactions, hydrophobic (non-specific) interactions, and ion exchange mechanisms (Hale et al., 2017; Yu et al., 2009). Polar interactions include H-bond and charge-assisted H-bond interactions. Non-specific hydrophobic interactions can more accurately be described as high cavity formation energy which results from the sum of forces that limit solubility of large, non-polar molecules in water (Arp et al., 2006; Sigmund et al., 2022). Electrostatic interactions involve both attraction and repulsion. Cation bridging is one form of electrostatic attraction.

1.3 Valorization of sewage sludge

Recycling and the valorization of waste have become key areas of interest in research and development aimed at achieving a transition to a more circular economy (Ahmad et al., 2014). In recent years, the European Union has invested substantial funding in projects aimed at developing remedial techniques for the treatment of soil and water contaminated with PFAS (see Section 5.4) (European Commission, 2020; ECHA, 2020). One of the most promising techniques developed so far is an *in situ* treatment that involves applying sorbents which immobilize PFAS from the bioavailable aqueous phase by strong sorption to biochar (Ahmad et al., 2014; Sørmo et al., 2021; Kupryianchyk et al., 2016b).

1.3.1 Sewage sludge biochar as sorbent for PFAS

Biosolids are the residual semi-solid material waste left over from wastewater treatment. They are produced in large quantities, and are expensive to dispose of because they often contain heavy metals, micro plastics and organic pollutants (Raheem et al., 2018). High moisture and ash contents, as well as the presence of heavy metals and a cocktail of organic contaminants contained in sewage sludge, make treatment and disposal difficult (Li et al., 2019). Incineration or landfilling disposal are methods that are often resorted to. These release sustantial amounts of greenhouse gases (GHG), fly ash, and PAHs (Huang et al., 2022). Incineration and landfilling are associated with an increased risk of contaminants leaching into soils and groundwater (Propp et al., 2021).

Wastewater treatment plants (WWTPs) have started to look at possible ways to process biosolids and raw sewage sludge in a more sustainable and cost-effective manner (Raheem et al., 2018). One possibility involves generating energy from waste. With the help of microorganisms, it is possible to produce digestate, a liquid residual fraction from the anaerobic

treatment of sewage sludge and other organic wastes. This digestate is already being used in the commercial production of biogas. In some cases, biosolids are applied to agricultural fields as fertilizers (Moodie et al., 2021). However, high contents of micro and macro plastics as well as heavy metals may limit the use of biosolids in agriculture (Mohajerani and Karabatak, 2020).

Research into the production of biochar, using digestate and raw sewage sludge as feedstocks, represents a promising novel strategy for finding sustainable ways to valorize organic waste. Production of biochar is particularly attractive because it is considered one of the most promising carbon sequestration technologies, taking a problematic waste material and transforming it into an economically valuable resource (Arvaniti et al., 2014a). After pyrolysis, biochar from sewage sludge has a higher ash content than cleaner, wood-based substrates' content of inorganic constituents (Fan et al., 2020). One benefit of a higher ash content is a lower loss of volatile carbon. This is attributed to the fact that inorganic ions in the ash raise the bond dissociation energy of organic and inorganic carbon (Cantrell et al., 2012).

Even today, industrial production of sorbents by pyrolysis of sewage sludge is still in a pioneering phase. Some of the challenges include: 1) Sewage sludge biochar has a lower carbon content than more homogeneous, wood-based feedstocks. It likely has a low surface area and porosity, and hence, poor sorption strength. Due to sewage sludge biochar's lower porosity, it is expected that its uptake of PFAS may be lower than that of AC. In order to achieve an acceptable quality of treatment for contaminated soil and water, it may be necessary to use a higher dosage of biochar, or change biochar filters more frequently. 2) Non-activated biochar possesses more oxygen and nitrogen-containing functional groups, making it more polar. This in turn results in its being able to attract charged and polar contaminants to a greater extent. Non-activated biochar contains a higher non-carbonized fraction. It interacts with contaminants in a way that is different from fully condensed, aromatic structures. One of the main focuses of this thesis is discussing the relevance and benefits of this more heterogeneous matrix for the sorption of PFAS. 3) Due to the heterogeneity of sewage sludge, biochar will vary in composition. This could mean that biochar will exhibit inconsistent sorption capacities. 4) Bio oils and syn-gas are by-products from the production of biochar. These are expected to contain organic pollutants, and constitute a possible source of greenhouse gases, particulate matter, and heavy metals. Research partners conducted pollution control measurements at the same time as the present research was conducted. These showed that microplastics and organic pollutants disappeared and heavy metals were immobilized (10% available at low pH) during sludge pyrolysis at > 600 °C, and that only 5-10% of PFAS measured in the raw sludge remained after pyrolysis at 700-800 °C (Erlend Sørmo, preliminary data). Complete results from Sørmo's study will provide important information relevant to an overall life cycle assessment (LCA) of biochar.

1.4   Application of sorbents in real-world conditions

To understand remediation of PFAS-contaminated soil and water through the use of sorbents *in situ*, it is important to understand the complexity of such soil and water systems and how the contaminants are already distributed in the various phases. Soils, sediments, sewage sludge and other solid materials relevant for wastewater treatment or soil remediation, have an intrinsic affinity to PFAS. These contribute to lowering freely dissolved concentrations of PFAS to some degree (Arvaniti et al., 2014b; Zhang et al., 2013). The heterogeneous composition of the various solid phases, size fractions and other contaminants found in such systems are complex,

and therefore difficult to explain.

The following is an attempt to summarize some overarching trends from previous literature. Researchers agree that organic matter (OM) is the most important soil and water parameter governing sorption of PFAS into the environment (Zareitalabad et al., 2013). Soil organic matter (SOM) is divided into several different categories, and constitutes a diverse range of the organic fractions present in soil (Cornelissen et al., 2005). Biopolymers such as polysaccharides, proteins and lipids are fresh and amorphous. Soot and charcoal-like material, collectively termed black carbon, are hard, aromatic and condensed. Humic substances fall somewhere in between (Cornelissen and Gustafsson, 2004). The various OM-fractions have different affinities to PFAS. Hydrophobicity increases for the more condensed and aromatic carbon fractions. Therefore, PFAS has higher affinities to black carbon, a characteristic which it shares with biochar. Therefore, soils rich in highly condensed carbon have a natural buffer-system for organic pollutants. Cornelissen et al. (2005) provides an informative sketch that compares the difference between humic organic matter and black carbon in terms of sorption strength to organic molecules (Figure 1.1). This figure shows that organic contaminants are more tightly bound to black carbon (100 times stronger) than to humic substances. One benefit of black carbon is that it is more recalcitrant. Once it sorbs organic contaminants, they are removed from the bioavailable phase "forever" (Cornelissen and Gustafsson, 2006). Natural systems contain only a minor fraction of black carbon. Most organic matter is typically present as humic acids. These are large and complex organic molecules that consist of aromatic and aliphatic regions with a high number of functional groups.
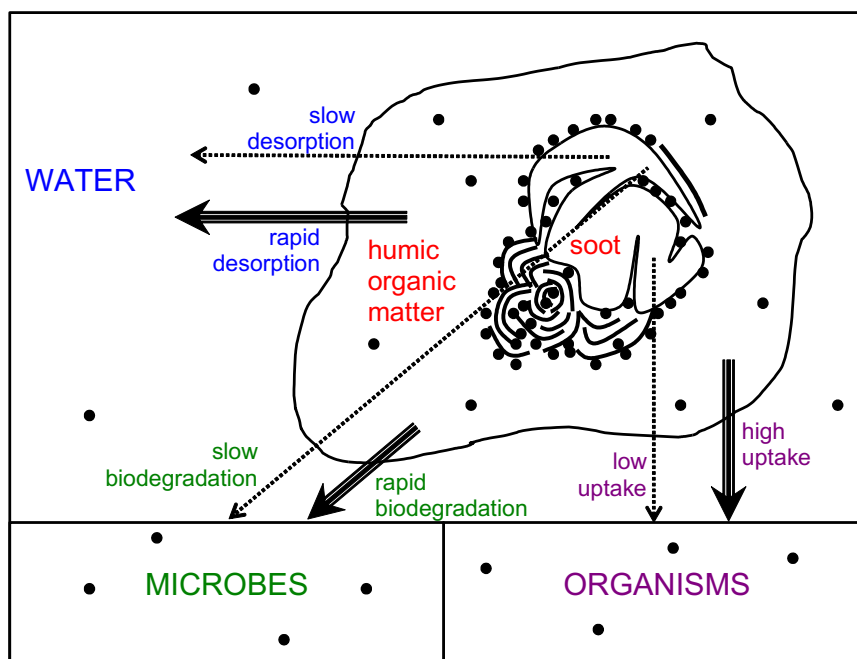
Figure 1.1: Sketch adapted from Cornelissen et al. (2005) shows the differences in sorption strength of organic molecules (black dots) between humic organic matter and black carbon, affecting bio-availability for microbes and organisms. Note: PFAS is never rapidly desorbed nor degraded, so the green scheme is not relevant for the present discussion.

1.4.1   Attenuation

Attenuation is defined as the weakening of the sorption strength of a sorbent by the presence of soil and/or competing molecules. The large-sized humic acids pose challenges when it comes to using biochar to remediate contaminated soil (Mahinroosta and Senevirathna, 2020). Large organic molecules prevent efficient sorption of PFAS by clogging the pore throats of the BC, reducing by factors between 7-150 the expected BC-water partitioning coefficient (K_d) derived from clean water systems (Hale et al., 2009; Teixido et al., 2013; Cornelissen and Gustafsson, 2004). Dissolved organic matter (DOM) reduces the mass transfer of the adsorbates into biochar pores by the deposition of large and complex molecules onto pore openings (Pignatello et al., 2006). Furthermore, smaller humic molecules can compete with PFAS for sorption sites, thus reducing the sorption capacity of biochar (Du et al., 2014). This clogging effect by the presence of OM becomes a more significant challenge for sorbents with lower porosity. Therefore, activated carbon is commonly used for remediation of OM-rich soils (Sørmo et al., 2021). This study will examine the properties of the sewage sludge biochars in an effort to evaluate if these sorbents have sufficient porosity to function as sorbents for PFAS in soil.

Sorbent-water partition coefficients are usually determined during equilibrium conditions. Sorption equilibrium between biochar and clean water has been shown to be achieved after 14 days (Kupryianchyk et al., 2016b). However, diffusion through clogged pore throats can take much longer, up to three years, in the presence of soil or sediment. It was shown that AC sorption capacity for DDT in sediment was reduced from a factor 32 after one month, to no attenuation after 2.5 years (Hale et al., 2009). This shows that pore blocking by SOM could be a kinetic effect more than a competitive effect. In the Hale et al. (2009) study, OM did not affect the sorption capacity of biochar, but influenced the diffusion rate of adsorbate molecules into the pores. Bearing this in mind, it is possible to define what PFAS removal-rate is needed for any given remedial application by testing sorption of the target contaminants to biochar in the medium in need of remediation over an extended time-frame. In treatment of wastewater, 2.5 years is not a realistic time-frame for reaching effective PFAS removal since water is expected to flow through the carbon filter at a constant flow rate. In soil remediation, knowledge of the diffusion rate of biochar applied to the specific soil in need of remediation is important. This to study the attenuation effect by SOM versus biochar contact time. In remediation of contaminated soil, it may be urgent to apply sorbents that will sorb PFAS quickly in order to prevent further leaching of PFAS into groundwater. Soils rich in OM may bind PFAS to a sufficient degree that the biochar applied achieves the intended remediation within an acceptable time-frame.

Apart from attenuation by OM, the presence of contaminants other than PFAS has been shown to suppress sorption (Cornelissen and Gustafsson, 2006). The result is a "cocktail effect" which means that when a system is overwhelmed by different adsorbing contaminants, molecules experience attenuated sorption depending on their relative physicochemical properties and concentrations. There is overall agreement among researchers that competition between sorbates and/or SOM are the most important parameters that lead to attenuated sorption of PFAS in natural systems (Zareitalabad et al., 2013; Higgins and Luthy, 2006; Teixido et al., 2013).

Chapter 2

Research objectives and hypotheses

2.1 Objectives

The aim of this thesis is to study whether biochar from various waste materials can be used as sorbents in the remediation of PFAS-contaminated soil and water. The overall goal of this study is to test the degree to which sewage sludge-based biochars (SS-BCs) can be used as effective sorbents for PFAS in the remediation of contaminated water and soil. To achieve this, the sub-goals are to:

I Compare the relative abilities of SS-BCs and clean wood chip BCs to sorb PFCA

II Identify possible sorption mechanisms of PFCA for biochar from different feedstocks

III Study the effects of perfluorinated carbon chain-length on PFCA sorption to SS-BCs

IV Study the attenuation effect of competing sorbates and the presence of soil, on sorption, and to evaluate the effectiveness of SS-BCs as sorbents in real-world conditions

To achieve these objectives, sorption isotherms were determined for biochar from three different feedstocks: raw sewage sludge, digested sewage sludge, and clean wood chips. Six perfluorinated carboxylic acids (PFCA) with increasing chain lengths from C5-C10 were selected for spiking the sorption isotherms, both individually and as mixtures of these compounds. To study sorption attenuation, isotherms with biochar only, and isotherms with biochar mixed with a sandy, low-TOC soil were prepared.

2.2 Hypotheses

This thesis sought to test the following four hypotheses:

i Biochar from sewage sludge is not as effective a sorbent for PFAS as biochar produced from clean wood chips due to its lower carbon-content and porosity, though it can be used as a low-cost, lower quality-class sorbent.

ii The dominant mechanism by which PFCAs sorb to sewage sludge biochars is electrostatic attraction due to mineral-rich components.

iii Following from hypothesis (ii), sorption to sewage sludge biochars is not chain-length dependent and is due to electrostatic interactions by the negatively charged PFCA functional groups, whereas sorption increases with chain length for clean wood chips due to predominating hydrophobic interactions with the more carbonaceous biochar matrix of this biochar.

iv Sorption of PFCA to biochar is attenuated by the presence of soil and other PFCAs.

Chapter 3

Materials and methods

A series of batch shaking tests was conducted to test the sorption strength of waste-based biochars to PFAS, and to determine possible sorption mechanisms. Experiments to investigate how chain length affects sorption, both with and without the presence of soil, were conducted using six perfluorinated carboxylic acids (PFCAs) (C5-C10). Both single compound and a cocktail of C5-C10 batch tests were performed to determine attenuation factors. A methods flowchart is given in Figure 3.1. The main work and laboratory experiments were conducted in the environmental chemistry laboratory at the Norwegian Geotechnical Institute (NGI), Oslo, Norway. Quantification analysis of the batch test filtrates was performed by LC-MS/MS at the Institute for Chemistry, Norwegian University of Science and Technology (NTNU), Trondheim, Noway.
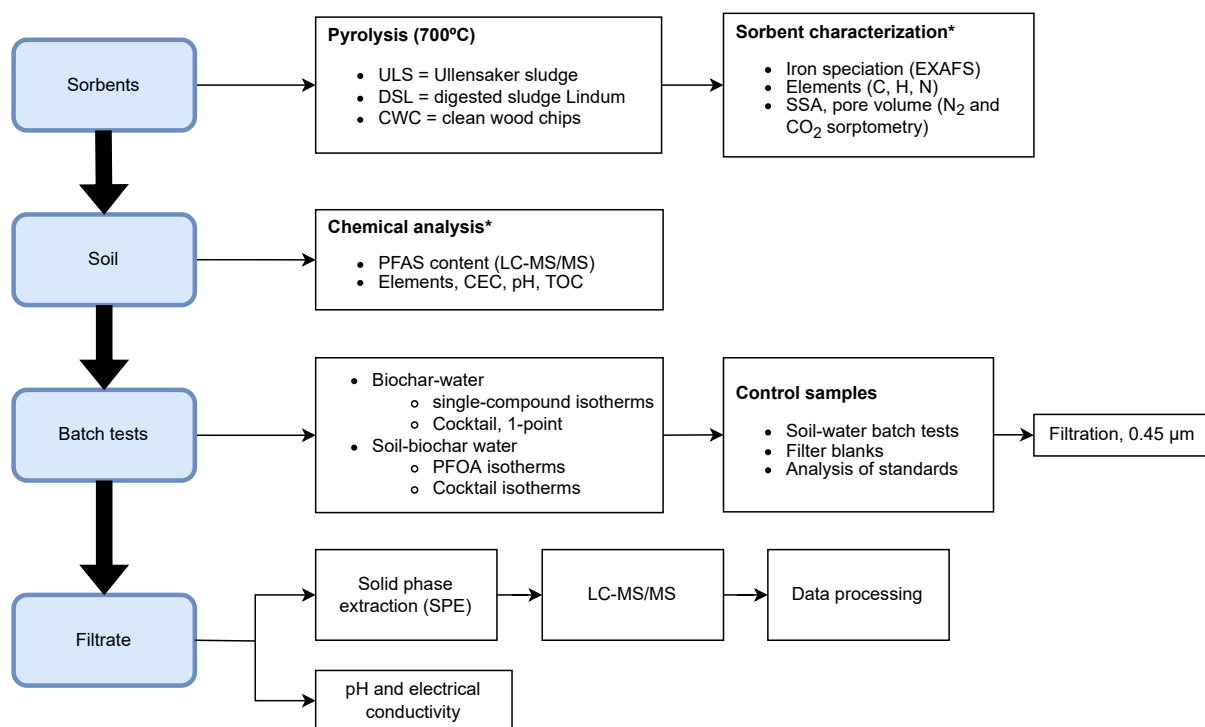
Figure 3.1: Overview of the methods conducted for this thesis. * = analyses conducted by commercial laboratories or that were delegated to project partners.

12

3.1 Biochar sorbents

3.1.1 Feedstock

Three feedstocks were selected for use as sorbents for the sorption experiments:

- **Ullensaker sludge (ULS)**: raw sewage sludge biosolids from Ullensaker wastewater treatment plant located North-East of Oslo, Norway.

- **Digested sludge Lindum (DSL)**: a solid residue (digestate) left over from anaerobic digestion of food waste and organic material for the production of commercial biogas.

- **Clean wood chips (CWC)**: clean, fresh softwood timber, without additives, that has been shredded, dried, and compressed into 8 mm pellets. The wood pellets were commercially available from Hallingdal Trepellets (Kleivi næringspark, Ål, Norway)

These feedstocks were dried and pelletized before pyrolysis.

3.1.2 Pyrolysis

The ULS, DSL, and CWC biochars were provided as sample biochars for the sorption experiments conducted for this thesis. The biochars were produced at Lindum AS (Drammen, Norway) by using Biogreen$^{©}$ technology, provided by the French company, ETIA (Evaluation Technologique, Ingénierie et Applications). The CWC, ULS, and DSL biochars were produced by slow pyrolysis at 700 °C and a residence time of 20 minutes for CWC and 40 minutes for ULS.

First, the pyrolysis chamber was electrically heated to a stable pyrolysis temperature. Feedstock pellets were added to a feeding container where a heated rotating screw (Spirajoule$^{®}$) led the feedstock through the pyrolysis chamber for the desired residence time. The biochar product was then transported to an external collection container where it was dispensed into sampling bags Figure 3.2. Syn-gas from pyrolysis was led through a condensing pipe, and condenses into bio-oil at two points, depending on boiling point. Syn-gas that does not condense at this point was led into a combustion chamber where a steady inflow of propane ensured clean combustion of the remaining compounds.

A biochar sub-sample (100 g) was taken by random grab-sampling from the bulk volume ($\sim$ 5 kg) of the biochar produced during pyrolysis. The biochars were crushed using a ball mill (Retsch ISO 9001) at 50 rpm for 5 minutes, then sieved into fine-powdered biochar (D <1 mm), and transferred to LDPE zipper bags for storage (4 °C).

3.1.3 Biochar properties

Surface area and pore volume

Total specific surface area (SA) and pore volume (PV) were determined by nitrogen (N_2) and carbon dioxide (CO_2) gas sorptiometry conducted by research partners at the Particle Engineering Research Center, University of Florida (Gainesville, USA) using a Quantachrome Autosorb 1 surface area analyzer according to the methods described by Kwon and Pignatello (2005). N_2 sorptiometry was performed at the boiling point for liquid nitrogen (-195.8 °C). Due to slow diffusion at this low temperature, N_2 cannot enter the smallest pores <1.5 nm, and

Figure 3.2: DSL feedstock pellets (left) and DSL biochar (right).

thus, sorption of N_2 represents the largest pores of >1.5 nm. CO_2 sorptiometry was performed at 0 °C, enabling the gas to diffuse into smaller nanopores between 0.4-1.5 nm. N_2 SA was interpreted using both Brunauer, Emmett and Teller (BET) and density functional theory (DFT). N_2 PV was interpreted with Barret-Joyner-Halenda (BJH) and DFT. CO_2 SA and PV were interpreted using DFT.

Element analysis

The analysis of biochar total element composition was performed by project partners at the Norwegian University of Life Sciences (NMBU, Ås, Norway) according to DIN 51732. Total carbon (C) was analyzed by the dry combustion method described by Nelson and Sommers (1982). The samples were crushed with a mortar before quantification by a Leco CHN628 from Leco Corporations (Sollentuna, Sweden). The sample was combusted at 1050 °C until complete oxidation of the C into CO_2. The concentration of CO_2 was measured by an infrared cell. Total nitrogen (N) was determined according to the *Dumas* method (Bremmer and Mulvaney, 1982) by the same principles as that of total C. The N-containing constituents were reduced by copper into N_2. Nitrogen gas concentration was measured by thermal conductivity, also performed with Leco CHN628.

The biochar composition of the remaining main elements (Ca, Fe, K, Mg, Na, P, S and Si) and trace elements (As, Ba, Cd, Co, Cr, Cu, Mo, Ni, Pb, Sr, V and Zn) were determined by NO_3-digestion at 260 °C in an Ultraclave from Milstone, followed by dilution and analysis using either an Agilent Triple QQQ 8800 ICP-MS with a reaction-collision cell (As, Ba, Cd, Co, Cr, Cu, Mo, Ni, Pb, S, Sr and V), or an ICP-OES (Ca, Fe, K, Mg, Na, P, Si and Zn). In these analyses, the NJV 94-5 and NCS ZC 73007 certified reference materials were used for quality control purposes.

Iron speciation

Iron speciation of DSL and ULS were analyzed by Fe K-edge X-ray absorption fine structures (EXAFS) at the synchrotron SOLEIL (Gif-sur-Yvette, France) (beamline SAMBA) by one of the project partners at NGI, with practical assistance by the author of this thesis. To prepare the biochars for analysis, each sample ($\sim$50 mg) was crushed to a fine powder in a mortar (250μm). The samples were then mixed with boron nitride (BN, 300 mg) to a homogeneous powder, and then pelletized. The BN matrix was used for sample dilution because it absorbs very little of the photon beam at the absorption edge. The resulting biochar pellets were analyzed by X-ray absorption spectroscopy.

The overall principle of EXAFS is to determine the structural composition of a sample by examining its X-ray absorption spectrum. This plots absorbance, μx, as a function of photon energy, eV (Vlaica and Olivi, 2004). The sample is then submitted to an X-ray beam where a spectrophotometer measures the beam's intensity as it passes through the sample. The difference in intensity, measured both before and after passing through the sample, is translated into an absorption coefficient, following Beer-Lambert's Law:

$$\mu x = \log \frac{I}{I_0} \tag{3.1}$$
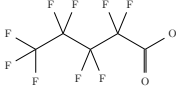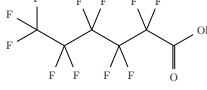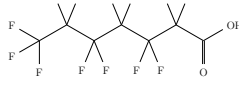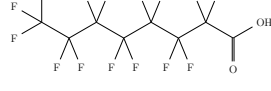
where μx is a dimensionless absorbance coefficient (AU), I is the transmitted light intensity, and I_0 is the incident light intensity. The energy of the photon beam can be determined by the angle of a crystal monochromator, tuned so that the sample is bombarded by a range of photon energies between which the absorption edges of the target element is expected to be located (Vlaica and Olivi, 2004). An adsorption K-edge occurs when the transmitted photon energy equals the energy required to excite a core electron, and is observed as a vertical jump (K) in μx on the spectrum (Vlaica and Olivi, 2004). The neighboring elements interfere with the photon wave which then translates into oscillations on the absorption spectrum following the absorption edge. Each element has a different oscillation pattern. The frequency and amplitude of these oscillations are (partially) determined by the type and number of neighboring atoms. The absorption edge energy and oscillations thus contain information on the valency of the element, as well as the number and type of neighboring atoms, that is to say, the element speciation.

Fe(II) species will have their K edge at a lower energy than Fe(III) species because a higher photon energy is required to excite an electron from the more electronegative Fe(III). In addition, the following oscillation pattern will differ depending on the Fe mineral. The different iron species present in the sample can be derived by interpreting the resulting X-ray absorption spectrum.

3.2   PFAS analytes

6 perfluorinated carboxylic acids (PFCAs) were selected as target compounds for the batch test experiments. These were: PFPeA, PFHxA, PFHpA, PFOA, PFNA, PFDA, with perfluorinated carbon units 4-9 respectively (Full names are listed in Table 3.1). 10 mL stock solutions for each PFCA were prepared by weighing the pure compound salt/liquid (Table 3.1), and then

Table 3.1: PFAS compounds investigated in this study. Note: PFCAs appear in dissociated form at environmentally relevant pH's due to low pK_a's.

Chemical	Acronym	Short	CAS number	Molecular structure	Stock form	Purity
Perfluoropentanoic acid	PFPeA	C5	2706-90-3		liquid	>97 %
Perfluorohexanoic acid	PFHxA	C6	307-24-4		liquid	>97 %
Perfluoroheptanoic acid	PFHpA	C7	375-85-9		crystalline	>99 %
Perfluorooctanoic acid	PFOA	C8	335-76-2		powder	>95 %
Perfluorononaoic acid	PFNA	C9	375-95-1		crystalline	>97 %
Perfluorodecanoic acid	PFDA	C10	335-67-1		flakes	>98%

dissolving them in methanol in volumetric flasks. Additional safety precautions were taken during this procedure by using double latex gloves.

Two spiking standards at high (STD1) and low (STD2) concentrations were prepared from the stock solution used for spiking the batch tests at various concentrations (standard concentrations in Table A.3). The working standards were analyzed by LC-MS/MS of a twice diluted standard at an optimum concentration for the instrument calibration curve (10-20 μg/L). All further calculations of spike dilutions were corrected by means of the measured standard concentrations. See Appendix A for expected vs. analytical concentrations. A detailed description of the LC-MS/MS analytical procedure is given in Section 3.5.2.

3.3 Batch tests

Batch testing is a laboratory method that involves shaking biochar in a closed container using a specified water-to-solid (L/S) ratio, contact time, and different concentrations of PFAS. After shaking, the concentration of PFAS in the water phase is analyzed. An illustration of the batch test experimental procedure used for PFAS and biochar in this thesis is shown in Figure 3.3.

The batch tests prepared in this thesis were used to determine sorption isotherms for the biochars. A sorption isotherm is a curve that represents the distribution of a substance between the aqueous and sorbed phase at different concentrations (Limousin et al., 2007). Sorption of PFAS to biochar is weakened at higher concentrations caused by a gradual saturation of sorption sites (Schwarzenbach et al., 2005). This means that sorption isotherms for biochar are linear at low concentrations and gradually become non-linear at higher concentrations. When designing the batch test experiments for this thesis, the goal was to represent sorption of PFAS across
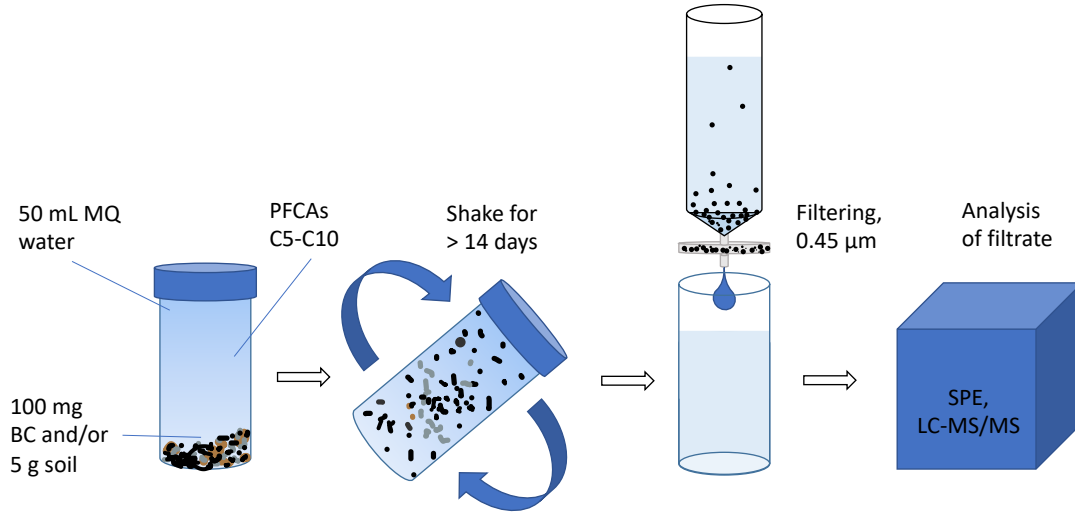
Figure 3.3: Experimental procedure for the laboratory batch shaking tests.

both the linear and non-linear regions, this to determine at which concentration BC sorption sites start to get saturated. A more detailed description of this trend, called attenuation, is provided in Section 3.4.2.

3.3.1   PFAS spike concentrations

To achieve detectable equilibrium aqueous concentrations (C_w), determining appropriate spike concentrations was based on several factors: 1) obtaining biochar-water distribution coefficients (K_{BC}) for the corresponding PFCAs from literature Xiao et al. (2017a) Table A.2, 2) biochar dose, 3) LOQ of the analytical method (Table A.4), and 4) available volumes of pipette tips. The relationships between K_{BC} (L kg^{-1}), the sorbed concentration, C_s (μg kg^{-1}), and the freely dissolved aqueous concentration, C_w (μg L^{-1}), are expressed as:

$$K_{BC} = \frac{C_s}{C_w} \tag{3.2}$$

and was used to estimate the expected C_w. By rearranging eq. (3.2), C_w can be expressed as a function of the mass PFCA spiked (m_{TA}), the estimated K_d, the biochar dose (m_{BC}), and sample water volume (V_w):

$$C_w = \frac{\frac{m_{PFAS}}{\left(\frac{m_{BC} \times K_{BC}}{V_w}\right)+1}}{V_w} \tag{3.3}$$

The lowest spike concentration for each isotherm was established as two times the method LOQ in order to account for uncertainties when estimating resulting C_w. The remaining points were spread evenly over a 10^4 concentration interval.

Two preliminary batch tests were prepared to check how well the estimates from points 1) - 4) above matched the expected sorption strength of the biochar samples. A description of the preliminary tests is given in Appendix A).
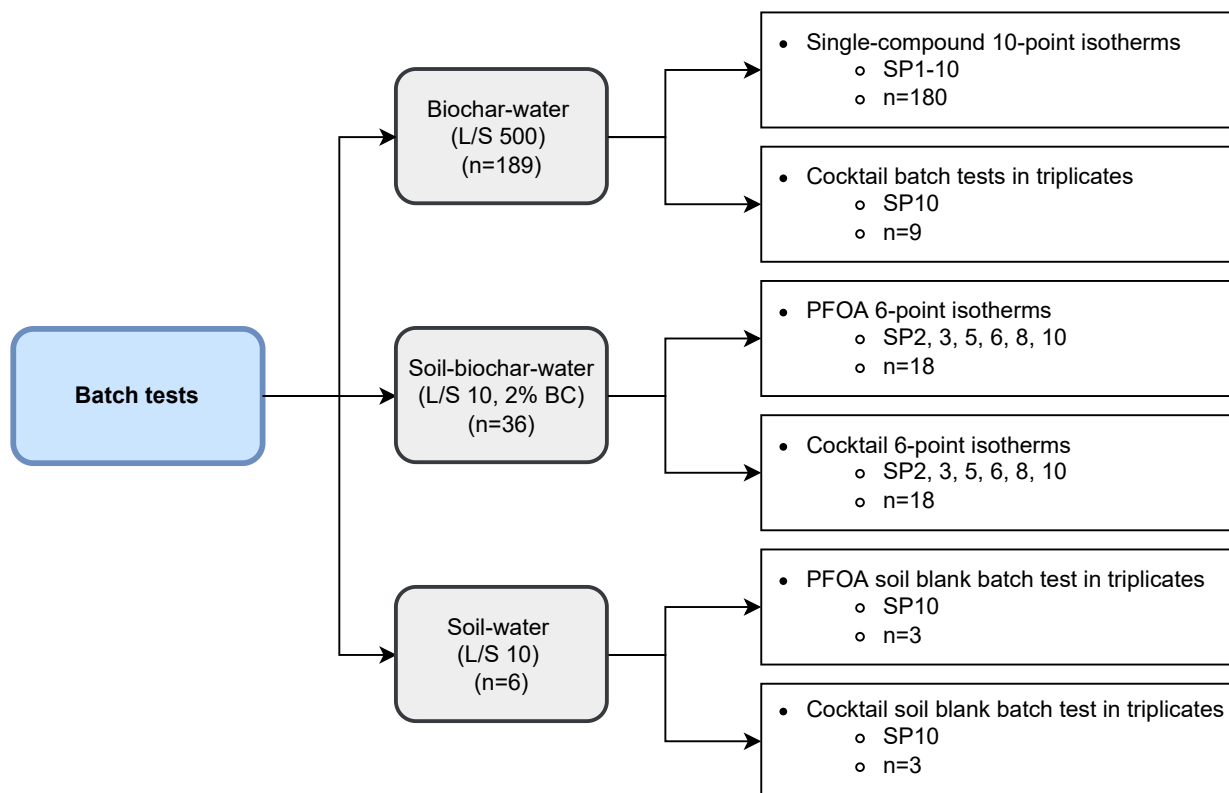
Figure 3.4: Experimental design of the batch tests prepared in this study. SC = spike concentration (the acronym was changed to SP in the remaining discussions). SP10 = highest spiked concentration.

3.3.2 Preparation of batch test

An overview of the experimental design of the batch tests is given in Figure 3.4. The batch tests were prepared with a liquid-to-solid mass ratio (L/S) of 500 for biochar, and an L/S of 10 for soil amended with 2% biochar in accordance with CEN EN 12457, and with modifications described in (Hale et al., 2017; Kupryianchyk et al., 2016a). The different batch test categories prepared were:

- **BC-single**: biochar-water spiked with single PFCAs

- **BC-mix**: biochar-water spiked with a PFCA cocktail

- **BC-soil-PFOA**: soil-biochar-water spiked with single PFOA only

- **BC-soil-mix**: soil-biochar-water spiked with a PFCA cocktail

- **Soil-single**: soil-water spiked with single PFCAs

- **Soil-mix**: soil-water spiked with a PFCA cocktail

All samples were prepared in 50 mL polypropylene (PP) centrifuge tubes that were rinsed three times with 50% MeOH to extract any potential PFAS contamination prior to sample preparation. 100$\pm$4 mg biochar and/or 5.000$\pm$0.005 g soil were added to the sample tubes and spiked with single PFCA compounds and a PFCA cocktail at the concentrations specified in Table 3.2. These were then filled with Milli-Q water to a final volume of 50 mL. A volume

Table 3.2: Spike concentrations (SC) in μg/L used for the batch tests, corrected for the analytical standards.

Compound	SC1	SC2	SC3	SC4	SC5	SC6	SC7	SC8	SC9	SC10	SC10-MIX*	SC10-MIX-S†
PFPeA	0.019	21	43	64	86	107	128	150	171	191	191	283
PFHxA	0.033	37	73	110	146	184	220	256	292	330	330	836
PFHpA	0.012	11	25	38	52	65	79	92	106	117	117	153
PFOA	0.195	216	435	651	871	1 087	1 302	1 522	1 742	1 953	1 953	1 974
PFNA	0.141	156	313	471	625	784	942	1 097	1 255	1 409	1 409	2 310
PFDA	0.383	425	850	1 275	1 700	2 126	2 551	2 976	3 401	3 830	3 830	5 288

* cocktail of C5-C10 spiked to biochar-water batch tests
† cocktail of C5-C10 spiked to biochar-soil-water and soil-water batch tests

calibration was performed to control for variations in sample volumes and is in Appendix C. Cocktail samples were spiked with the same relative amounts of each PFCA as the single-spike samples at SC10 (SC10-MIX and SC10-MIX-S). The concentrations spiked were compared to literature values for the critical micelle concentrations (CMC) of the different PFCAs, and were not an issue for the concentration range considered (Bhhatarai and Gramatica, 2011; Ding and Peijnenburg, 2013). The samples were assured to contain <1% MeOH, which is the upper limit to ensure that methanol does not influence sorption (Arvaniti et al., 2014b).

In order to reach equilibrium, batch tests were shaken end-over-end (9 rpm) and/or agitated on a shaking table (160 rpm) at room temperature (23°C) for at least 14 days (Kupryianchyk et al., 2016a). The samples were filtered through a 0.45μm Minisart® regenerated cellulose syringe filter into new PP tubes using methods described in Sorengard et al. (2019). Prior to filtration, the samples containing soil were centrifuged to remove as many particles from suspension as possible. However, filtration still required frequent filter changes due to clogging (up to three times per sample). Loss of biochar that adhered to the walls of the syringe was quantified in the event that a full mass balance was required for analysis of PFCA distribution Appendix C. However, a 100% mass balance was assumed when calculating the distribution between sorbent and water. The calculation was done by subtracting the initial spike concentration from the measured filtrate concentration.

3.3.3 Soil

Soil used for batch tests in the presence of soil, was an unaged, sandy soil that was obtained from a remote field area, 17 km from Uppsala, Sweden (59.733 N, 17.667 E). The soil carbon content was determined through dry combustion according to ISO10694 (1995) using an elemental analyzer for macro samples (TruMac®CN, Leco corp, St. Joseph, MI, USA). This analysis was performed by research partners at the Swedish University of Agricultural Sciences (SLU), Uppsala, Sweden. The soil was classified as a fine sand (0.1 to 0.3 mm), with 1.3 % total organic carbon (TOC, pH 5.38 $\pm$ 0.02, CEC 2.63 $\pm$ 0.06 meqv/100 g). Total element concentrations and exchangeable ion concentrations are presented in Appendix D, Table D.2. The soil was dried at 100 °C for 24 h, and then crushed and sieved to <2 mm.

Filter clogging by soil

Prior to filtration, the batch tests with soil contained different degrees of suspended particles despite being centrifuged. This made it difficult to filter the samples that contained the most
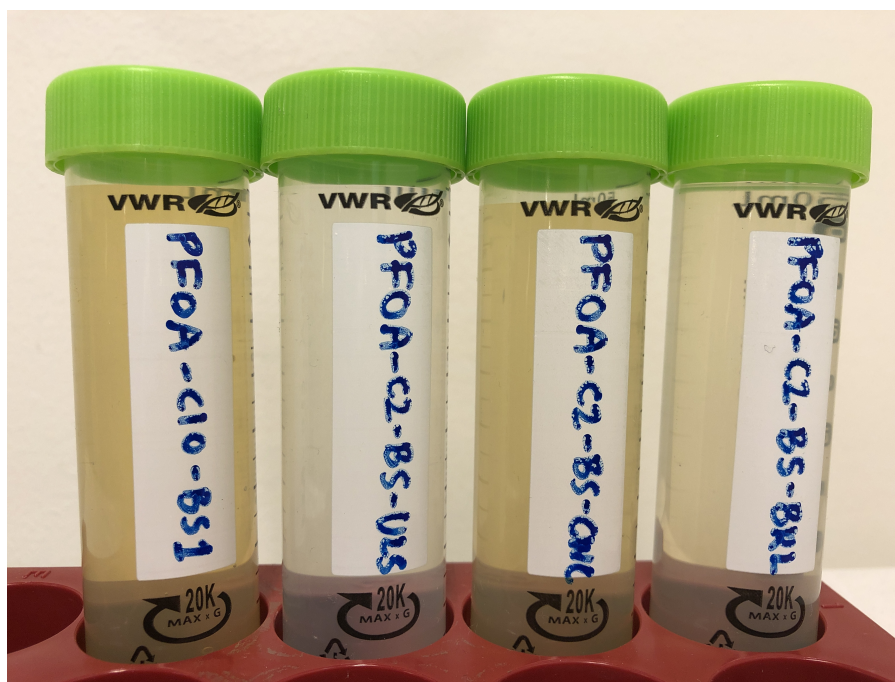
Figure 3.5: Color of filtrate for each biochar batch test. From left to right: soil only, soil+ULS, soil+CWC, and soil+DSL.

suspended particles. Filtration led to clogged filters that had to be changed up to three times per sample. Frequently clogged filters likely resulted in reduced filter pore size associated with the fact that some DOC was retained. This may have led to underestimating C_w, and thereby overestimating K_d for the soil samples. This, in turn, became an issue when deriving Freundlich distribution coefficients for biochar in the presence of soil. In the next section, additional considerations for calculating PFAS-distribution in batch tests with biochar in the presence of soil will be discussed. Filter blanks (Section 3.3.4) were only prepared for BC-water samples that showed no significant effect (see Table A.5). Hence, the effect of reduced filter size by clogging could not be quantified.

The resulting soil batch test filtrates varied in color Figure 3.5. The sludge biochar soil samples were more transparent than soil only, and soil-CWC. The remarkable difference in DOC could be attributed to DOC complexation with inorganic species present in the sludge chars, but not in CWC biochar, as inorganic ions are not a dominating component of clean wood-derived biochar. In summary, the observations made during filtration of the BC soil batch tests indicate that sewage sludge biochar binds DOC, and that DOC in the filtrate is potentially responsible for an underestimation of C_w, and hence, an overestimation of the soil-water distribution coefficient ($K_{d,s}$).

3.3.4   Sample blanks

To correct for potential PFCA-loss to the filter paper, and thereby underestimation of C_w, filtration blanks for each compound were prepared in triplicates for each PFCA at an optimum concentration range for the instrument (see Section 3.2).

3.3.5   pH and electrical conductivity

pH and conductivity were measured in a slurry of biochar and water (1:5). This involved pre-stirring (15 min) and then letting the particles settle (>24 hrs) before measurement (n=3).

3.4   Sorption models

There are several empirical and theoretical models that can be used to fit a line between the concentration points that were generated from analysis of the batch test filtrates (Wang and Guo, 2020). This study applied a linear sorption model to evaluate sorption to soil, and the Freundlich sorption model for the data points from batch tests that contained biochar. In this study, sorption isotherms were determined at equilibrium which was assumed to be reached after 14 days.

3.4.1   The biochar-water distribution coefficient (K_d)

Linear sorption assumes that sorption increases proportionally with concentration and is commonly used to determine distribution at one concentration point. Linear sorption is expressed by:

$$C_s = K_d \times C_w \tag{3.4}$$

where C_s is the sorbed amount, C_w is the equilibrium aqueous concentration, and K_d is the resulting distribution coefficient. Since sorption to biochar is non-linear, K_d-values cannot be extrapolated beyond the concentration point where they were determined at. Also, a comparison of $K_d s$ across samples can only be done if the $K_d s$ have the same equilibrium aqueous concentration.

3.4.2   The Freundlich sorption model

The Freundlich sorption model provides a way of deriving distribution coefficients that represent solid-water phase distribution across a wider concentration range (Zhang et al., 2013). The Freundlich equation is expressed as:

$$C_s = K_F \times C_w^{n_F} \tag{3.5}$$

where C_s is the amount sorbed in μg/kg, K_F is the Freundlich distribution coefficient in L/kg, C_w is the equilibrium aqueous concentration in μg/L, and n_F is the coefficient of non-linearity. Because this model does not consider all sites on the adsorbent surface to be equal, but rather predicts that adsorption becomes progressively more difficult as more and more adsorbate accumulates, it is usually used for sorbents such as biochar that have heterogeneous surfaces(Yin et al., 2022; Schwarzenbach et al., 2005). The Freundlich model assumes a log-normal sorption distribution (Schwarzenbach et al., 2005). Taking the log of each side of eq. (3.5) results in a linear expression:

$$\log C_s = \log K_F + n_F \times \log C_w \tag{3.6}$$

A linear regression line can be fitted between the log C_w (x-axis) and log C_s (y-axis) concentration points for each sample. The resulting regression equation is the Freundlich equation (eq. (3.6)) where the y-intercept is the Freundlich distribution coefficient (log K_F), and the slope is the coefficient of non-linearity (n_F). n_F represents how linear the isotherm is within the concentration intervals achieved and is <1. n_F is usually between 0.7 and 1.0 (Cornelissen et al., 2005).

The modeling of the soil-inclusive experiments is complicated since distribution behavior between soil-water and biochar-water must be considered together. The K_d of soil must be determined separately and corrected in order to determine K_F, BC in the presence of soil. Sorption to soil-only is most often linear and is therefore represented by eq. (3.4). The mass balance for the distribution between water, soil and biochar (BC) is obtained by expanding the Freundlich equation (eq. (3.5)). The mass balance between the three phases can be deduced as follows:

$$m_{tot} = m_w + m_s + m_{BC} \tag{3.7}$$

$$m_{tot} = C_w V_w + C_s M_s + C_{bc} M_{BC} \tag{3.8}$$

$$m_{tot} = C_w V_w + K_d C_w M_s + K_F C_w^{n_F} M_{BC} \tag{3.9}$$

where m is the mass PFAS in ng or μg, and M is the mass soil or sorbent in kg. Substituting eq. (3.9) in the Freundlich equation yields:

$$m_{tot} - C_w V_w - K_d C_w M_s = K_F C_w^{n_F} M_{BC} \tag{3.10}$$

Equation (3.10) contains the expression for the amount of PFAS in the BC on the left hand side, and an expression for the aqueous PFAS concentration on the right hand side. To get the linear Freundlich expression, the log of each side is taken:

$$\log(m_{tot} - C_w V_w - K_d C_w M_s) = \log(K_F C_w^{n_F} M_{BC}) \tag{3.11}$$

Further modifications are made so as to simplify the Freundlich linear expression to $y = b + a \times x$:

$$\log(m_{tot} - C_w V_w - K_d C_w M_s) = \log K_F + \log C_w^{n_F} + \log M_{BC} \tag{3.12}$$

$$\log(m_{tot} - C_w V_w - K_d C_w M_s) = \log K_F + n_F \times \log C_w + \log M_{BC} \tag{3.13}$$

$$\log(m_{tot} - C_{aq} V_w - K_d C_w M_s) - \log M_{BC} = \log K_F + n_F \times \log C_w \tag{3.14}$$

For each point on the isotherm, eq. (3.14) can be plotted using $\log C_w$ on the x-axis, and $\log(m_{tot} - C_{aq} V_{aq} - K_d C_{aq} M_s) - \log M_{bc}$ on the y-axis. The resulting linear regression coefficients represent the same variables as the non-extended Freundlich expression (eq. (3.6), that is, n_F is the slope, and log K_F is the intercept.
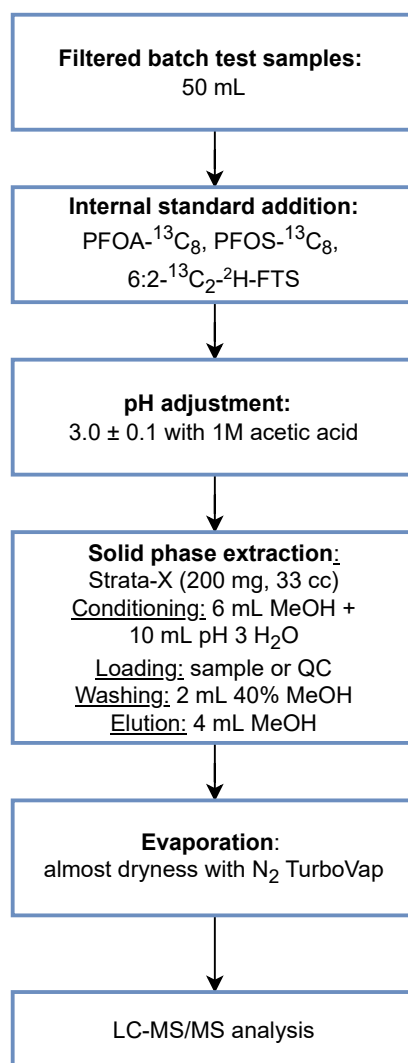
Figure 3.6: Schematic diagram of the analytical method applied for the determination of TCs in the batch test filtrates adapted from Arvaniti et al. (2012).

3.5 Instrumental analysis

3.5.1 Solid-phase extraction (SPE)

Solid-phase extraction (SPE) is a sample-preparation method used to extract and concentrate a large-volume sample to produce a solvent extract. The extract can then be subjected to analyte quantification using LC-MS/MS. The sample is passed through a cartridge with a porous sorbent polymer which serves as the extraction agent, and strongly retains polar compounds. The sorbed analytes are then eluted with an appropriate solvent, evaporated, and finally reconstituted to the desired extract volume. All samples are spiked with a mix of internal standards (ISs) to compensate for variations in extraction percentages and instrumental response by the mass spectrometer detectors (Arvaniti et al., 2014b).

Strata-X® 200 mg/6mL cartridges, supplied by Phenomenex, were used for extracting the target compounds in the filtered water samples. The sorbent polymer was a surface modified styrene divinylbenzene (Figure 3.7) with a 33 μm average particle diameter, and a surface area
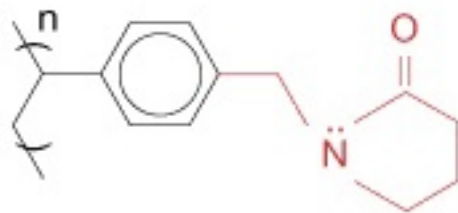
Figure 3.7: Polymer used as extraction agent in SPE, surface-modified styrene divinylbenzene.

of 800 m^2 g^{-1}. The internal standards used were $^{13}C_8$-perfluorooctanoic acid ($^{13}C_8$-PFOA), $^{13}C_8$-potassium perfluorooctanesulfonate ($^{13}C_8$-PFOS-K), and 6:2-$^{13}C_2$-^1H,^2H-perfluorooctane sulfonate (6:2 $^{13}C_2$-FTS) where a working standard of the three isotopic PFASs was prepared in methanol at 1 ppm, from a 50 ppm analytical standard supplied by Sigma Aldrich.

A schematic description of the SPE protocol is provided in Figure 3.6. The filtered batch test samples were adjusted to pH $\sim$3 with 800 μL 1 M acetic acid. However, samples containing soil required adding at least double this amount to reach the same pH. pH strips were used to test the pH of five randomly selected samples from each batch of 20. All samples were then spiked with IS. SC1 and SC2 samples were spiked with 10 μL IS, and SC3-SC10 samples were spiked with 20 μL IS. The difference in the amount of IS for the two low-spike samples was due to the fact that a more concentrated extract was needed (0.5 mL vs. 1 mL) for these samples so as to avoid signals below instrumental LOQ. The samples were vortexed prior to SPE.

The SPE cartridges were conditioned with 6 mL MeOH and 10 mL pH 3 milli-Q water (acidified by 100% acetic acid). MeOH was used for wetting to allow the mobile phase to flow into all the pores of the sorbent polymer. This ensured maximum chromatographic retention. Water with a low pH was used to protonate lone pair electrons on the polymer surface in order to maximize hydrophobic interaction with the analytes. The samples were loaded using glass pipettes, and allowed to pass through the cartridges by gravity. The flow rate was adjusted by modifying the opening of the cartridge openings by the use of LC liners so that the sample exited the cartridge as individual droplets.
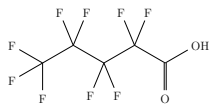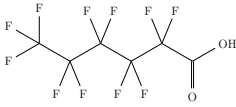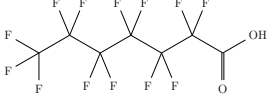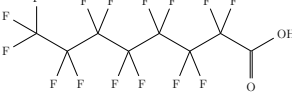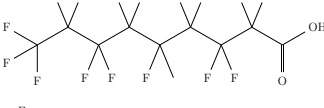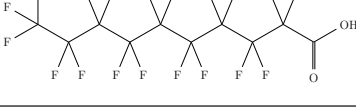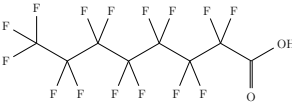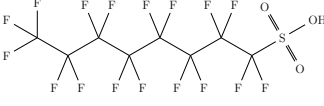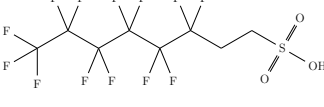
After extracting the samples, the SPE cartridges were washed with 2 mL MeOH:MQ (40:60, % v/v) in order to remove any matrix interferences. The cartridges were then dried with a vacuum pump at 20 mmHg until the extraction agent was visible as a dry powder. The analytes were then eluted with 4 mL MeOH into 15 mL PP centrifuge tubes, and concentrated to $\leq$0.5 mL using TurboVap® at 40 °C, and nitrogen gas (N_2) at 5 psi. The samples were reconstituted to 1 mL (0.5 mL for SCs 1 and 2) with MeOH and MQ, ending up at a final solvent ratio of 50:50 % v/v. The extracts were transferred to LC vials using glass pipettes and stored at -19 °C until sample analysis took place. To minimize risk of contamination during laboratory work, working benches were cleaned with acetone and covered with aluminum foil. Sterilized PP tubes were used during all steps of the procedure.

3.5.2   LC-MS/MS

Liquid chromatography separates compounds in a mixture based on polarity by using a stationary phase that retards hydrophobic compounds while allowing more polar compounds to pass through more quickly along with a polar mobile phase. Using high voltage, the compounds were

then ionized into fragment ions which were detected by a mass spectrometer that determined the mass of the transitions.

Table 3.3: Ion transitions for the target analytes and internal standards in this study.

Compound	Structure	Formula	M	Parent	Cone (V)	Transitions (CE)
PFPeA		$C_5HF_9O_2$	264.05	262.97	20	$262.97 \rightarrow 219\ (8)$
PFHxA		$C_6HF_{11}O_2$	314.05	312.97	10	$312.97 \rightarrow 118.95\ (18)$ $312.97 \rightarrow 269\ (8)$
PFHpA		$C_7HF_{13}O_2$	364	362.96	6	$362.96 \rightarrow 119.00\ (22)$ $362.96 \rightarrow 168.97\ (18)$
PFOA		$C_8HF_{15}O_2$	414.07	412.97	20	$412.97 \rightarrow 168.90\ (18)$ $412.97 \rightarrow 369.00\ (8)$
PFNA		$C_9HF_{17}O_2$	464.08	462.99	20	$462.99 \rightarrow 219\ (16)$ $462.99 \rightarrow 419\ (10)$
PFDA		$C_{10}HF_{19}O_2$	514.09	513.1	10	$513.10 \rightarrow 219.01\ (18)$ $513.10 \rightarrow 269.04\ (16)$
Internal standards (IS)						
PFOA $^{13}C_8$		$^{13}C_8HF_{15}O_2$	422.01	420.9	16	$420.90 \rightarrow 171.86\ (16)$ $420.90 \rightarrow 222.84\ (16)$
PFOS $^{13}C_8$		$^{13}C_8HF_{17}O_3S$	507.06	506.9	56	$506.90 \rightarrow 79.87\ (46)$ $506.90 \rightarrow 171.85\ (32)$
6:2 FTS $^{13}C_2$		$C_6^{13}C_2H_5F_{13}O_3S$	432	432.96	26	$432.96 \rightarrow 411.959\ (24)$ $432.96 \rightarrow 81.901\ (30)$

CE = collision energy
V = cone voltage

PFAS quantification was determined by LC-MS/MS using an Acquity UPLC I-Class system connected to a Xevo TQ-S triple quadrupole mass spectrometer, equipped with an ESI Z spray. Both were supplied by Waters (Milford, MA, USA). For chromatographic separation, a Kinetex C18 column (30 x 2.1 mm, 1.3 μm), serially connected to a Phenomenex C18 (2 x 2.1 mm i.d.) security guard (Torrance, CA, USA), was used. Mobile phases were A: 2 mM ammonium acetate in MQ water (water phase) and B: pure MeOH (organic phase) that were supplied at a constant flow rate of 250 μL/min to the LC column, and maintained at a constant temperature of 30 °C. The sample injection volume was 4 μL. The run-time for each sample was 6 minutes, with an initial and final mobile phase gradient of 20:80 (A:B). Analytes were

ionized by negative electrospray ionization (ESI-), and nitrogen was used as a drying gas at the ionization source. Two ion transitions were registered for each PFCA (Table 3.3), and these came within 60 seconds of the expected retention time for the compound. Peak integration was performed automatically by MassLynx software, obtaining 12 points per peak, and an average baseline peak width of 5 s. Data from LC-MS/MS was processed in MassLynx version 4.1, while quantification processing was performed with TargetLynx. Each peak was manually reviewed to remove peaks that were likely background noise, as well as corrections for inconsistencies in peak base width. Complete instrument programming and parameters are summarized in Appendix B.

3.5.3 Quality assurance and quality control

Accurate mass spectrometric quantitation was performed using the matrix-matched calibration method. The advantage of using this calibration is that the ionization influence of the sample matrix are corrected for. A detailed description of the matrix-matched calibration method is provided below, and a summary of the contents of each quality assurance and quality control (QA/QC) sample prepared for the quantitation of PFAS are listed in Appendix B, Table B.1.

Calibration curves

A 10-point calibration curve ranging from 0.01 to 50 ppb was prepared in methanol. The results demonstrated a satisfactory regression coefficient ($r^2 > 0.98$) for each analyte. This solvent blank calibration curve is used to derive analyte concentrations in samples not taken through the SPE protocol since they do not experience a matrix effect. A matrix-matched calibration curve was used to quantify MS samples brought through SPE. During calculations of results, only $^{13}C_8$-PFOA was used because it had the most similar retention time to the target analytes.

Blanks

Contamination that may have arisen during preparation of samples, and from laboratory materials, was evaluated through the analysis of sample and procedural blanks. One procedural blank was prepared by spiking IS directly into the SPE cartridge and eluting with methanol. Thereafter, the whole SPE procedure continued from this point. Contamination from test tubes, reagents, or other introductions of contamination, will show up on the instrument results from this quality assurance (QA) procedure. Two blank samples were prepared by bringing 50 mL pH 3 MQ water (sample matrix), spiked with IS, through the extraction protocol. Sample blanks determined any interferences caused by the the matrix itself. During analysis, solvent blanks (100 % MeOH), and a standard mixture of TAs at 10 ppb, were injected into the instrument every 15-20 samples in order to monitor potential cross-contamination, carryover, and to assure maintenance of sensitivity. An MeOH:MQ (50:50; v/v) 0.1 % formic acid wash solution was used to clean the injection needle before and after each injection.

Pre- and post- extraction spiked matrix samples

Pre and post-extraction matrix spike samples were prepared in triplicate at a concentration interval covering the expected concentration range of the test samples (2.5, 25 and 50 ppb). To spike the samples, a working standard of target analytes (C5-C10) was prepared at 1 ppm

in MeOH. Pre-extraction matrix spikes were prepared by spiking IS and TA standard at 2.5, 25 and 50 ppb in the 50 mL sample matrix. These were taken through the protocol in the same manner as the test samples. Matrix-matched samples were prepared by taking a 50 mL sample matrix through the SPE protocol, and spiking it with 2.5, 25 and 50 ppb TA and IS post-extraction. Concentration of TAs was determined by interpolation based on the resulting matrix-matched calibration curve.

Absolute recovery, relative recovery and matrix effect calculations

By comparing the pre- and post-extraction matrix spike signals, absolute recovery (AR), relative recovery (RR), and matrix effects (ME) were calculated for each target analyte. AR and RR were assessed using the following equations:

$$\%AR = 100\% \times \left(\frac{A_{ss}}{A_{se}} \right) \tag{3.15}$$

$$\%RR = \frac{\frac{A_{ss}}{A_{is}} - \frac{A_b}{A_{is}}}{\frac{A_{se}}{A_{is}} - \frac{A_b}{A_{is}}} \times 100\% \tag{3.16}$$

Where:

A	peak area of chromatogram signal,
ss	spiked sample (pre-extraction matrix spike),
se	spiked extract (post-extraction matrix matched),
is	internal standard,
b	solvent blank,
cc	calibration curve solvent spike

AR and RR values of 100 % indicate recovery of all analytes. Matrix effects were assessed by the following equation:

$$\%ME = 100\% \times \left(\frac{A_{se} - A_b}{A_{cc}} \right) - 1 \tag{3.17}$$

where ME >0% indicates ion enhancement, and ME <0% = ion suppression. In mass spectrometry, ion enhancement/suppression occurs when there is an enhanced/reduced detector response of the target analyte at the ionization source. This is caused by the sample matrix competing for ionization energy. The ARs, RRs and MEs are reported in Table 3.4

Table 3.4: Absolute recovery, relative recovery, and matrix effects for the target analytes from solid-phase extraction (SPE).

Analyte	Absolute recoveries			Relative recoveries			Matrix effects	
	2.5 ppb	25 ppb	50 ppb	2.5 ppb	25 ppb	50 ppb	25 ppb	50 ppb
PFPeA	12 %	8 %	6 %	0 %	6 %	7 %	65 %	63 %
PFHxA	103 %	80 %	83 %	128 %	89 %	106 %	87 %	80 %
PFHpA	90 %	95 %	93 %	111 %	106 %	118 %	111 %	100 %
PFOA	99 %	94 %	90 %	139 %	105 %	115 %	94 %	86 %
PFNA	100 %	101 %	93 %	132 %	113 %	119 %	88 %	81 %
PFDA	106 %	83 %	80 %	177 %	93 %	102 %	88 %	83 %

3.6   Data analysis

Raw data handling was conducted using Microsoft Excel (v.16.58). Statistical analysis and plotting were carried out using R software (v.4.1.2), and RStudio IDE (2022.02.0-443).

3.7   Uncertainty

Each of the many steps involved in determining the aqueous equilibrium concentrations of the target compounds will have an impact on the overall uncertainty of the results. Factors contributing to increase uncertainty incrementally, starts with the preparation of the PFAS standards used for spiking. Uncertainty is also associated with spiking each batch test, a process that involved up to three pipettings done per sample, as well as weighing sorbent doses,measuring water volume, and potential contamination during sample preparation and storage, filtering samples and co-sorption onto filters and tube walls. Further uncertainty is also associated with chemical analysis by solid-phase extraction (SPE) and LC-MS/MS, a combination of automatic and manual peak integration, and data treatment. Previous research on material choice for laboratory work with PFAS indicates some sorption to tube walls (Lath et al., 2019). 74-81 % recovery of PFOA for polypropylene (PP) has been measured. Sorption to tube walls follow Langmuir sorption, meaning that tube wall sorption sites saturate. This means that recoveries increase significantly with higher spike concentrations (e.g., recovery of PFOA increased from 53.7-85.5 %, and between spiked concentrations of 12-415μg/L) (Lath et al., 2019). Therefore, quantification of low concentrations may be subject to a higher degree of error, and in most cases will be an underestimation of dissolved concentrations. Recovery from regenerated cellulose syringe filter was measured at 74%, though filter loss in this study was insignificant (Table A.5). No causal relationship was established between losses of PFOA on syringe filter and increasing spike concentrations. It is therefore difficult to determine the absolute degree of uncertainty associated with all the steps in the sample-preparation and analysis processes. But based on previously reported estimates in similar studies, 20-30%, uncertainty can be expected. Further details related to the main sources of uncertainty expected are discussed in Appendix C.

Chapter 4

Results and discussion

4.1   Sorption isotherms

The Freundlich isotherms and fitting parameters of PFPeA, PFHxA, PFHpA, PFOA, PFNA and PFDA to the CWC, ULS and DSL biochars from the BC-single batch tests are shown in Figure 4.1, Figure 4.2 and Table 4.1. Overall, correlations were poor for the short-chain compounds, PFPeA and PFHxA. The isotherms for PFPeA-DSL, PFPeA-CWC and PFHxA-CWC had significant uncertainty, with $r^2 < 0.3$ and $p < 0.05$, and have therefore not been reported. This uncertainty can be attributed to poor sorption affinity to biochar at shorter chain lengths (Zhang et al., 2021), or to biochar heterogeneity, even for well-mixed and ground samples (Hale et al., 2011).

On average, non-linearity coefficients, n_F, were 0.64 ± 0.23. This average is close to the 0.67 average found from 90 other studies (Cornelissen et al., 2005). The slopes that had $n_F > 1$ (PFHxA-DSL: n=1.11 and PFHpA-ULS: 1.08) were not statistically higher than 1 (standard error $\pm$ 0.11 for both). Therefore, all n_F were < 1, in accordance with the Freundlich model assumptions provided in Section 3.4.2.

Freundlich sorption coefficients for C5-C10 varied over two to three orders of magnitude. Log K_F varied from 3.30 ± 0.15 $(\mu g/kg)/(\mu g/L)^{n_F}$ to 6.00 ± 0.04 $(\mu g/kg)/(\mu g/L)^{n_F}$. The Freundlich coefficients (log K_F) reported throughout this text are in units of $(\mu g/kg)/(\mu g/L)^{n_F}$.

Table 4.1: Freundlich sorption coefficients and linear regression statistics for the BC-single isotherms in CWC, ULS and DSL (n=9). The error is presented as standard error. All K_F data are in units of $(\mu g/kg)/(\mu g/L)^{n_F}$.

PFCA	ULS				DSL				CWC			
	log $K_{F,BC}$	$n_{F,BC}$	r^2	p	log $K_{F,BC}$	$n_{F,BC}$	r^2	p	log $K_{F,BC}$	$n_{F,BC}$	r^2	p
PFPeA	4.10 ± 0.13	0.67 ± 0.16	0.74	**			0.06	>0.05			0.30	>0.05
PFHxA	4.80 ± 0.06	0.34 ± 0.09	0.72	**	3.30 ± 0.15	1.11 ± 0.11	0.93	***			0.04	>0.05
PFHpA	5.98 ± 0.17	1.08 ± 0.11	0.93	***	4.67 ± 0.06	0.57 ± 0.09	0.86	***	4.44 ± 0.05	0.59 ± 0.11	0.80	**
PFOA	5.73 ± 0.02	0.65 ± 0.05	0.95	***	5.12 ± 0.02	0.60 ± 0.02	0.99	***	5.06 ± 0.08	0.39 ± 0.05	0.90	***
PFNA	5.89 ± 0.02	0.71 ± 0.03	0.99	***	5.33 ± 0.03	0.80 ± 0.07	0.94	***	4.88 ± 0.04	0.65 ± 0.04	0.98	***
PFDA	6.00 ± 0.04	0.35 ± 0.05	0.86	***	5.61 ± 0.02	0.61 ± 0.02	0.99	***	5.22 ± 0.07	0.45 ± 0.04	0.94	***

Significance codes: *** < 0.001, ** < 0.01
Insignificant regressions (p < 0.05) have been removed
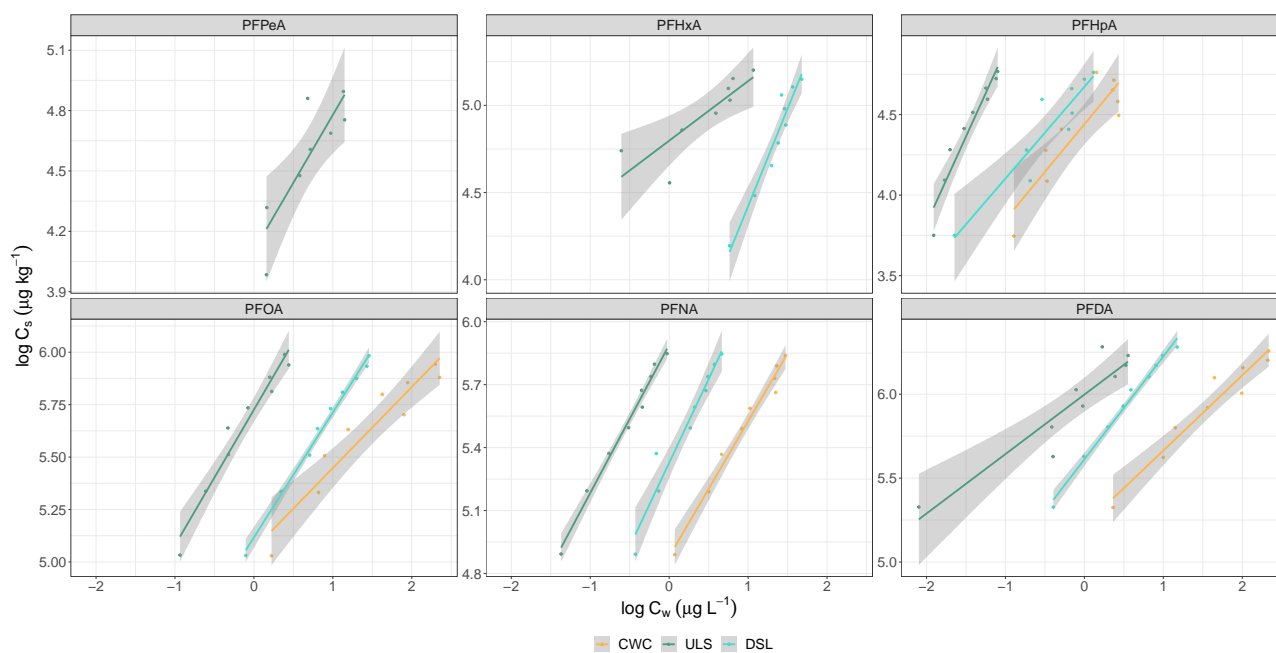
Figure 4.1: Freundlich sorption isotherms for PFPeA, PFHxA, PFHpA, PFOA, PFNA and PFDA in batch tests with three different biochars. Lines are obtained by linear regression.

Freundlich distribution coefficients for ULS ranged from 4.10 ± 0.13 to 6.00 ± 0.04. Log K_F increased in the order: PFPeA (CF4) < PFHxA (CF5) < PFOA (CF7) < PFHpA (CF6) < PFNA (CF8) < PFDA (CF9). Freundlich distribution coefficients for DSL ranged from 3.30 ± 0.15 to 5.61 ± 0.02. Log K_F increased in the order: PFHxA (CF5) < < PFHpA (CF6) < PFOA (CF7) < PFNA (CF8) < PFDA (CF9). Freundlich distribution coefficients for CWC ranged from 3.98 ± 0.36 to 5.22 ± 0.07. Log K_F increased in the order: PFPeA (CF4) < PFHpA (CF6) < PFHxA (CF5) < PFNA (CF8) < PFOA (CF7) < PFDA (CF9).

For all compounds, sorption was strongest for the two sludge chars. This was unexpected. Research on the sorption of PFAS to sewage sludge is relatively new. To the best of this author's knowledge, there is no current literature available that demonstrates distribution coefficients - for PFAS to other sewage sludge biochars - that are comparable to the ones found in this study. However, comparisons can be made between the log K_Fs found in this thesis, and commercially-produced activated carbons (AC) reported in previous studies. In this study, sorption coefficients for PFOA to ULS and DSL biochars (5.12-5.73) are similar to, or higher than, the log K_F for PFOA onto AC found in other literature: 5.60 (Kupryianchyk et al., 2016b), 4.45 (Hansen et al., 2010), and 4.74-5.42 (Silvani et al., 2019). Possible mechanisms that could account for the stronger sorption found for the sewage sludge biochars will be discussed throughout this chapter.
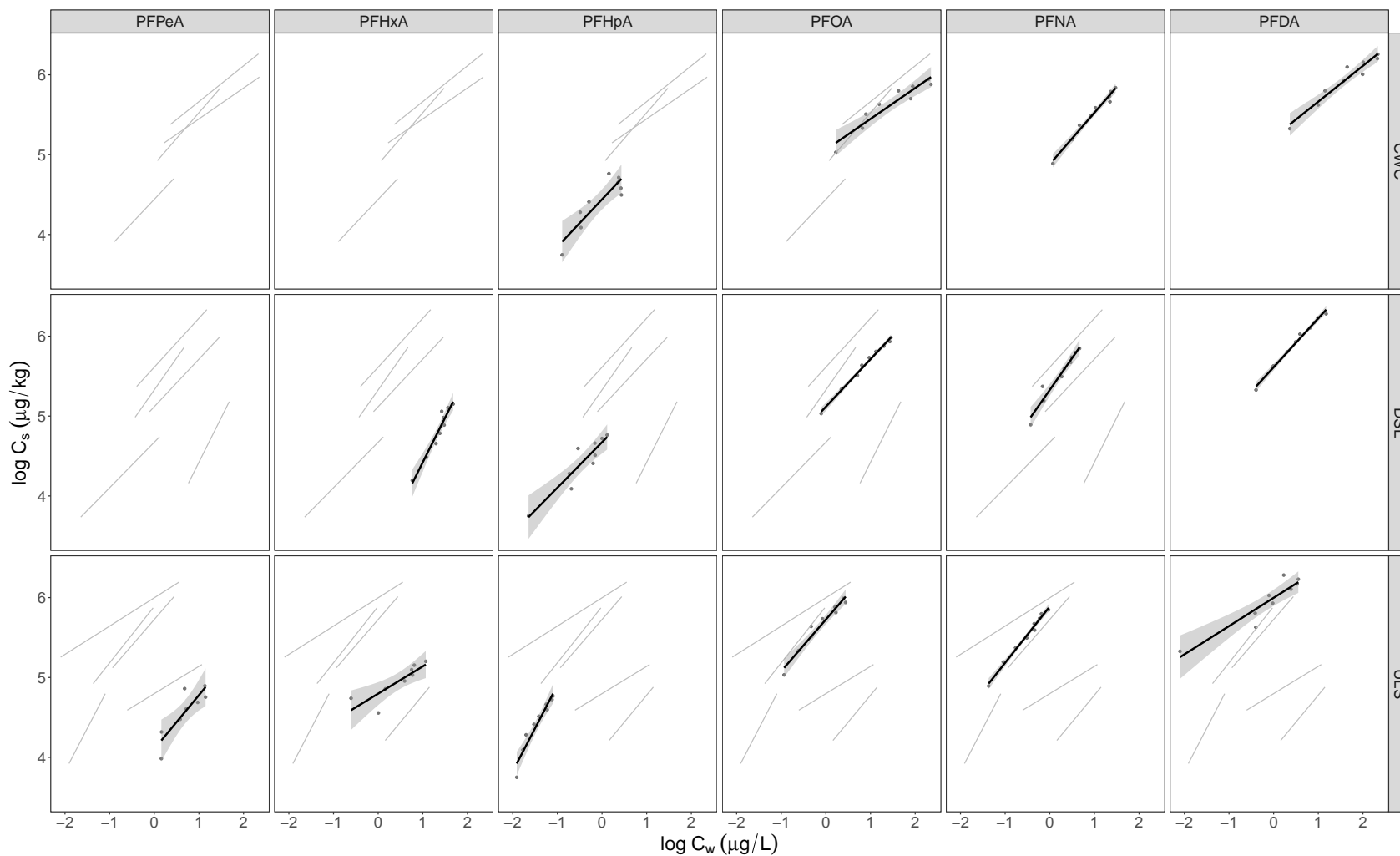
Figure 4.2: Single-compound Freundlich sorption isotherms for PFPeA, PFHxA, PFHpA, PFOA, PFNA and PFDA. Lines are obtained by linear regression. For comparison across chain length, the shaded gray lines are the isotherms from the other compounds with the same sorbent.

4.1.1 The relationship between K_F and physicochemical properties of PFAS

Perfluorinated carbon chain length

K_d increased with increasing perfluorinated chain length for ULS, DSL, and CWC biochars in the BC-single batch tests (Figure 4.3). This relationship was statistically significant for all three biochars (p<0.05), and is in accordance with previous studies (Sorengard et al., 2019; Fabregat-Palau et al., 2022; Ahmed et al., 2020). There was a difference of 1.2-1.9 log K_F units between the longest and the shortest PFCA compounds that were considered for the regressions.

Hydrophobicity of PFAS increases for each additional CF_2 moiety. Two main arguments based on the laws of thermodynamics can explain why perfluorinated carboxylic acids increase in hydrophobicity with increasing chain length. First, due to the perfluorinated tail's high molecular surface, a high cavity formation energy is needed to dissolve the compounds in water (Arp et al., 2006). For this reason, the compounds tend to be pushed towards water-solid interfaces such as a biochar surface. As a result, solvation becomes decreasingly entropically favorable as chain length increases (Sigmund et al., 2022). Second, compared to a hydrocarbon chain, the perfluorinated chain is capable of the lowest van der Waals dispersive forces per molecular surface area (Du et al., 2014). The result is that PFAS in the water cavity has a much weaker attraction to water molecules than hydrophobic organic compounds. For this reason, PFASs are both oil- and water repellent. Generally, water cavity formation energy, and van der Waals interactions, have been considered insignificant for sorption of short-chain PFAS to solid phases (<C6) (Du et al., 2014). They are, however, significant for long-chained PFAS (>C6) (Du et al., 2014). This supports the chain length dependency found in this study. In summary, hydrophobic interactions between condensed aromatic structures in the biochar matrix increase for PFAS with longer chain lengths. This contributes to stronger sorption, and suggests that hydrophobic interactions play the primary role in sorption of PFCA to the biochars tested in this study.

PFAS functional group

In the previous section, an increase in K_F with increasing perfluorinated chain length was established. Also, hydrophobic interaction was proposed as the dominant sorption mechanism for PFCA onto biochar. However, the interactions between the charge-assisted polar head of PFCA, especially for short-chain PFAS, and the biochar surface, cannot be disregarded.

Zhang et al. (2021) found that sorption increased in the order PFBA < PFBS < PFOA < PFOS for granular activated carbon and softwood-derived biochar. PFBA and PFOA are perfluorinated *carboxylic* acids (PFSA), meaning that their polar heads consist of a carboxylate functional group (C(=O)-O⁻). Here, the terminal carbon is bonded to two oxygen atoms that together make up the carboxylate group. PFBS and PFOS are perfluorinated *sulfonic* acids that contain a sulfonate functional group (S(=O)$_2$-O⁻) at the end of the perfluorinated chain. This means that PFBS and PFOS have one more perfluorinated carbon than PFBA and PFOA respectively. The order of sorption Zhang et al. (2021) found for these PFAS compounds demonstrates the probable dominance of hydrophobic interactions as sorption mechanism.

Furthermore, if sorption between a PFSA and PFCA with the same number of CF_2 moieties
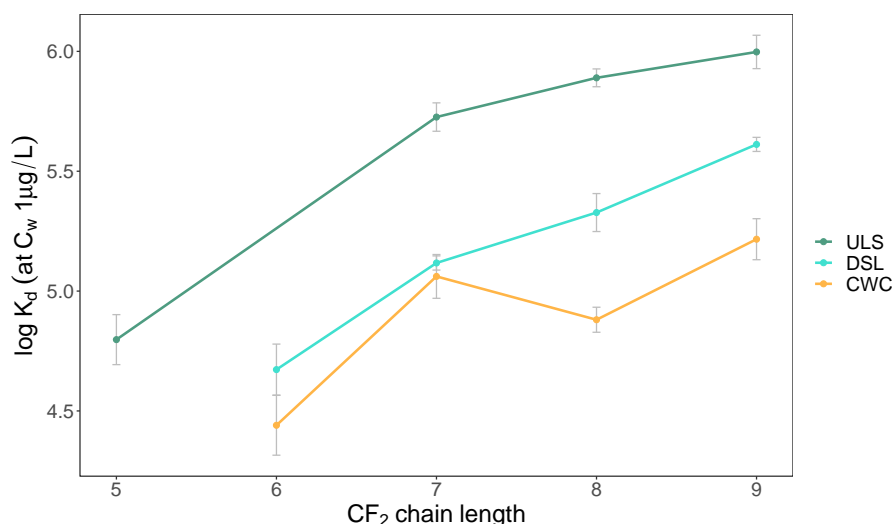
Figure 4.3: Relationship between log K_d at 1 μg/L and perfluorinated chain length derived from the Freundlich distribution coefficients for the BC-single batch tests. Linear regression coefficients for ULS: $r^2 = 0.92$, $p = 0.04$, DSL: $r^2 = 0.98$, $p = 0.01$, CWC: $r^2 = 0.68$, $p = 0.17$. Error bars are the propagated error of log K_F and n_F.

are compared, such as PFHpS to PFOA, the PFSA still sorbs better. Again, there are two main arguments based on the laws of thermodynamics that can explain this difference. First, there is a difference in molecular size between PFHpS and PFOA. This is because the sulfonate group is slightly larger than the carboxylate croup. This results in a greater cavity formation energy for PFSAs (Yin et al., 2022; Sigmund et al., 2022). Second, sulfonic acids are stronger acids than carboxylic acids. This results in a stronger ionic interaction to positive charges of mineral phases in biochar ash (Arvaniti and Stasinakis, 2015).

PFAS can engage simultaneously in hydrophobic interactions (perfluorinated chain), as well as in electrostatic interactions (attraction and repulsion), with both surface functional groups and dissolved ions (head) (Zhang et al., 2013; Sigmund et al., 2022). The arguments discussed in this section suggest that hydrophobic interactions plays a more important role for sorption of PFCAs than electrostatic interactions. Different electrostatic interactions (cation bridging, biochar surface attraction and repulsion) are discussed more in depth in Section 4.2.2.

4.2 Biochar properties

In this section, the sorption strength of ULS, DSL and CWC biochars was considered in relation to the following biochar properties: surface area (SA), pore volume (PV), main elements (C, H, O, N), and trace elements (Ca and Fe). Data for PFOA, PFNA and PFDA have been used in this discussion because they exhibited the best sorption isotherms. Conducting multivariate analyses between the biochar distribution coefficients and different biochar property parameters was desirable, but would not have been statistically valid due to the fact that there were only 3 samples (zero degrees of freedom). However, a brief discussion and respective correlation plots for C, Ca, and Fe have been added to Appendix E. Further discussion on the effects of biochar properties on sorption will be limited to discerning trends with SA, PV, carbon, calcium, and iron..

Table 4.2: Surface area (SA), pore volume (PV), element content (C, O, H, N), and ratios for the biochars evaluated in the laboratory experiments.

Biochar sorbent	CO$_2$ sorption (pores 0.4-1.5 nm)		N$_2$ sorption (pores >1.5 nm)		Elemental content				Element ratio		
	DFT SA (m^2/g)	DFT PV (cm^3/g)	BET SA (m^2/g)	BJH PV (cm^3/g)	C (%)	O (%)	H (%)	N (%)	O/C	H/C	N/C
CWC	683	0.186	323	0.017	91.4	5.50	1.01	0.69	0.06	0.01	0.008
ULS	165	0.047	128	0.126	29.6	57.1	1.24	1.13	1.9	0.04	0.04
DSL	87	0.027	110	0.111	13.5	61.4	1.05	0.82	4.6	0.08	0.06

4.2.1 Surface area and pore volume

Total surface area (SA, m^2/g) and pore volume (PV, cm^3/g) for the three biochars used in the sorption experiments in this study are provided in Table 4.2.

Pore size distribution between 0.4-1.5 nm

For pores between 0.4-1.5 nm, surface area (SA) of CWC biochar (683 m^2/g) was ~six times higher than that of ULS and DSL biochars (165 and 87 m^2/g, respectively). CWC biochar also had the highest pore volume (PV) 0.186 cm^3/g, followed by ULS (0.047 cm^3/g), and DSL biochars (0.027 cm^3/g). High internal SA and PV are desirable for strong sorption of organic contaminants (Ahmed et al., 2020; Hale et al., 2016). These increase available sorption sites and pore-filling capacity (Rajabi et al., 2021). The high SA and PV of CWC biochar suggested that CWC biochar had the highest fraction of active sites and the highest pore-filling capacity as compared to ULS and DSL biochars within the micropore range ($\leq$ 2 nm). However, the distribution of pores between 0.4-1.5 nm shown in Figure 4.4, makes clear that nearly 80% of the SA, and 60% of the PV in CWC biochar were located in pores that were smaller than 0.6 nm. These pores are referred to as ultra micropores (Bardestani et al., 2019). To find out whether PFCAs can be absorbed into these ultra micropores, determining the molecular size of the adsorbates is important. Table 4.3 lists effective cross-sectional diameter (D_{eff}) and maximum diameter (D_{max}) of each PFCA (the definitions of D_{eff} and D_{max} are illustrated in Figure 4.5). PFCAs C5-C10 range from 0.45-0.72 nm (D_{eff}) to 0.96-1.54 nm (D_{max}). This means that most pores ($<$ 0.6 nm) were inaccessible to the PFCA molecules (Yu et al., 2009). The perfluorinated chains of PFAS molecules are large and rigid. Therefore, pores that are too small make it difficult for the compounds to adjust their shape to the pore walls in order to be able to come close enough to sorb to the biochar surface. This also means that chains that are too long to enter a pore can get stuck in a cross-sectional position, preventing diffusion of more sorbates.

Maximum sorption is achieved when the molecular dimensions of PFAS match the pore size and shape of the sorbent (Hale et al., 2016). Since the distribution of pores between 0.4-1.5 nm was dominated by ultra micropores, sorption of PFPeA, PFHxA, and PFHpA was only possible *if* the congeners entered the pores at the exact right angle. PFOA, PFNA, and PFDA experienced size exclusion as their molecules were too large in any direction. This means that sorption of PFCA in pores smaller than 1.5 nm was insignificant and could not explain the differences in sorption between biochar feedstocks, especially since strongest sorption was measured for long-chain PFCAs.
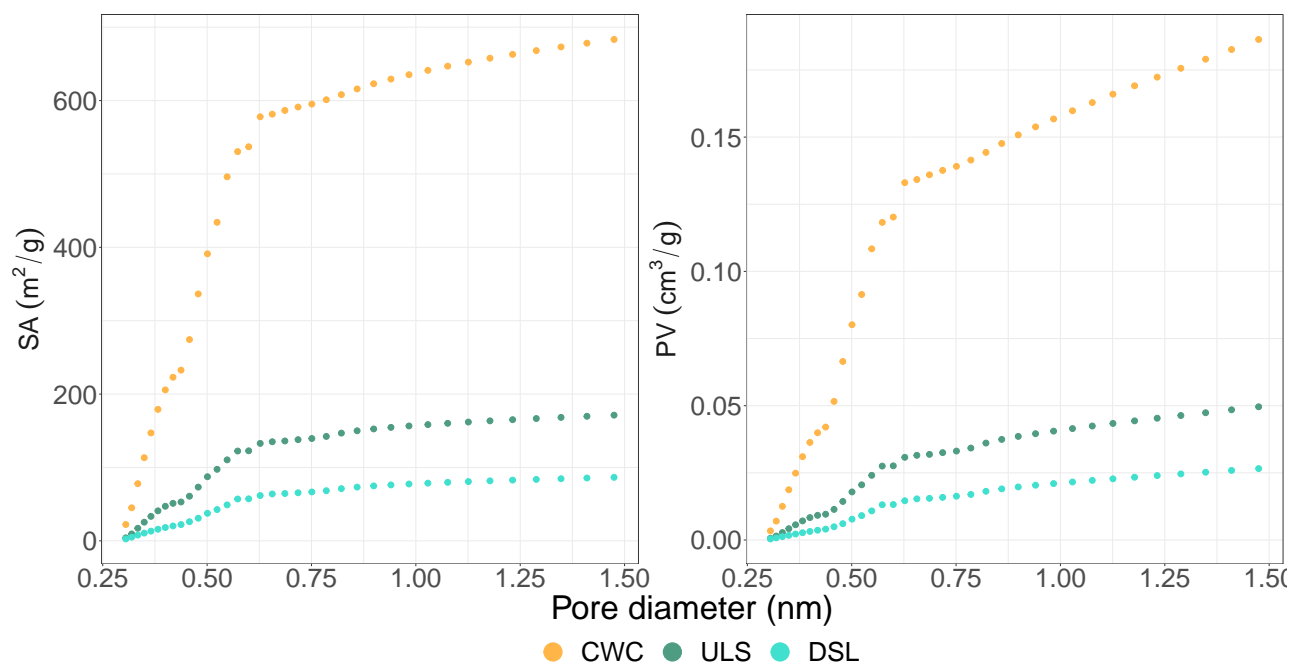
Figure 4.4: Cumulative pore size distribution for 0.4-1.5 nm-sized pores using DFT with (a) surface area (SA) and (b) pore volume (PV).

Pore size distribution for pores >1.5 nm

CWC biochar had the largest cumulative SA (323 m^2 g^{-1}), but the lowest PV (0.017 cm^3 g^{-1}) for pores >1.5 nm. ULS biochar had slightly larger SA than DSL biochar (128 versus 110 m^2 g^{-1}), as well as a slightly larger PV (0.126 versus 0.111 cm^3 g^{-1}). The pore size distributions plotted in Figure 4.6 show remarkable differences in the distribution of SA and PV with increasing pore diameters between CWC biochar and the sludge biochars. For CWC biochar, SA and PV are almost exclusively allocated to pores between 1.5-3 nm. By contrast, SA and PV for the ULS and DSL biochars increase steadily up to a maximum pore size of 35 nm. The difference in porosity between CWC biochar and the sewage sludge biochars can possibly explain why the sewage sludge biochars had higher sorption strengths than CWC biochar.

Table 4.3: Effective cross-sectional diameter (D_{eff}) and maximum diameter (D_{max}) of TCs interpolated and extrapolated by linear regression from calculations performed by Inoue et al. (2012) on PFOA and other PFCAs with chain lengths 11-18.

Compound	Chain length	D_{eff} (nm)	D_{max} (nm)
PFPeA	5	0.45	0.96
PFHxA	6	0.50	1.08
PFHpA	7	0.56	1.19
PFOA[*]	8	0.61	1.36
PFNA	9	0.67	1.42
PFDA	10	0.72	1.54

[*] Value from Inoue et al. (2012)
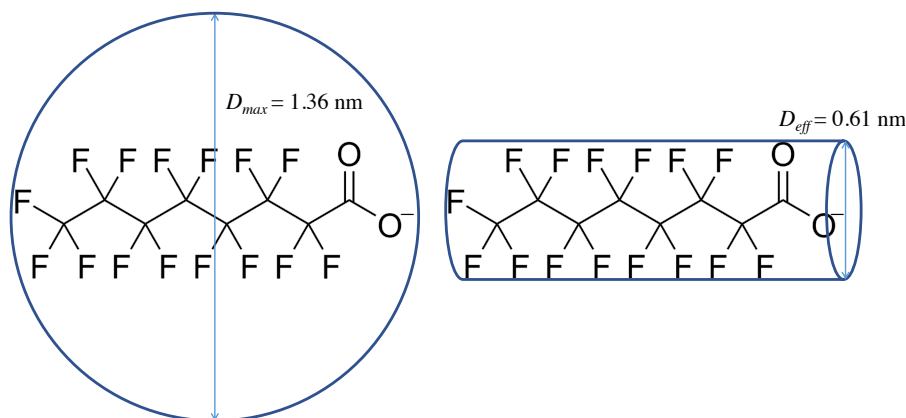
Figure 4.5: Effective cross-sectional diameter (D_{eff}) and maximum diameter (D_{max}) of PFOA.

Apart from SA and PV, carbon content has, in previous literature, been a good predictor of sorption affinity to PFAS (Hale et al., 2016; Cornelissen et al., 2005). Since ULS biochar had only slightly larger porosity compared to DSL biochar (Figure 4.6), the higher carbon content in ULS biochar (30 % versus 14 %) than DSL biochar indicates that more hydrophobic interactions were possible for ULS biochar. The difference in carbon content between ULS and DSL biochars is the most plausible explanation for why ULS biochar sorbed better than DSL biochar.

Three important conclusions can be drawn from this information: 1) CWC biochar had pores that were predominantly too small to accommodate PFCA, 2) CWC biochar had much lower PV for pores >1.5 nm, and this greatly restricted pore-filling mechanisms, and 3) ULS biochar had a higher PV, SA and C-content than DSL biochar. This probably explains why 1) ULS biochar was a better sorbent than DSL biochar, 2) high porosity and sufficiently large pores were the two most important parameters responsible for high sorption capacity, and 3) a carbon-rich pore wall enhanced sorption by increasing hydrophobic interactions.

The higher sorption of PFCAs to the ULS and DSL biochars stands in contrast to findings in previous literature that consistently report that a higher carbon content is a good predictor for increased sorption (Fabregat-Palau et al., 2022). However, previous PFAS sorption studies have been conducted on activated biochar and charcoal, more carbon-rich and porous feedstocks than biochar from sewage sludge (Sørmo et al., 2021; Zhang et al., 2021). Despite lower carbon contents in the ULS and DSL biochars, this study supports previous literature that concluded that the importance of electrostatic interaction to sorption is secondary to the hydrophobic effect.

4.2.2 Biochar surface chemistry

Surface hydrophobicity and degree of carbonization can be described by the oxygen to carbon (O/C), hydrogen to carbon (H/C), and nitrogen to carbon (N/C) ratios (Chun et al., 2004). The O/C ratio of CWC (0.06) was within the same range as other non-activated biochars pyrolyzed at 700°C (Lehmann and Joseph, 2015; Chun et al., 2004; Kupryianchyk et al., 2016a). By contrast, the high oxygen content of DSL and ULS (61.4 and 57.1 % respectively) resulted in higher O/C ratios (4.6 and 1.9) respectively (Table 4.2). The difference between the O/C ratio
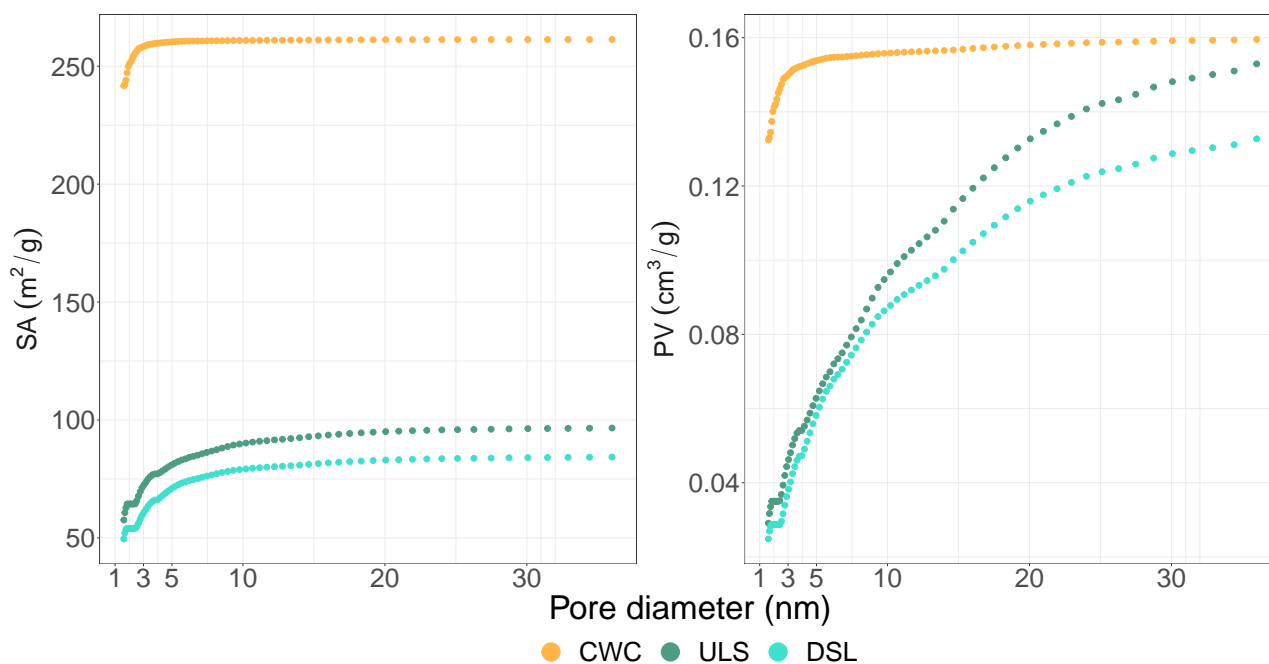
Figure 4.6: Cumulative pore size distribution for pores > 1.5 nm using DFT theory with (a) surface area (SA) and (b) pore volume (PV).

<1 for CWC compared to ratios >1 for ULS and DSL indicate a significantly different degree of carbonization between the two feedstock types. At the same time, H/C ratios for all three biochar feedstocks were similar, and were within the same range reported in previous literature (Chun et al., 2004; Kupryianchyk et al., 2016a).

Some studies have found that a higher O/C and N/C ratio—indicative of more polar functional groups (hydroxyl, carbonyl, metal-containing groups, amines and amides)—are beneficial for PFAS sorption (Du et al., 2014; Fabregat-Palau et al., 2022). Researchers suggest several sorption mechanisms related to the surface polar groups that may contribute to enhanced sorption. Basic functional groups such as amines have high pK_as and are protonated at environmentally relevant pH levels, providing anion exchange capacity and electrostatic attraction to the carboxylic acid heads (Deng et al., 2010). Basic sites in π-electron-rich, carbon-rich materials are important for PFAS sorption (Saeidi et al., 2020). N/C ratios for ULS and DSL biochars were one order of magnitude higher than for CWC biochar. A high nitrogen/carbon (N/C) ratio can be indicative of more amine groups in the periphery of the condensed carbon structure. The positive charge on several nitrogen-containing functional groups can interact electrostatically with the PFCA carboxylate group. In addition, it is possible that they also engage in weak, non-specific electrostatic interactions with the negative dipole of the CF-chain (Xiao et al., 2011). The latter mechanism could explain the positive chain-length dependency on sorption seen for sewage sludge biochars (Figure 4.3). Sewage sludge contains a mixture of proteins and inorganic nutrients that will denaturate in some form during thermal treatment. To the author's knowledge, no data exists on how speciation of nitrogen changes during pyrolysis. Even though a higher N/C ratio is only an indication for nitrogen functional groups, the presence of amines is likely.

In this study, highest sorption was seen for the biochars that had the highest composition of elements other than C, O, H, and N. CWC biochar contained only 1.4% of other elements,

Table 4.4: Mean pH (± standard error) measurements for the different batch test slurries (n=3) where S is soil and BC/S/L is the biochar:soil:liquid ratio.

Biochar	pH	BC/S/L
ULS	7.10 ± 0.03	1/0/500
DSL	7.31 ± 0.01	1/0/500
CWC	7.36 ± 0.04	1/0/500
ULS+S	7.18 ± 0.01	1/50/500
DSL+S	7.14 ± 0.00	1/50/500
CWC+S	7.09 ± 0.03	1/50/500
S	7.08 ± 0.03	0/1/10

whereas the sludge biochars, ULS and DSL, contained substantially more (10.9% and 23.2% respectively). A table with the total biochar elemental composition is given in Appendix D. Some of these elements are commonly found as freely dissolved ions. Since dissolved ions were not analyzed, we can only assume that, by and large, the alkalis (K and Na), and earth alkalis (Mg and Ca), are present as dissolved cations that originate from the biochar ashes. It is likely that Fe is predominantly incorporated in the biochar matrix. Iron speciation will be further discussed in Section 4.2.2. The higher content of other elements than C, H, O, and N in ULS and DSL biochars suggests that sorption of PFCAs onto the sludge chars were likely influenced by the presence of charged species, both in the solution, as well as on the biochar surface. Coexisting inorganic ions complicate the sorption behavior of PFCAs because sorption can both be suppressed and enhanced by different electrostatic mechanisms (Du et al., 2014). This will be further discussed below.

The relationship between solution and biochar surface chemistry

Solution chemistry, pH, and the composition of elements other than C, O, H and N, may provide further insight into how the pore walls of CWC, ULS and DSL biochars differ from one another, as well as how these elements can influence sorption. pH varied little across sample types with an average pH of 7.18 ± 0.02 (Table 4.4). Therefore, pH levels for the biochar-water batch tests slurries have only been used to discuss expected surface charges. Surface charges for biochar are pH-dependent, and are usually negatively charged at neutral pH (Zhang et al., 2013). However, point-of-zero charge measurements for the biochars did not become available in time for incorporation into this discussion. Therefore, a net negative biochar surface is assumed, but was not confirmed (Saeidi et al., 2020). By contrast, the protonation state of the carboxylic functional group of PFCA is not pH dependent at environmental pH levels due to the strong electron-withdrawing fluorine atoms (Goss, 2008).

Sorption can be suppressed by electrostatic repulsion of the carboxylate group on PFCA by the negatively charged biochar surface, or by competitive sorption of anions to positive BC sites (Sigmund et al., 2022). Electrostatic repulsion can contribute to the weaker sorption observed for the shorter-chain PFCAs in this study (Table 4.1). The repulsion effect becomes weaker for the longer-chain PFCAs where the hydrophobic effect becomes more dominant. Electrostatic repulsion is reduced at lower pH because more negative biochar-sites are protonated, and thereby neutralized (Zhang et al., 2013). This allows for a PFCA anion- π-bond interaction with biochar (Sigmund et al., 2022). Sorption can be enhanced through electrostatic attraction to

Table 4.5: Composition of a selection of elements in the biochar samples in g/kg.

	Ca	Fe	K	Mg	Na	P	S	Si
CWC	8	0.1	4.0	0.9	0.05	0.4	0.09	0.2
DSL	26	180	3.7	4.7	1.8	8.0	7.2	0.6
ULS	21	23	6.8	5.3	2.4	45	2.9	1.7

positively charged biochar functional groups, and by divalent cation bridging (Du et al., 2014). Cation bridging is the electrostatic linking of negatively charged PFCAs to negatively charged biochar surfaces by means of a divalent ion that acts as a "bridge" between them (Sigmund et al., 2022). Ca^{2+} and Mg^{2+} are common divalent ions present in biochar ash that contribute to bridging.

The concentration of Ca^{2+} and Mg^{2+} was three to six times higher in the sludge biochars than in CWC biochar (Table 4.5. Correlation plots between K_d and Ca-content are provided in Appendix E, Figure E.4, but have not been further elaborated on in the main discussion due there being only three biochar samples.

Bridging has been shown to be an important sorption mechanism in, for example, sediments, mineral materials, and black carbon (Higgins and Luthy, 2006). Apart from bridging between the BC surface and PFAS functional groups, divalent ions can chain individual PFAS molecules together (Wang and Shih, 2011). This creates an even more hydrophobic complex that can sorb more strongly to biochar. For this reason, more frequent formation of divalent cation bridges for the ULS and DSL biochars is expected. Although sorption *capacity* has not been measured directly, the above mechanisms for PFAS interaction with charged and polar functional groups may be a contributor to the higher sorption found for the more heterogeneous, mineral-rich matrices of sewage sludge biochars.

The positive correlation between log K_F and chain length for all three biochars (Figure 4.3) in this study indicates that electrostatic interactions play a minor role for sorption to these biochars. If electrostatic interactions played an equally important role as hydrophobic interactions, sorption across differing PFCA chain lengths would be more similar.

Iron speciation

Due to a lack of corresponding reference compounds for some of the EXAFS signals, no satisfying fit was obtained for the iron species present in sewage sludge biochar samples. This suggests that iron is not only present as iron oxides. The Fe K-edge XANES spectra (Figure G.1) and EXAFS spectra (Figure G.2) show that DSL and ULS are similar in valence and speciation. They consist mainly of reduced forms of Fe (Fe(II)), and DLS is slightly more reduced than ULS. Total Fe concentration is especially high for DSL (180 mg/kg, Table 4.5), making up as much as 18% of its matrix (3.3% and 0.01% for ULS and CWC respectively). The Fe concentration will therefore significantly affect the surface morphology of DSL. PFAS has been shown to form inner-sphere complexes via covalent metal-ligand bonds (Fe-carboxylate) by means of the following reaction (Du et al., 2014):

$$\equiv Fe - OH_2^+ \ + \ CF_3(CF_2)_nCOO^- \rightarrow \ \equiv Fe - OOC(CF_2)_nCF_3 \ + \ H_2O \qquad (4.1)$$
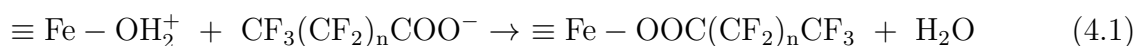
The triple bond represents chelation of Fe to the biochar matrix. Point of zero charge (PZC) for Fe(oxyhydr)oxides, such as ferrihydrite and goethite, are around 7, similar to the solution pH measured for the water-biochar systems (see Section 4.2.2). The iron species are expected to be neutral for the systems analyzed, and will likely not be one of the dominating sorption mechanisms for PFCA.

4.3   Sorption attenuation

This section discusses sorption attenuation for the different batch test categories that were prepared (Section 3.3). In this study, the same equilibrium concentrations were not achieved across all samples. Therefore, K_d-values with the same *total* concentrations were compared. Figure 4.7a shows how much K_d is suppressed by the presence of soil and/or a mixture of PFCAs at the highest spike point, SC10. A description of considerations that were taken for the determination of K_d values in soil is in Appendix E, Appendix E.2. The difference in log K_d between BC single and the other sample types is directly related to how much sorption was attenuated by the presence of soil and/or other PFCAs. As visualized by the order of the colored points, attenuation increased in the following order: BC-single (reference) > BC-soil-single > BC-mixed $\sim$ BC-soil-mixed > soil-single and soil-mixed. Attenuation factors (AF) were calculated for each category:

$$AF = \frac{K_{BC-single}}{K_{BC-x}} \tag{4.2}$$

where $K_{BC-single}$ is the expected sorption, and K_{BC-x} is the measured distribution coefficient for the mixed, soil-mixed, or soil-single batch tests. In Figure 4.7b, the AFs for PFOA, PFNA, and PFDA have been plotted for each biochar. AFs ranged from 3-10 for BC-S-PFOA, 6-140 for BC-mix, and 8-138 for BC-S-mix (Table 4.6). These factors were very high due to five other compounds having been to a total concentration of 10 mg/L. The PFCA cocktail used in batch testing consisted of 18% PFOA, 21% PFNA, and 49% PFDA (Table 3.2). Since the concentrations for each compound were different, no sorption attenuation trends with chain length were derived. It was difficult to evaluate any trends in AFs between biochar samples or PFCA chain lengths.

A comparison of attenuation factors between batch test categories gave interesting implications. Since the AFs varied widely within each category, mean and median values for each category were calculated to evaluate trends. BC-S-PFOA: mean = 6, median = 4, BC-mix: mean = 43, median = 29, and BC-S-mix: mean = 59, median = 49. Based on these statistics, attenuation for the cocktail samples were one to two orders of magnitude higher than attenuation by soil alone. The presence of soil with a cocktail caused additional attenuation of 27% ($AF_{soil} = 59 - 43 = 16$.

To the best of the author's knowledge, there are no existing attenuation factors for sewage sludge biochar to PFAS. However, these AFs are in the same range as in previous literature where it was established that sorption was attenuated by a factor of 10 for phenanthrene by means of adding other PAHs (Cornelissen and Gustafsson, 2006), 32 for a mixture of DDT (Hale et al., 2009), and 100-500 for sulfamethazine (SMT) in soil after a longer residence-time to soil Teixido et al. (2013). The high attenuation for sulfamethazine seen by Teixido

Table 4.6: Attenuation factors (AF) calculated as K_{BC_singe}/K_{BC_x} and respective log K_d-values at SC10.

Compound	type	CWC		DSL		ULS	
		log K_d	AF	log K_d	AF	log K_d	AF
PFOA	BC-mix	2.84	6	3.17	23	4.13	29
PFNA	BC-mix	2.33	109	3.03	140	4.40	29
PFDA	BC-mix	2.95	9	3.60	32	5.09	9
PFOA	BC-S-mix	2.73	8	3.24	19	3.47	134
PFNA	BC-S-mix	2.68	48	3.33	71	3.73	138
PFDA	BC-S-mix	2.91	10	3.67	27	4.16	78
PFOA	BC-S-PFOA	3.19	3	3.98	4	4.61	10

et al. (2013) is in the same order as the AFs found in the present study. Sorption of both SMT (a structure that consists of a sulfonamide functional group that links two aromatic rings with nitrogen-substitutions, methyls and an amine), and PFAS to biochar seems to be more affected by the presence of soil than does sorption of the hydrophobic organic contaminants (HOCs), phenanthrene and DDT. Though speculative, and taking into account that sorbents and conditions vary, this could indicate that HOCs can more easily penetrate the humic acid pore blockages than can PFAS and SMT. A hypothesis that could explain this is that SMT and PFAS are more similar in hydrophobicity as humic acids. This means that they share a level playing field in the competition for sorption sites. However, since humus is larger than PFAS, pores remain non-penetrable. A more extensive determination of structure-property relationships and attenuation would be needed to confirm this hypothesis.

On a final note, one cannot know if the AFs derived after 14 days study would be further reduced by increasing soil-BC-mix and BC-water-mix contact times, as was seen by Hale et al. (2009) who found that sorption of DDT was no longer attenuated by the presence of soil (AF = 1) after 26 months. Attenuation depends mainly on two factors: 1) sediment-BC contact time, and 2) concentration of the cocktail used for sorption (Teixido et al., 2013). A sorption capacity test would have to be conducted to determine if sorption sites for CWC, ULS, and DSL biochars truly were saturated and at equilibrium after 14 days. Or whether diffusion and occupation of all sorption sites would increase with increased contact time. This would be particularly interesting for the high spike-concentration batch tests, BC-mix and BC-S-mix.

4.3.1 Sorption of PFOA in the presence of soil and other PFCAs

Figure 4.8 shows the effect of attenuation on the PFOA isotherms for BC soil single, and BC soil mixed. The isotherms were spiked with the same C_i as BC single. But only six of the ten points were selected for the attenuation isotherms (Section 3.3. For all biochars, BC single has the highest sorption, followed by BC soil single, and BC soil mixed. This trend gives a good indication of the order of factors that influence attenuation, and is consistent with the results discussed in the previous section. The isotherms have similar C_s concentrations, but varying C_w, depending on sample type. Due to pore blocking and competitive sorption by natural organic matter and natural compounds, more sorbate in solution is needed to push the
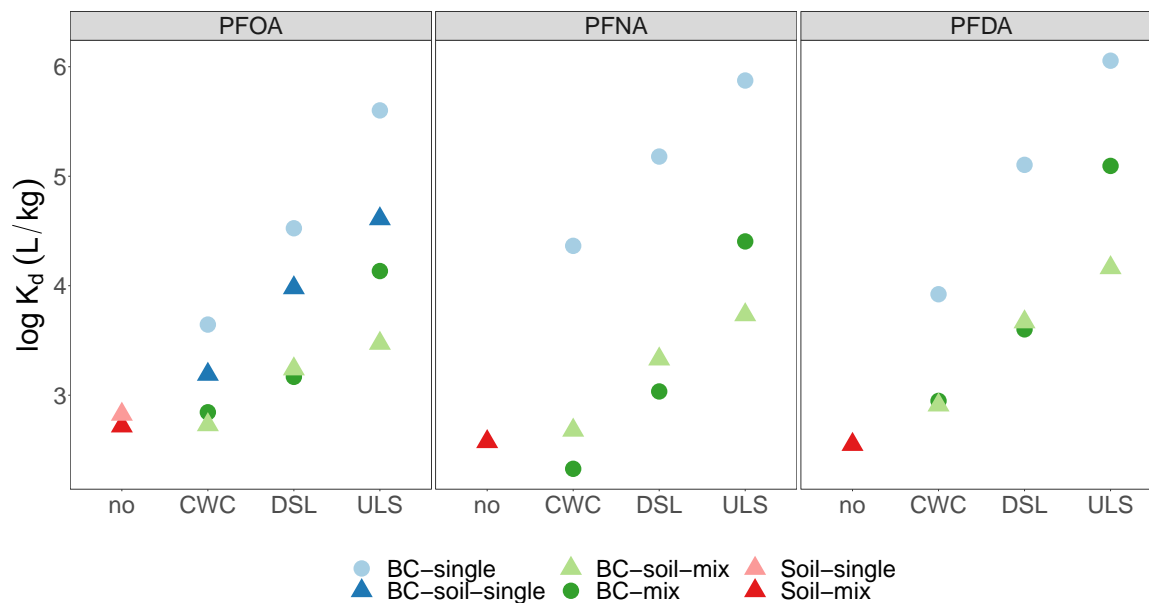
(a) log K_d for PFOA, PFNA, and PFDA spiked at SC10 (1 953, 1 409, and 3 830 μg/L respectively) for the different biochar feedstocks (CWC, DSL, ULS) and soil-only (no biochar). log K_d for BC single (light blue circles) are the predicted sorption by biochar.
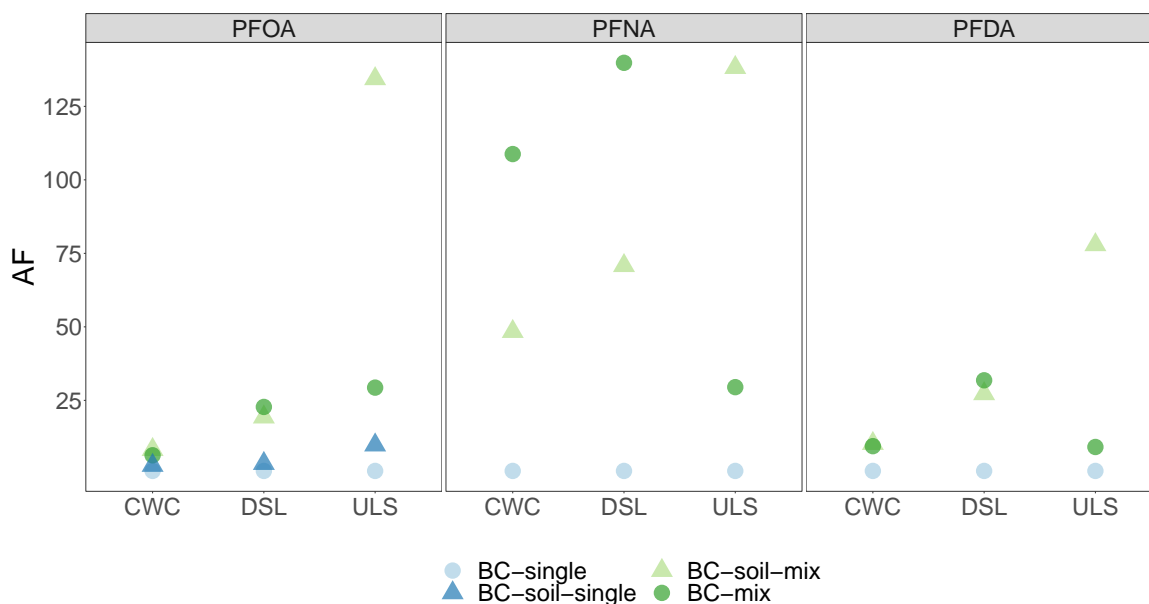
(b) Attenuation factors (AF) at SC10 for PFOA, PFNA, and PFDA calculated as $K_{d,BCsingle}/K_{d,x}$ where $K_{d,x}$ are batch test categories. See Table 3.2 for spike concentrations used for each PFCA in the single-spike and cocktail-spike batch tests.

Figure 4.7: Reduction in **(a)** log K_d at SC10 and **(b)** attenuation factors at SC10.

same number of molecules onto the solid phase in the presence of soil, an effect that can be further enhanced by the presence of both soil and a cocktail since this isotherm has the highest C_w and lowest C_s. This particular quality is due to the fact that PFCAs with longer chain lengths (PFNA and PFDA) have an advantage over PFOA when competing for sorption sites (Sørmo et al., 2021). Supported by the trends in Figure 4.7, the cocktail attenuation effect is more significant than attenuation by soil. Parallel isotherms mean that attenuation is the same across the whole concentration range, as, for instance, between BC-single and BC-soil-single for ULS. For some isotherms, attenuation is minimal at low concentrations and increases with increasing spike concentration. This is the case for the DSL isotherms, and can be explained by the non-linear sorption at higher concentrations. So, when spike concentration increases, sorption attenuation also increases.

Siriwardena et al. (2019) measured attenuation factors for PFOA to two granulated activated carbons (GAC), one coal-based and one coconut-based. GAC is an adsorption media with extremely high internal surface area. It is produced from organic material such as coconut shells, coal, peat, or wood. In the presence of the co-contaminants, kerosene, ethanol, and trichloroethylene, the coal-based carbon had an AF of 3.3 and the coconut-based carbon had an AF of 1.7. The cumulative initial concentration used was 4.1 mg/L, half the total concentration spiked in the present study. AFs of 23 and 29 for PFOA, in BC-mix for DSL and ULS respectively, (Table 4.6) are slightly higher than those found by Siriwardena et al. (2019).
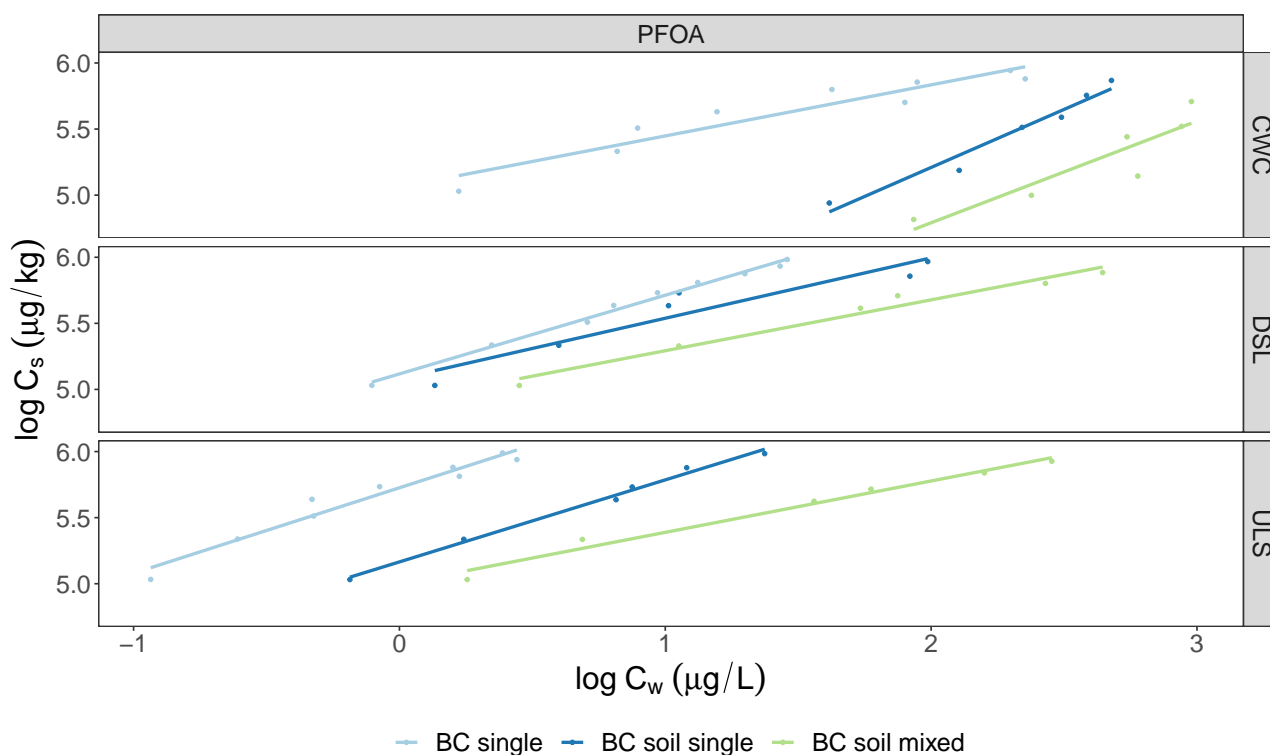
Figure 4.8: Sorption isotherm comparison for PFOA single-compound spike in biochar (BC single), single-compound spike in soil-biochar (BC soil single), and PFOA spiked in a cocktail in soil-biochar showing attenuation by soil and competing congeners.

4.3.2 Freundlich sorption non-linearity

The non-linear sorption isotherms for PFOA in Figure 4.9 show how sorption is attenuated at higher concentrations, and how attenuation changes in the presence of soil and soil with other PFCAs. The resulting Freundlich coefficients (log K_F and n_F) for PFOA are given in Table 4.7, and the remaining compounds are in Appendix ETable E.2. Two general conclusions can be drawn from these figures: 1) attenuation is higher in the presence of soil, and even higher when soil and cocktail are added together. And 2) the concentration intervals for some of the isotherms were too narrow (average Δ log $C_w = 1.3$) to properly determine representative Freundlich coefficients for a wider concentration range. Therefore, conversion of log K_F to either higher or lower units can be expected to be associated with greater uncertainty.

Both concentration intervals and n_F should be considered together in order to predict the sorption capacity of biochars. Figure 4.10 shows the non-linear BC-single isotherms for PFOA, PFNA and PFDA, where the degree of non-linearity is more easily visualized than the n_F-values alone. For example, Figure 4.10 shows that the CWC biochar isotherms have more attenuation than DSL and ULS biochars, and that C_ws have measurements across a wider concentration range. These findings are consistent with lower log K_Fs found for CWC. Figure 4.10 also shows that the isotherms for PFNA-DSL and PFNA-ULS are nearly linear, and span aqueous concentrations only within the same order of magnitude. Higher spike concentrations, or lower BC dosages, should have been used to get isotherms that cover the regions of attenuated sorption for these biochars and compounds. What is significant is that this suggests that sludge biochars have higher sorption capacities than CWC.

The concentration range achieved for C_w for the sorption isotherms was an average of 1.3 log units, in contrast to the desired concentration range over 4 log units. Poor signals were achieved for the SC1 points, and as a result were removed from the data analysis. This resulted in the spike concentration interval being reduced to two orders of magnitude (Table 3.2). In retrospect, spike concentrations at each log unit should have been selected instead of spreading the ten concentrations evenly across the concentration range. The CWC isotherms had the widest concentration intervals for C_w. This can be accounted for by the fact that CWC is the weakest sorbent of the three biochars studied.

Electrostatic interactions between PFCAs and sediment can contribute to enhancing saturation of adsorption sites as well as intermolecular electrostatic repulsion between individual molecules (Higgins and Luthy, 2006; Yin et al., 2022). Yin et al. (2022) presents two main explanations for why sorption of PFCAs to biochar is non-linear: 1) successive saturation of adsorption sites, and 2) the complex composition of biochar with negative, positive and neutral charges within same matrix.

4.3.3 Attenuation by organic matter

Colored filtrate and humus aggregation seen during analysis of the soil batch tests indicate that sorption of organic matter (OM) to biochar is likely (see Section 3.3. Large humic acids (300-600 nm) clog the pores, preventing diffusion of PFAS (Cornelissen and Gustafsson, 2006; Klučáková, 2018). Furthermore, the size of the organic molecules is a critical factor, as humic molecules, whose size is similar to that of PFAS, represent the greatest competition to PFAS in terms of diffusion (Du et al., 2014). By the co-existence of OM and dissolved organic carbon (DOC), sorption attenuation occurs by a combination of competitive and weaker sorption of

Table 4.7: Freundlich distribution coefficients and standard errors for the PFOA isotherms. Freundlich coefficients for the soil samples are the collective distribution coefficients for soil and biochar because K_d for soil alone was not accurate enough. All K_F data are in units of $(\mu g/kg)/(\mu g/L)^{n_F}$.

Compound	Biochar	type	log K_F	n_F	r^2	p
PFOA	CWC	BC-S-mix	3.25 ± 0.48	0.77 ± 0.18	0.82	*
PFOA	CWC	BC-S-sing	3.45 ± 0.21	0.88 ± 0.09	0.96	**
PFOA	CWC	BC-sing	5.06 ± 0.08	0.39 ± 0.05	0.90	***
PFOA	DSL	BC-S-mix	4.91 ± 0.06	0.39 ± 0.03	0.97	***
PFOA	DSL	BC-S-sing	5.08 ± 0.10	0.46 ± 0.08	0.90	*
PFOA	DSL	BC-sing	5.12 ± 0.02	0.60 ± 0.02	0.99	***
PFOA	ULS	BC-S-mix	5.00 ± 0.05	0.39 ± 0.03	0.98	***
PFOA	ULS	BC-S-sing	5.16 ± 0.03	0.62 ± 0.03	0.99	***
PFOA	ULS	BC-sing	5.73 ± 0.02	0.65 ± 0.05	0.95	***

Significant codes: *** ~ 0.001, ** ~ 0.01, * ~ 0.05
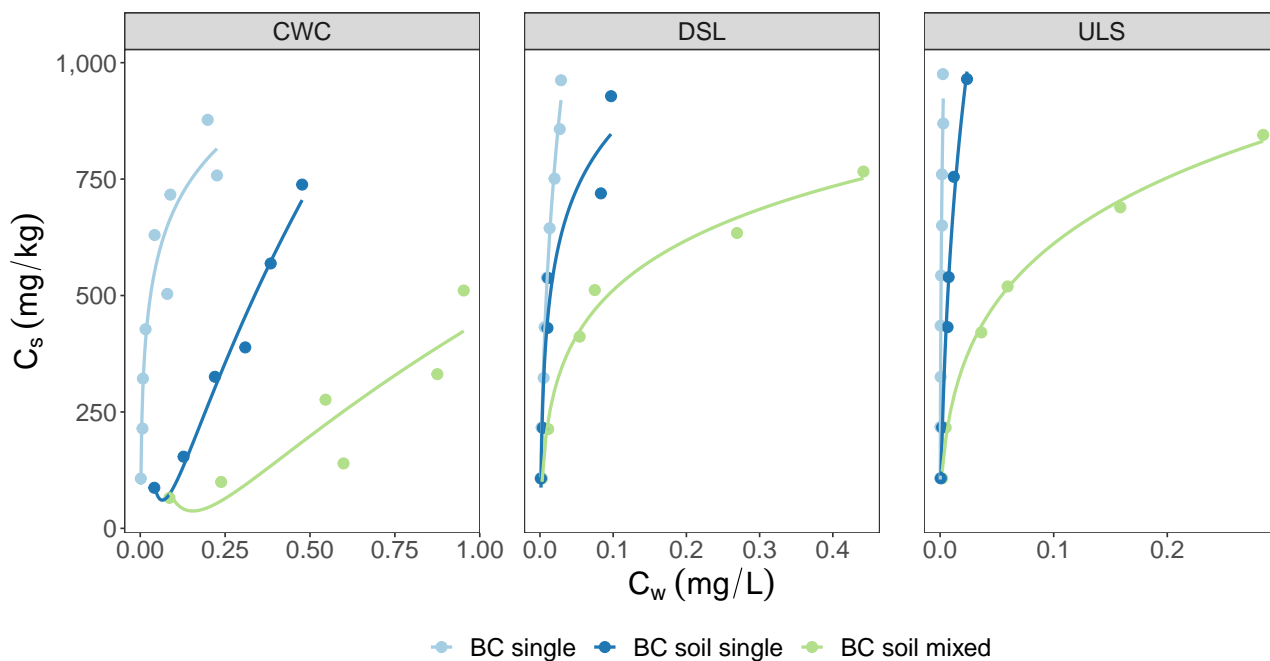
Figure 4.9: Non-linear sorption isotherms for PFOA in the BC-single, BC-mixed and BC-soil-mixed batch tests. Lines are fitted by a polylogarithmic function.
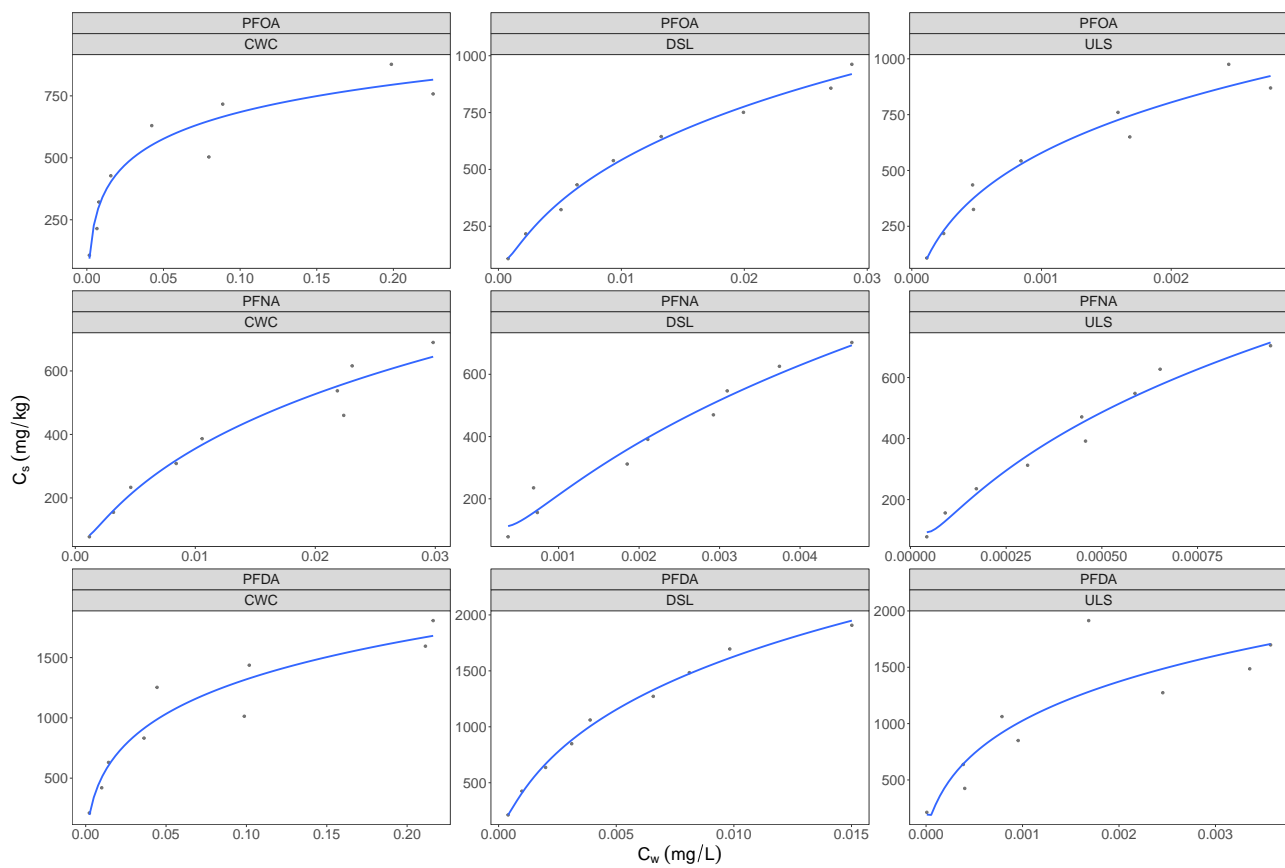
Figure 4.10: Plots showing sorption attenuation by the presence of other PFCAs with increasing spiked concentrations. Lines are fitted by a polylogarithmic function.

PFAS to OM and DOC, and the competitive sorption of OM to biochar. PFAS binds to OM, and it is possible that PFAS also binds to the dissolved fraction of OM (DOC). Since DOC is sorbed it is thus possible that there is sorption of DOC-PFAS complexes. Given that DOC-assisted PFAS sorption has yet not been proven, and investigating size fractionation for humic molecules was not a part of this study, the points presented here could only take place on a theoretical level.

Chapter 5

Implications, conclusion and recommendations for further work

The data generated in this research has yielded promising results for the future use of sewage sludge-based biochar (SS-BC) as a sorbent. To begin the summary of the results obtained, the initial hypotheses that represented a point of departure for the research presented, are reiterated:

i Biochar from sewage sludge is not as effective a sorbent for PFAS as biochar produced from clean wood chips due to its lower carbon-content and porosity, though it can be used as a low-cost, lower quality-class sorbent.

ii The dominant mechanism by which PFCAs sorb to sewage sludge biochars is electrostatic attraction due to mineral-rich components.

iii Following from hypothesis (ii), sorption to sewage sludge biochars is not chain-length dependent and is due to electrostatic interactions by the negatively charged PFCA functional group, whereas sorption increases with chain length for clean wood chips due to predominating hydrophobic interactions with the more carbonaceous matrix of this biochar.

iv Sorption of PFCA to biochar is attenuated by the presence of soil and other PFCAs.

Hypotheses (i), (ii) and (iii) were rejected. Hypothesis (i) was falsified by discovering that the SS-BCs tested in this research were *better* sorbents for PFCAs than biochar from clean wood chips (CWC). Log K_F, in units of $(\mu g/kg)/(\mu g/L)^{n_F}$, were in the range 5.73-6.00 for ULS biochar, 5.12-5.61 for DSL biochar, and 5.06-5.22 for CWC biochar for PFOA, PFNA, and PFDA (Table 4.1). Despite the fact that CWC biochar had the largest surface area, the majority of its pores were too small to accommodate PFAS. The higher fraction of mesopores (2-50 nm) in the sewage sludge biochars compared to those found in clean wood chips (CWC) probably explains why the SS-BCs turned out to be such effective sorbents. Furthermore, better sorption to ULS biochar was explained by a higher carbon content (30%) than that of DSL biochar (14%).

Hypothesis (ii) was rejected by the observation of higher log K_d's (at $C_w = 1\mu g/L$) with increasing perfluorinated chain length for all biochar feedstocks (Figure 4.3). Since no apparent correlations were found between Ca or Fe-content and log K_d, electrostatic interactions are likely not the primary sorption mechanism for the SS-BCs. Since strongest sorption was

measured for the biochars with higher porosity and carbon content, hydrophobic interactions is likely the dominant sorption mechanism for PFCAs to the SS-BCs. Although mechanisms responsible for the stronger sorption of ULS and DSL were proposed, these could not be fully verified due to the limited sample size of only three biochars.

The conclusions drawn from hypothesis (ii) are directly linked to hypothesis (iii) which was also rejected for the same reasons. The poor Freundlich sorption isotherm correlations acquired for the short-chain PFCAs (PFPeA, PFHxA and PFHpA) supports the chain length-dependency of PFCAs to ULS, DSL, and CWC biochars. This relationship suggests that sorption of PFCA to SS-BCs was mainly governed by hydrophobic interactions between the C-F chain and carbonaceous aromatic surfaces. Since mineral contents were high in the strong-sorbing SS-BCs, a larger sample size is needed to understand how these influence sorption strength and mechanisms.

Finally, hypothesis (iv) proved to be correct. Attenuation factors (AFs) ranged from 3-10 for PFOA in the presence of soil, 6-140 for PFOA, PFNA, and PFDA in a mixture of PFCAs, and 8-138 for PFOA, PFNA, and PFDA in the presence of soil and other PFCAs (Table 4.6). Despite large variations in AFs, the presence of other PFCAs was responsible for a stronger degree of attenuation than the presence of soil. The presence of soil in the PFCA-mixture increased attenuation by an additional 27%. This suggests that the sorbents could be more effective for filtration in waste water treatment than in soil remediation, and especially in moderately contaminated wastewater.

5.1 Application of sewage sludge biochar in the treatment of wastewater

The results from this study demonstrate that the ULS and DSL biochars bind PFCA strongly at concentrations that are many times higher than most environmental concentrations. Based on these results, some rough estimates have been made to say something about how effective the ULS and DSL biochars are for removing PFAS from wastewater in Norway. And following from this, what the commercial implications of such an application might be.

Since the sorption data generated in this study represents equilibrium PFAS water concentrations, the estimates that will be made in this section assumed no kinetic limitations during the wastewater treatment procedure, equilibrium conditions, and a water/BC ratio of 500. Linear sorption ($n_F = 1$) was also assumed for the application of fresh, unused, SS-BC to Norwegian wastewater (i.e., log K_F = log K_d) because the wastewater concentrations that will be discussed here are two orders of magnitude below the lowest spiked concentration for the isotherms. The BC-soil-mix isotherms were chosen because one can expect attenuation when they are applied to the treatment of wastewater.

The example presented here is an estimate of the removal efficiency of PFOA from Norwegian wastewater. log K_d for ULS and DSL biochars to PFOA were 5.00 and 4.91 respectively. Based on samples obtained by a Norwegian survey conducted in late 2020 (Gabriela Castro Varela, NTNU, unpublished data), Norwegian wastewater treatment plant influents contain total levels of PFAS between 0.1-1 μg/L. To be conservative, the following estimate is based on a PFOA concentration of 1μg/L. Distribution coefficients for ULS and DSL biochars of 5.00 and 4.91, and an initial PFOA concentration of 1μg/L. This would result in a potential reduction of

PFOA from wastewater by 99.5 and 99.4%, which equate to remediated wastewater PFOA concentrations of 0.005 and 0.006 μg/L. These concentrations are between the annual average environmental quality standard (AA-EQS) in freshwater of 0.00065 $\mu g/L$ and the maximum acceptable concentration (MAC-EQS) of 32 $\mu g/L$ for PFOS set by the EU Water Framework Directive (Council of the European Union, 2013). It is worth noting that, the Danish limit of 0.002 $\mu g/L$ PFOA, PFOA, PFNA, and PFHxS for safe drinking water would not be reached (Danish Environmental Protection Agency, 2021). Clearly, ULS and DSL biochars have the potential to be effective in reducing PFAS levels significantly. But more work is needed to ensure that safe PFAS levels will be obtained.

Equilibrium aqueous concentrations measured at higher concentrations say something about the sorption capacities of the ULS and DSL biochars, and can therefore give an indication of how long carbon filters used for wastewater treatment can be expected to reduce PFAS concentration to an acceptable level. As is widely accepted, and supported by the findings of this thesis, sorption to biochar is weaker (attenuated) at higher contaminant concentrations. Due to the kinetic aspects of the sorption process, the following assessment is only *indicative* of filtration capacity as there are differences between a batch test with a spiked concentration, and the steady flow of a lower concentration. Using the same assumptions underlying the previous example, but now with an initial PFOA concentration of 1.9 mg/L in a total PFCA cocktail concentration of 10 mg/L, 85.5 and 77.7% would be retained by ULS and DSL respectively, versus >99% at 1 μg/L. The sorption capacity of ULS and DSL biochars at this point would result in equilibrium aqueous PFOA concentrations of 0.28 and 0.44 mg/L—post-treatment levels that would be unacceptable. Hence, the filter would need to be exchanged before this point. Tests that account for wastewater residence time, flow rate, bed volumes, and sorbent dose, are factors that would need to be considered in order to design a water purification solution that uses SS-BCs, and is beyond the scope of the present study.

5.1.1   Considerations for commercializing sludge chars as sorbents

The sorption strength of sewage sludge biochars was tested in a controlled laboratory environment, with low-TOC soil, and artificially spiked PFCAs. The results from this research do not, therefore, take into account the heterogeneity of sewage sludges, variations in the organic matter contents of soils that the sorbents will potentially be applied to, and the potential competition for sorption sites from a range of other possible contaminants in soil and water in need of remediation. All of the variables mentioned above will influence the sorption strength of SS-BCs.

Since the results from this study showed poor sorption affinity to PFPeA, PFHxA, and PFHpA, consideration should also be given to ensure that short-chain PFASs do not slip through wastewater treatment systems that use SS-BC. For this reason, Lindum considers the application of SS-BCs more as a pre-treatment sorbent, to be followed by treatment using a stronger sorbent that is more effective in retaining short-chain PFAS. Also important to consider is the potential risk of residual contaminants in biochars produced from contaminated feedstocks.

5.2   Revenue estimates for commercial production of sewage sludge biochar

The following is a case example that gives a rough idea of the revenue potential of a scenario in which 100 % of the activated carbon used for wastewater treatment is replaced with SS-BC. VEAS, a Norwegian WWTP, purchases 2 tonnes of AC annually for wastewater treatment. Market prices for AC range from 600 - 1,000 €/tonne. For VEAS, replacing AC with SS-BC would result in annual savings from 200 - 1,000 €, equivalent to a cost reduction of 17-50%. This assumes that SS-BC has a starting price of 500 €/tonne.

A second case presents a prime example of a circular economy scenario. Wastewater from Ullensaker WWTP, the project partner that provided the ULS sludge analyzed in this thesis, contains 3.8 μg/L (Varela, unpublished). This is the highest level of PFAS concentration found among the six Norwegian WWTPs monitored. High concentrations of PFAS at the Ullensaker WWTP have been attributed to the use of aqueous film forming foam at a nearby firefighting training facility (Hale et al., 2017). In this scenario, Ullensaker WWTP adapts pyrolysis technology that can produce biochar from the high PFAS-level wastewater they are paid to remediate. The resulting ULS biochar is applied directly as a PFAS sorbent to wastewater. With an influent total PFAS concentration of 3.8 μg/L in Ullensaker wastewater, linear sorption can be assumed. Based on the BC-S-mix isotherm used in this study, log $K_d s$ for ULS biochar are 5.00, 5.22, and 5.62 for PFOA, PFNA, and PFDA. reduces water concentrations to <20 ng/L (>99.5%). Applying this solution at the Ullensaker WWTP site would mean eliminating transportation-related costs. In addition, SS-BCs have low production costs that are estimated to be 100 €/tonne. If SS-BCs can be produced for 100€/tonne, and sold for 500 €/tonne, the revenue from pyrolyzing all sewage sludge in Norway would be 3,600,000 €/year = 36 million NOK annually.

In summary, there appear to be several benefits associated with replacing AC with SS-BC: 1) PFAS present in wastewater can, for all intents and purposes, be eliminated by pyrolysis. Preliminary data from one of the partners in this study shows reductions from 90-95% (Erlend Sørmo unpublished), 2) biochar that previously contained PFAS can now be applied to sorb even more PFAS-contaminated sludge right at the production site, 3) reduced annual expenses for the purchase of currently available commercial sorbents, and 4) WWTPs can increase their profitability and at the same time contribute to carbon sequestration. A rough calculation of the carbon sequestration potential of SS-BCs has been made and is presented in the following section.

5.3   Carbon sequestration potential

Since a commercial trade in carbon credits has opened up, the potential sale of SS-BCs at a global scale could be highly attractive. Assuming that SS-BC replaces the entire annual demands for AC in Norway and Europe, it is possible to make a rough estimate of the carbon sequestration potential of SS-BCs. Carbon dioxide equivalents (CO_2-eq) can be calculated, where one $CO_2 - eq$ is the equivalent of one tonne of sequestered CO_2. Annual demands for AC in Norway are approximately 1,700 tonnes/year, and 165,000 tonnes/year for Europe as a whole (Schmidt et al., 2019). On average, sewage sludge biochars contain 20% carbon (C), of which 70-80 % is assumed to be stable over time (Schmidt et al., 2019). This is equivalent to

1,000 and 100,000 annual CO_2-eq for Norway and Europe respectively. Considering the current EU CO_2 trading price of 90 €/CO_2-eq, this translates into annual carbon credit values of 90,000 and 8,800,000 €. Biochar could be one of the areas that help countries meet their commitments to reducing the amount of C02 released into the atmosphere

For the production of the 1,700 tonnes of SS-BC needed annually to replace AC, assuming 30% yield, a mere 7% of the 200,000 tonnes w.w. (30,000 d.w.) of sewage sludge generated in Norway each year would be needed. This fraction could be much higher if soil remediation can also be done using SS-BC as well as the application of SS-BC as fertilizers in agriculture. For Norway, pyrolysis of all sewage sludge would result in 120,000 €/CO_2-eq, and 10.6 million €carbon credits annually. However, to realize such an expansive future vision, much more research is needed.

Despite a wide range of both technical and legislative challenges, a great deal of research is currently being done to corroborate initial research which suggests that nearly all microplastics, heavy metals, and organic pollutants, including PFAS, are either combusted or immobilized at high pyrolysis temperatures (Sørmo, unpublished). In a best-case-scenario, the 93% of sewage sludge remaining after sorbent production could still be pyrolyzed into BC, and used, for example, in place of bio-based fertilizers in agriculture. *Raw* biosolids contain microplastics, heavy metals, and various organic pollutants. These same masses can potentially be safely applied to agricultural fields *after* pyrolysis. In addition, pyrolyzed sludge could prove to increase soil fertility more effectively than non-pyrolyzed biosolids. Not only would this represent increased carbon sequestration, but it would serve as an additional incentive for SS-BC manufacturers to maximize their biochar yields from raw sewage sludge, creating products that are attractive on the voluntary carbon credit market.

It is tempting to further speculate on the revenues a company like Lindum AS could expect by processing all sewage sludge using pyrolysis. They currently generate revenues by 1) treating sewage sludge, and 2) using some of the fractions to produce bio-gas. Managing to utilize the final fraction, digestate, could further increase the company's revenues per tonne of processed raw sewage sludge. SS-BC production costs of 100 €/tonne will likely represent a tiny fraction of the total revenue that can be expected from each tonne of raw sewage sludge received.

5.4 Waste-based biochar for sustainable development

The European Green Deal of July 14, 2021 lists development of biochar as one of the most important economic means to achieve the goal of making Europe the first climate-neutral continent in the world. Biochar, with its numerous applications, has the potential to contribute to the following 2030 United Nations Sustainable Development Goals (SDGs) (United Nations, 2015):

- **SDG 6**: Clean water and sanitation

- **SDG 9**: Industry, innovation and infrastructure

- **SDG 11**: Sustainable cities and communities

- **SDG 12**: Responsible consumption and production

- **SDG 13**: Climate action

- **SDG 14**: Life below water

- **SDG 15**: Life on land

Within Norway and the EU, a number of research initiatives have been taken to study possible applications of waste-based biochar sorbents that could contribute to achieving the SDGs and the European Green Deal. The International Biochar Initiative (IBI) is a collaborative platform for science, industry, agriculture, government, and non-governmental organizations, as is the European Biochar Certificate (EBC) which creates awareness about the benefits of biochar, and develops biochar standards for safe and sustainable use. The 4 per mille initiative, Soils for Food Security and Climate, was launched by France during the UN climate change conference in December, 2015 (COP21). The 4 per 1000 mission is to increase soil carbon stocks in the first 30-40 cm of soil by 4 ‰ annually as a means of complementing what is necessary efforts to compensate for global fossil-based GHG emissions. The goal is to scale biochar for global agricultural and remediation markets. If applied correctly, biochar can play an important role in sequestering carbon, and at the same time serve as a soil amendment and fertilizer in agriculture. However, this must be done carefully because the application of biochar to soil has been shown to have a priming effect on soil-native C by improving microbial populations, thereby influencing the decomposition rate of organic matter (Ahmad et al., 2014). In most cases however, negative priming is seen, and biochar actually helps to increase natural organic matter content in soils (Chen et al., 2019; Weng et al., 2018). With many initiatives and research groups working on the national, continental, and global levels, not only within the biochar-world of remediation and agricultural science, but also in many other scientific, as well as humanitarian disciplines, one can only hope that the sum of these contributions will help to slow global warming.

5.5   Final recommendations

This thesis has proposed a set of mechanisms that are expected to explain the differences in sorption of PFCAs to biochar derived from raw sewage sludge, digested sludge, and clean wood chips. It has indicated the significant potential of biochar for application as a sorbent for wastewater and soil contaminated with PFAS. This study is one of the first to show that biochar made from two different sewage sludge substrates can be used to reduce PFAS concentrations in water by $88 \pm 22\%$ at a dosage of only 0.1 g. The SS-BCs tested have shown to sorb equally strongly, or stronger than, several activated carbons (AC) reported in previous literature. The results and analyses from this thesis also raise new research questions within the relatively novel research area of PFAS-sorption to sewage sludge biochars. Conducting multivariate regression analyses between PFAS sorption strenght and factors such as surface area, pore volume, carbon content, and mineral contents (mainly Ca and Fe) will be necessary to confirm the sorption mechanisms proposed in this work, and to draw more definitive conclusions than those presented here. Additional research could also determine capacity tests for sewage sludge-based biochar filters, sorption strength to other PFAS groups, especially PFSA, competition with PAHs, and other contaminants that are commonly present in wastewater. Further tests are also needed to determine how these biochars work *in situ* soil remediation. Studying the effect of activation of sludge chars on sorption strength could be highly useful, especially for application to OM-rich soils. Attention could also be given to investigating the relationship between soil organic carbon, and the biochar dosage required to reduce PFAS pore water concentrations to an acceptable

level.

Increased potential for carbon sequestration, and increased commercial valorization of sewage sludge in a circular economy, are highly promising for the incorporation, and ultimately, the replacement of existing fossil-derived sorbents with sewage-sludge based sorbents. Should further studies corroborate the findings presented in this study, the commercial and environmental benefits would be nothing less than sensational.

Bibliography

Ahmad, M., Rajapaksha, A. U., Lim, J. E., Zhang, M., Bolan, N., Mohan, D., Vithanage, M., Lee, S. S., and Ok, Y. S. (2014). Biochar as a sorbent for contaminant management in soil and water: a review. *Chemosphere*, 99:19–33.

Ahmed, M., Johir, M., McLaughlan, R., Nguyen, L. N., Xu, B., and Nghiem, L. D. (2020). Per-and polyfluoroalkyl substances in soil and sediments: Occurrence, fate, remediation and future outlook. *Science of the Total Environment*, 748:141251.

Alhashimi, H. A. and Aktas, C. B. (2017). Life cycle environmental and economic performance of biochar compared with activated carbon: a meta-analysis. *Resources, Conservation and Recycling*, 118:13–26.

Arp, H. P. H., Niederer, C., and Goss, K.-U. (2006). Predicting the partitioning behavior of various highly fluorinated compounds. *Environmental science & technology*, 40(23):7298–7304.

Arvaniti, O. S., Andersen, H. R., Thomaidis, N. S., and Stasinakis, A. S. (2014a). Sorption of perfluorinated compounds onto different types of sewage sludge and assessment of its importance during wastewater treatment. *Chemosphere*, 111:405–411.

Arvaniti, O. S., Asimakopoulos, A. G., Dasenaki, M. E., Ventouri, E. I., Stasinakis, A. S., and Thomaidis, N. S. (2014b). Simultaneous determination of eighteen perfluorinated compounds in dissolved and particulate phases of wastewater, and in sewage sludge by liquid chromatography-tandem mass spectrometry. *Analytical Methods*, 6(5):1341–1349.

Arvaniti, O. S. and Stasinakis, A. S. (2015). Review on the occurrence, fate and removal of perfluorinated compounds during wastewater treatment. *Science of the Total Environment*, 524:81–92.

Arvaniti, O. S., Ventouri, E. I., Stasinakis, A. S., and Thomaidis, N. S. (2012). Occurrence of different classes of perfluorinated compounds in greek wastewater treatment plants and determination of their solid–water distribution coefficients. *Journal of hazardous materials*, 239:24–31.

Ball, P. (2012). Like attracts like? *Nature*.

Bardestani, R., Patience, G. S., and Kaliaguine, S. (2019). Experimental methods in chemical engineering: specific surface area and pore size distribution measurements—bet, bjh, and dft. *The Canadian Journal of Chemical Engineering*, 97(11):2781–2791.

Beesley, L., Moreno-Jiménez, E., Gomez-Eyles, J. L., Harris, E., Robinson, B., and Sizmur, T.

(2011). A review of biochars' potential role in the remediation, revegetation and restoration of contaminated soils. *Environmental pollution*, 159(12):3269–3282.

Bhhatarai, B. and Gramatica, P. (2011). Prediction of aqueous solubility, vapor pressure and critical micelle concentration for aquatic partitioning of perfluorinated chemicals. *Environmental science & technology*, 45(19):8120–8128.

Bremmer, J. M. and Mulvaney, C. (1982). Nitrogen-total. In Miller, R. and Keeney, D., editors, *Methods of soil analysis Part 2 Agronomy*, volume 9, chapter 31, pages 595–624. American Society of Agronomy Inc., Madison, Wisconsin, USA, 2 edition.

Brendel, S., Fetter, É., Staude, C., Vierke, L., and Biegel-Engler, A. (2018). Short-chain perfluoroalkyl acids: environmental concerns and a regulatory strategy under reach. *Environmental Sciences Europe*, 30(1):1–11.

Cabrerizo, A., Muir, D. C., De Silva, A. O., Wang, X., Lamoureux, S. F., and Lafrenière, M. J. (2018). Legacy and emerging persistent organic pollutants (pops) in terrestrial compartments in the high arctic: sorption and secondary sources. *Environmental science & technology*, 52(24):14187–14197.

Cantrell, K. B., Hunt, P. G., Uchimiya, M., Novak, J. M., and Ro, K. S. (2012). Impact of pyrolysis temperature and manure source on physicochemical characteristics of biochar. *Bioresource technology*, 107:419–428.

Chen, L., Jiang, Y., Liang, C., Luo, Y., Xu, Q., Han, C., Zhao, Q., and Sun, B. (2019). Competitive interaction with keystone taxa induced negative priming under biochar amendments. *Microbiome*, 7(1):1–18.

Chun, Y., Sheng, G., Chiou, C. T., and Xing, B. (2004). Compositions and sorptive properties of crop residue-derived chars. *Environmental science & technology*, 38(17):4649–4655.

Cornelissen, G. and Gustafsson, Ö. (2004). Sorption of phenanthrene to environmental black carbon in sediment with and without organic matter and native sorbates. *Environmental science & technology*, 38(1):148–155.

Cornelissen, G. and Gustafsson, o. (2006). Effects of added pahs and precipitated humic acid coatings on phenanthrene sorption to environmental black carbon. *Environmental Pollution*, 141(3):526–531.

Cornelissen, G., Gustafsson, ö., Bucheli, T. D., Jonker, M. T., Koelmans, A. A., and van Noort, P. C. (2005). Extensive sorption of organic compounds to black carbon, coal, and kerogen in sediments and soils: mechanisms and consequences for distribution, bioaccumulation, and biodegradation. *Environmental science & technology*, 39(18):6881–6895.

Council of the European Union (2013). Directive 2013/39/eu of the european parliament and of the council of 12 august 2013 amending directives 2000/60/ec and 2008/105/ec as regards priority substances in the field of water policy text with eea relevance. `https://eur-lex.europa.eu/legal-content/EN/TXT/PDF/?uri=CELEX:32013L0039&from=EN`.

CRCCARE (2017). Assessment, management and remediation guidance for perfluorooctanesulfonate (pfos) and perfluorooctanoic acid (pfoa)–part 5: management and remediation of pfos and pfoa, crc care technical report no. 38.

Danish Environmental Protection Agency (2021). Bekendtgørelse om vandkvalitet og tilsyn med vandforsyningsanlæg. Technical Report 2361, The Danish Environmental Protection Agency (Miljøministeriet). Appendix (bilag) 1 d.

Das, S. K., Ghosh, G. K., and Avasthe, R. (2020). Application of biochar in agriculture and environment, and its safety issues. *Biomass Conversion and Biorefinery*, pages 1–11.

Deng, S., Yu, Q., Huang, J., and Yu, G. (2010). Removal of perfluorooctane sulfonate from wastewater by anion exchange resins: Effects of resin properties and solution chemistry. *Water Research*, 44(18):5188–5195.

Ding, G. and Peijnenburg, W. J. (2013). Physicochemical properties and aquatic toxicity of poly-and perfluorinated compounds. *Critical reviews in environmental science and technology*, 43(6):598–678.

Du, Z., Deng, S., Bei, Y., Huang, Q., Wang, B., Huang, J., and Yu, G. (2014). Adsorption behavior and mechanism of perfluorinated compounds on various adsorbents—a review. *Journal of hazardous materials*, 274:443–454.

ECHA (2020). Annex xvii to reach - conditions of restriction c9-c14 linear and/or branched perfluorocarboxylic acids, their salts and c9-c14 pfcas-related substances. Technical report, ECHA.

EPA (2014). Emerging contaminants-perfluorooctane sulfonate (pfos) and perfluorooctanoic acid (pfoa). Technical Report EPA 505-F-14-001, US EPA.

European Commission (2020). Commission staff working document: poly- and perfluoroalkyl substances (pfas). Technical report, European Commission.

Fabregat-Palau, J., Vidal, M., and Rigol, A. (2022). Examining sorption of perfluoroalkyl substances (pfas) in biochars and other carbon-rich materials. *Chemosphere*, page 134733.

Fan, J., Li, Y., Yu, H., Li, Y., Yuan, Q., Xiao, H., Li, F., and Pan, B. (2020). Using sewage sludge with high ash content for biochar production and cu (ii) sorption. *Science of the Total Environment*, 713:136663.

Fathianpour, A., Taheriyoun, M., and Soleimani, M. (2018). Lead and zinc stabilization of soil using sewage sludge biochar: optimization through response surface methodology. *CLEAN–Soil, Air, Water*, 46(5):1700429.

Figueiredo, C., Lopes, H., Coser, T., Vale, A., Busato, J., Aguiar, N., Novotny, E., and Canellas, L. (2018). Influence of pyrolysis temperature on chemical and physical properties of biochar from sewage sludge. *Archives of Agronomy and Soil Science*, 64(6):881–889.

Filipovic, M., Woldegiorgis, A., Norström, K., Bibi, M., Lindberg, M., and Österås, A.-H. (2015). Historical usage of aqueous film forming foam: A case study of the widespread distribution of perfluoroalkyl acids from a military airport to groundwater, lakes, soils and fish. *Chemosphere*, 129:39–45.

Gebbink, W. A., Van Asseldonk, L., and Van Leeuwen, S. P. (2017). Presence of emerging per-and polyfluoroalkyl substances (pfass) in river and drinking water near a fluorochemical production plant in the netherlands. *Environmental science & technology*, 51(19):11057–11065.

Goss, K.-U. (2008). The p k a values of pfoa and other highly fluorinated carboxylic acids. *Environmental science & technology*, 42(2):456–458.

Goss, K.-U. and Arp, H. P. H. (2009). Comment on "experimental p k a determination for perfluorooctanoic acid (pfoa) and the potential impact of p k a concentration dependence on laboratory-measured partitioning phenomena and envrinomental modeling". *Environmental science & technology*, 43(13):5150–5151.

Hagemann, N., Spokas, K., Schmidt, H.-P., Kägi, R., Böhler, M. A., and Bucheli, T. D. (2018). Activated carbon, biochar and charcoal: linkages and synergies across pyrogenic carbon's abcs. *Water*, 10(2):182.

Hale, S. E., Arp, H. P. H., Kupryianchyk, D., and Cornelissen, G. (2016). A synthesis of parameters related to the binding of neutral organic compounds to charcoal. *Chemosphere*, 144:65–74.

Hale, S. E., Arp, H. P. H., Schliebner, I., and Neumann, M. (2020). Persistent, mobile and toxic (pmt) and very persistent and very mobile (vpvm) substances pose an equivalent level of concern to persistent, bioaccumulative and toxic (pbt) and very persistent and very bioaccumulative (vpvb) substances under reach. *Environmental Sciences Europe*, 32(1):1–15.

Hale, S. E., Arp, H. P. H., Slinde, G. A., Wade, E. J., Bjørseth, K., Breedveld, G. D., Straith, B. F., Moe, K. G., Jartun, M., and Høisæter, Å. (2017). Sorbent amendment as a remediation strategy to reduce pfas mobility and leaching in a contaminated sandy soil from a norwegian firefighting training facility. *Chemosphere*, 171:9–18.

Hale, S. E., Hanley, K., Lehmann, J., Zimmerman, A. R., and Cornelissen, G. (2011). Effects of chemical, biological, and physical aging as well as soil addition on the sorption of pyrene to activated carbon and biochar. *Environmental science & technology*, 45(24):10445–10453.

Hale, S. E., Tomaszewski, J. E., Luthy, R. G., and Werner, D. (2009). Sorption of dichlorodiphenyltrichloroethane (ddt) and its metabolites by activated carbon in clean water and sediment slurries. *Water research*, 43(17):4336–4346.

Hansen, M. C., Børresen, M. H., Schlabach, M., and Cornelissen, G. (2010). Sorption of perfluorinated compounds from contaminated water to activated carbon. *Journal of Soils and Sediments*, 10(2):179–185.

Higgins, C. P. and Luthy, R. G. (2006). Sorption of perfluorinated surfactants on sediments. *Environmental science & technology*, 40(23):7251–7256.

Huang, C., Mohamed, B. A., and Li, L. Y. (2022). Comparative life-cycle assessment of pyrolysis processes for producing bio-oil, biochar, and activated carbon from sewage sludge. *Resources, Conservation and Recycling*, 181:106273.

Inoue, Y., Hashizume, N., Yakata, N., Murakami, H., Suzuki, Y., Kikushima, E., and Otsuka, M. (2012). Unique physicochemical properties of perfluorinated compounds and their bioconcentration in common carp cyprinus carpio l. *Archives of environmental contamination and toxicology*, 62(4):672–680.

Klučáková, M. (2018). Size and charge evaluation of standard humic and fulvic acids as crucial factors to determine their environmental behavior and impact. *Frontiers in chemistry*, 6:235.

Knutsen, H., Mæhlum, T., Haarstad, K., Slinde, G. A., and Arp, H. P. H. (2019). Leachate emissions of short-and long-chain per-and polyfluoralkyl substances (pfass) from various norwegian landfills. *Environmental Science: Processes & Impacts*, 21(11):1970–1979.

Krafft, M. P. and Riess, J. G. (2015). Per-and polyfluorinated substances (pfass): Environmental challenges. *Current opinion in colloid & interface science*, 20(3):192–212.

Kupryianchyk, D., Hale, S., Zimmerman, A. R., Harvey, O., Rutherford, D., Abiven, S., Knicker, H., Schmidt, H.-P., Pumpel, C., and Cornelissen, G. (2016a). Sorption of hydrophobic organic compounds to a diverse suite of carbonaceous materials with emphasis on biochar. *Chemosphere*, 144:879–887.

Kupryianchyk, D., Hale, S. E., Breedveld, G. D., and Cornelissen, G. (2016b). Treatment of sites contaminated with perfluorinated compounds using biochar amendment. *Chemosphere*, 142:35–40.

Kwon, S. and Pignatello, J. J. (2005). Effect of natural organic substances on the surface and adsorptive properties of environmental black carbon (char): pseudo pore blockage by model lipid components and its implications for n2-probed surface properties of natural sorbents. *Environmental science & technology*, 39(20):7932–7939.

Lam, G. C., Sum, K. N. W., Bashir, M., and Sethupathi, S. (2017). Adsorption of trimethyltin, arsenic and zinc by palm oil mill sludge biochar prepared by microwave. In *AIP Conference Proceedings*, volume 1828, page 020030. AIP Publishing LLC.

Langberg, H. A., Arp, H. P. H., Breedveld, G. D., Slinde, G. A., Høiseter, Å., Grønning, H. M., Jartun, M., Rundberget, T., Jenssen, B. M., and Hale, S. E. (2021). Paper product production identified as the main source of per-and polyfluoroalkyl substances (pfas) in a norwegian lake: Source and historic emission tracking. *Environmental Pollution*, 273:116259.

Lath, S., Knight, E. R., Navarro, D. A., Kookana, R. S., and McLaughlin, M. J. (2019). Sorption of pfoa onto different laboratory materials: Filter membranes and centrifuge tubes. *Chemosphere*, 222:671–678.

Lau, C., Anitole, K., Hodes, C., Lai, D., Pfahles-Hutchens, A., and Seed, J. (2007). Perfluoroalkyl acids: a review of monitoring and toxicological findings. *Toxicological sciences*, 99(2):366–394.

Lee, J.-W., Lee, H.-K., Lim, J.-E., and Moon, H.-B. (2020). Legacy and emerging per-and polyfluoroalkyl substances (pfass) in the coastal environment of korea: occurrence, spatial distribution, and bioaccumulation potential. *Chemosphere*, 251:126633.

Lehmann, J. and Joseph, S. (2015). *Biochar for environmental management: science, technology and implementation*. Routledge.

Leng, L., Xiong, Q., Yang, L., Li, H., Zhou, Y., Zhang, W., Jiang, S., Li, H., and Huang, H. (2021). An overview on engineering the surface area and porosity of biochar. *Science of the Total Environment*, 763:144204.

Li, L., Zou, D., Xiao, Z., Zeng, X., Zhang, L., Jiang, L., Wang, A., Ge, D., Zhang, G., and Liu, F. (2019). Biochar as a sorbent for emerging contaminants enables improvements in waste management and sustainable resource use. *Journal of Cleaner Production*, 210:1324–1342.

Li, Y., Oliver, D. P., and Kookana, R. S. (2018). A critical analysis of published data to discern the role of soil and sediment properties in determining sorption of per and polyfluoroalkyl substances (pfass). *Science of the Total Environment*, 628:110–120.

Limousin, G., Gaudet, J.-P., Charlet, L., Szenknect, S., Barthes, V., and Krimissa, M. (2007). Sorption isotherms: A review on physical bases, modeling and measurement. *Applied geochemistry*, 22(2):249–275.

Mahinroosta, R. and Senevirathna, L. (2020). A review of the emerging treatment technologies for pfas contaminated soils. *Journal of environmental management*, 255:109896.

Masoner, J. R., Kolpin, D. W., Cozzarelli, I. M., Smalling, K. L., Bolyard, S. C., Field, J. A., Furlong, E. T., Gray, J. L., Lozinski, D., Reinhart, D., et al. (2020). Landfill leachate contributes per-/poly-fluoroalkyl substances (pfas) and pharmaceuticals to municipal wastewater. *Environmental Science: Water Research & Technology*, 6(5):1300–1311.

McPhedran, K. N., Seth, R., and Drouillard, K. G. (2013). Hydrophobic organic compound (hoc) partitioning behaviour to municipal wastewater colloidal organic carbon. *Water research*, 47(7):2222–2230.

Merck (2022a). Pfo cas 307-34-6.

Merck (2022b). Pfoa cas 335-67-1.

Mohajerani, A. and Karabatak, B. (2020). Microplastics and pollutants in biosolids have contaminated agricultural soils: An analytical study and a proposal to cease the use of biosolids in farmlands and utilise them in sustainable bricks. *Waste Management*, 107:252–265.

Moodie, D., Coggan, T., Berry, K., Kolobaric, A., Fernandes, M., Lee, E., Reichman, S., Nugegoda, D., and Clarke, B. O. (2021). Legacy and emerging per-and polyfluoroalkyl substances (pfass) in australian biosolids. *Chemosphere*, 270:129143.

Morin, N. A., Andersson, P. L., Hale, S. E., and Arp, H. P. H. (2017). The presence and partitioning behavior of flame retardants in waste, leachate, and air particles from norwegian waste-handling facilities. *Journal of Environmental Sciences*, 62:115–132.

Nelson, D. and Sommers, L. (1982). Total carbon, organic carbon, and organic matter. In Miller, R. and Keeney, D., editors, *Methods of soil analysis Part 2 Agronomy*, volume 9, chapter 29, pages 539–579. American Society of Agronomy Inc., Madison, Wisconsin, USA, 2 edition.

Pandey, S. K. and Roy, K. (2021). Qspr modeling of octanol-water partition coefficient and organic carbon normalized sorption coefficient of diverse organic chemicals using extended topochemical atom (eta) indices. *Ecotoxicology and Environmental Safety*, 208:111411.

Pignatello, J. J., Kwon, S., and Lu, Y. (2006). Effect of natural organic substances on the surface and adsorptive properties of environmental black carbon (char): attenuation of surface activity by humic and fulvic acids. *Environmental science & technology*, 40(24):7757–7763.

Presser, V., McDonough, J., Yeon, S.-H., and Gogotsi, Y. (2011). Effect of pore size on carbon dioxide sorption by carbide derived carbon. *Energy & Environmental Science*, 4(8):3059–3066.

Propp, V. R., De Silva, A. O., Spencer, C., Brown, S. J., Catingan, S. D., Smith, J. E., and Roy, J. W. (2021). Organic contaminants of emerging concern in leachate of historic municipal landfills. *Environmental Pollution*, 276:116474.

Raheem, A., Sikarwar, V. S., He, J., Dastyar, W., Dionysiou, D. D., Wang, W., and Zhao, M. (2018). Opportunities and challenges in sustainable treatment and resource reuse of sewage sludge: a review. *Chemical Engineering Journal*, 337:616–641.

Rajabi, H., Mosleh, M. H., Prakoso, T., Ghaemi, N., Mandal, P., Lea-Langton, A., and Sedighi, M. (2021). Competitive adsorption of multicomponent volatile organic compounds on biochar. *Chemosphere*, 283:131288.

Rankin, K., Mabury, S. A., Jenkins, T. M., and Washington, J. W. (2016). A north american and global survey of perfluoroalkyl substances in surface soils: Distribution patterns and mode of occurrence. *Chemosphere*, 161:333–341.

Reemtsma, T., Berger, U., Arp, H. P. H., Gallard, H., Knepper, T. P., Neumann, M., Quintana, J. B., and Voogt, P. d. (2016). Mind the gap: Persistent and mobile organic compounds— water contaminants that slip through.

Saeidi, N., Kopinke, F.-D., and Georgi, A. (2020). Understanding the effect of carbon surface chemistry on adsorption of perfluorinated alkyl substances. *Chemical Engineering Journal*, 381:122689.

Sajjadi, B., Chen, W.-Y., and Egiebor, N. O. (2019). A comprehensive review on physical activation of biochar for energy and environmental applications. *Reviews in Chemical Engineering*, 35(6):735–776.

Schlabach, M., Bavel, B. v., Lomba, J. A. B., Borgen, A., Wing, G., Gabrielsen, Götsch, A., Halse, A.-K., Hanssen, L., Krogseth, I. S., Nikiforov, V., Nygård, T., Nizzetto, P. B., Reid, M., Rostkowski, P., and Samanipour, S. (2018). Screening programme 2017 – amap assessment compounds. Report 1080-2018, Miljødirektoratet.

Schmidt, H.-P., Anca-Couce, A., Hagemann, N., Werner, C., Gerten, D., Lucht, W., and Kammann, C. (2019). Pyrogenic carbon capture and storage. *Gcb Bioenergy*, 11(4):573–591.

Schwarzenbach, R. P., Gschwend, P. M., and Imboden, D. M. (2005). *Environmental organic chemistry*. John Wiley & Sons.

Sigmund, G., Arp, H. P. H., Aumeier, B. M., Bucheli, T. D., Chefetz, B., Chen, W., Droge, S. T., Endo, S., Escher, B. I., Hale, S. E., et al. (2022). Sorption and mobility of charged organic compounds: How to confront and overcome limitations in their assessment. *Environmental Science & Technology*.

Silvani, L., Cornelissen, G., Smebye, A. B., Zhang, Y., Okkenhaug, G., Zimmerman, A. R., Thune, G., Saevarsson, H., and Hale, S. E. (2019). Can biochar and designer biochar be used to remediate per-and polyfluorinated alkyl substances (pfas) and lead and antimony contaminated soils? *Science of the Total Environment*, 694:133693.

Siriwardena, D. P., Crimi, M., Holsen, T. M., Bellona, C., Divine, C., and Dickenson, E. (2019). Influence of groundwater conditions and co-contaminants on sorption of perfluoroalkyl compounds on granular activated carbon. *Remediation Journal*, 29(3):5–15.

Smith, P. (2016). Soil carbon sequestration and biochar as negative emission technologies. *Global change biology*, 22(3):1315–1324.

Sorengard, M., Kleja, D. B., and Ahrens, L. (2019). Stabilization of per-and polyfluoroalkyl substances (pfass) with colloidal activated carbon (plumestop®) as a function of soil clay and organic matter content. *Journal of environmental management*, 249:109345.

Sørmo, E., Silvani, L., Bjerkli, N., Hagemann, N., Zimmerman, A. R., Hale, S. E., Hansen, C. B., Hartnik, T., and Cornelissen, G. (2021). Stabilization of pfas-contaminated soil with activated biochar. *Science of the Total Environment*, 763:144034.

Teixido, M., Hurtado, C., Pignatello, J. J., Beltrán, J. L., Granados, M., and Peccia, J. (2013). Predicting contaminant adsorption in black carbon (biochar)-amended soil for the veterinary antimicrobial sulfamethazine. *Environmental science & technology*, 47(12):6197–6205.

Tindall, R., Apffel-Marglin, F., and Shearer, D. (2017). *Sacred soil: biochar and the regeneration of the earth.* North Atlantic Books.

United Nations (2015). The united nations sustainable development goals. Technical report, United Nations.

Van Zwieten, L., Kimber, S., Morris, S., Chan, K., Downie, A., Rust, J., Joseph, S., and Cowie, A. (2010). Effects of biochar from slow pyrolysis of papermill waste on agronomic performance and soil fertility. *Plant and soil*, 327(1):235–246.

Vlaica, G. and Olivi, L. (2004). Exafs spectroscopy: a brief introduction. *Croatica chemica acta*, 77(3):427–433.

Wang, F. and Shih, K. (2011). Adsorption of perfluorooctanesulfonate (pfos) and perfluorooctanoate (pfoa) on alumina: Influence of solution ph and cations. *water research*, 45(9):2925–2930.

Wang, J. and Guo, X. (2020). Adsorption isotherm models: Classification, physical meaning, application and solving method. *Chemosphere*, 258:127279.

Wang, Z., MacLeod, M., Cousins, I. T., Scheringer, M., and Hungerbühler, K. (2011). Using cosmotherm to predict physicochemical properties of poly-and perfluorinated alkyl substances (pfass). *Environmental Chemistry*, 8(4):389–398.

Weng, Z. H., Van Zwieten, L., Singh, B. P., Tavakkoli, E., Kimber, S., Morris, S., Macdonald, L. M., and Cowie, A. (2018). The accumulation of rhizodeposits in organo-mineral fractions promoted biochar-induced negative priming of native soil organic carbon in ferralsol. *Soil Biology and Biochemistry*, 118:91–96.

Xiao, F., Zhang, X., Penn, L., Gulliver, J. S., and Simcik, M. F. (2011). Effects of monovalent cations on the competitive adsorption of perfluoroalkyl acids by kaolinite: experimental studies and modeling. *Environmental science & technology*, 45(23):10028–10035.

Xiao, X., Ulrich, B. A., Chen, B., and Higgins, C. P. (2017a). Sorption of poly-and perfluoroalkyl substances (pfass) relevant to aqueous film-forming foam (afff)-impacted groundwater by biochars and activated carbon. *Environmental science & technology*, 51(11):6342–6351.

Xiao, X., Ulrich, B. A., Chen, B., and Higgins, C. P. (2017b). Supporting information for "sorption of poly-and perfluoroalkyl substances (pfass) relevant to aqueous film forming foam

(afff)-impacted groundwater by biochars and activated carbon". *Environmental science & technology*.

Yin, C., Pan, C.-G., Xiao, S.-K., Wu, Q., Tan, H.-M., and Yu, K. (2022). Insights into the effects of salinity on the sorption and desorption of legacy and emerging per-and polyfluoroalkyl substances (pfass) on marine sediments. *Environmental Pollution*, 300:118957.

Yu, Q., Zhang, R., Deng, S., Huang, J., and Yu, G. (2009). Sorption of perfluorooctane sulfonate and perfluorooctanoate on activated carbons and resin: kinetic and isotherm study. *Water research*, 43(4):1150–1158.

Zareitalabad, P., Siemens, J., Hamer, M., and Amelung, W. (2013). Perfluorooctanoic acid (pfoa) and perfluorooctanesulfonic acid (pfos) in surface waters, sediments, soils and wastewater–a review on concentrations and distribution coefficients. *Chemosphere*, 91(6):725–732.

Zhang, C., Yan, H., Li, F., Hu, X., and Zhou, Q. (2013). Sorption of short-and long-chain perfluoroalkyl surfactants on sewage sludges. *Journal of hazardous materials*, 260:689–699.

Zhang, D., He, Q., Wang, M., Zhang, W., and Liang, Y. (2021). Sorption of perfluoroalkylated substances (pfass) onto granular activated carbon and biochar. *Environmental technology*, 42(12):1798–1809.

Zheng, Y., Li, Q., Yuan, C., Tao, Q., Zhao, Y., Zhang, G., and Liu, J. (2019). Influence of temperature on adsorption selectivity: Coal-based activated carbon for ch4 enrichment from coal mine methane. *Powder Technology*, 347:42–49.

Appendix A

Batch test experiment preparations

A.1 Preliminary batch tests

The batch tests were prepared by spiking 50 mL Milli-Q water with PFOA to 1.3 mg/L and added 1 g CWC and 100 mg ULS in two PP tubes and placed in an end-over-end shaker for 14 d. DSL was not included in this step because the samples were not provided at this point. The aqueous concentration in the two test tubes were determined according to DIN38407-42 by the accredited laboratory Eurofins Norway. Sorption of PFCA to ULS was expected to be lower than for CWC. However, the test run for sorption of PFOA to ULS showed sorption two orders of magnitude higher than expected. Therefore, the same K_d values were used for calculating spike concentrations for the ULS, DSL, and CWC. A 100 mg biochar dose was decided to be ideal to balance convenient spike concentrations with sufficient sorption. Table A.1 shows the results from the preliminary sorption experiments.

Table A.1: Partition coefficients (K_d) for PFOA from the preliminary batch tests with CWC and ULS.

Biochar	C_i $(\mu g/L)$	C_s $(\mu g/kg)$	C_w $(\mu g/L)$	K_d (L/kg)	log K_d
CWC	1 335	66 652	0.099	673 250	5.83
ULS	1 335	630 824	2.7	233 638	5.37

Table A.2: Biochar-water distribution coefficients (K_{BC}) for PFCAs derived from Xiao et al. (2017b).

Compound	log K_{BC} (Xiao et al., 2017b)	est. log K_{BC}
PFPeA	4.16	4.16
PFHxA	4.15	4.15
PFHpA	4.49	4.49
PFOA	4.76	4.76
PFNA	*4.89	4.89
PFDA	*5.09	5.09

* not included in (Xiao et al., 2017b), so the values are extrapolated from the shorter chain lengths.

Table A.3: Expected versus analytic standard concentration of working standards used to spike the batch shaking tests.

Compound	Working standard single (mg/L)			Working standard cocktail (ug/L)		
	Expected	Analytic	% deviation	Expected	Analytic	% deviation
PFPeA	5.2	3.3	36	9.4	8.8	6
PFHxA	14.2	7.8	45	18.7	26.1	-39
PFHpA	3.3	3.0	9	4.0	4.8	-19
PFOA	13.2	22.7	-71	35.7	61.7	-73
PFNA	17.8	16.2	9	48.5	72.2	-49
PFDA	16.8	13.1	22	153.0	165.2	-8

Table A.4: Purity, stock form and LOQs of the PFCAs used for the sorption isotherms. iLOQ = instrumental LOQ for the extract, mLOQ = method LOQ.

Compound	Purity	Stock form	iLOQ (ng mL^{-1})	mLOQ (ng L^{-1})
PFPeA	97 %	liquid	0.05	0.50
PFHxA	97 %	liquid	0.10	1.00
PFHpA	99 %	crystalline	0.01	0.10
PFOA	95 %	powder	0.05	0.50
PFNA	97 %	crystalline	0.05	0.50
PFDA	98 %	flakes	0.10	1.00

Table A.5: Analysis results of a dilution of the standards (STD) used for spiking and filter blanks (FB) prepared at the same concentrations in $\mu g/L$.

Compound	STD-1	STD-2	STD-3	FB-1	FB-2	FB-3
PFPeA	1.38	1.40	1.18	1.31	1.19	3.86
PFHxA	30.3	33.3	30.2	23.6	26.9	30.2
PFHpA	0.042	2.30	2.07	2.15	1.96	2.01
PFOA	87.8	88.0	88.8	89.1	88.8	101.3
PFNA	11.5	11.4	12.1	11.8	12.5	11.8
PFDA	8.04	5.16	8.81	10.7	5.11	8.39

Appendix B

LC-MS/MS

Table B.1: Quality assurance and quality controls.

Code	Sample matrix	TA (addition pre-extraction)	IS (addition pre-extraction)	TA (addition post-extraction)	IS (addition post-extraction)	Solvent (MQ:MeOH)
Procedural blank	NO		✓			50:50
Blank 1	YES		✓			50:50
Blank 2	YES		✓			50:50
Spike 2.5 ppb	YES	✓	✓			50:50
Spike 25 ppb	YES	✓	✓			50:50
Spike 50 ppb	YES	✓	✓			50:50
Matrix matched 2.5 ppb	YES			✓	✓	50:50
Matrix matched 25 ppb	YES			✓	✓	50:50
Matrix matched 50 ppb	YES			✓	✓	50:50
Solvent blank[*]	NO					0:100
Calibration 0 ppb	NO			✓	✓	0:100
Calibration 0.01 ppb	NO			✓	✓	0:100
Calibration 0.05 ppb	NO			✓	✓	0:100
Calibration 0.1 ppb	NO			✓	✓	0:100
Calibration 0.2 ppb	NO			✓	✓	0:100
Calibration 0.5 ppb	NO			✓	✓	0:100
Calibration 1 ppb	NO			✓	✓	0:100
Calibration 2 ppb	NO			✓	✓	0:100
Calibration 5 ppb	NO			✓	✓	0:100
Calibration 10 ppb[*]	NO			✓	✓	0:100
Calibration 25 ppb	NO			✓	✓	0:100
Calibration 50 ppb	NO			✓	✓	0:100

[*] Injected every 15-20 samples
TA = target analytes, IS = internal standard

Table B.2: Gradient between the two mobile phases used during UPLC-MS/MS. Water phase (A): Milli-Q water with 2 mM ammonium acetate, organic phase (B): pure MeOH. Run time = 6 min.

Time (min)	Flow	% A	% B	Step
0	0.25	80	20	Init
0.1	0.25	80	20	6
0.2	0.25	50	50	6
0.8	0.25	30	70	6
1.5	0.25	20	80	6
2.8	0.25	15	85	5
4.5	0.25	0	100	6
5.5	0.25	0	100	6
5.6	0.25	80	20	6
6	0.25	80	20	6

Table B.3: Tune parameters for UPLC-Xevo TQS instrument.

ESI (-)	
Capillary (kV)	2
Cone (V)	25
Source Offset (V)	40
Desolvation temperature (°C)	450
Desolvation Gas flow (L/h)	650
Cone (L/h)	150
Nebuliszer (Bar)	6
Source Temperature (°C)	150

Appendix C

Miscellaneous laboratory tests

C.1 pH and conductivity

Table C.1: Mean pH and conductivity and standard error (μS cm^{-1}) measurements for the different batch test slurries (n=3). BC/S/L is the biochar:soil:liquid ratio.

	pH	Conductivity	BC/S/L
ULS	7.10 ± 0.03	45.7 ± 1.8	1/0/500
DSL	7.31 ± 0.01	40.9 ± 0.6	1/0/500
CWC	7.36 ± 0.04	46.5 ± 0.4	1/0/500
ULS+S	7.18 ± 0.01	34.9 ± 0.2	1/50/500
DSL+S	7.14 ± 0.00	35.7 ± 0.9	1/50/500
CWC+S	7.09 ± 0.03	44.9 ± 0.9	1/50/500
S	7.08 ± 0.03	23.3 ± 0.9	0/1/10

C.2 Biochar loss during filtration

CWC left in the syringe after filtration. To quantify BC loss in the syringe was important in the case of conducting a complete mass balance of PFAS by analyzing both the filtrate and the biochar, however, this was not conducted due to difficulties with extracting PFAS from the char. Filtering of the biochar-water samples varied in how char was transferred to the filter in saw close to complete transfer of the char to the filter paper whereas for CWC much of the char was stuck at the bottom of the syringe during filtration. A mass balance test was performed to quantify the loss of CWC (Table C.2).

Table C.2: Mass CWC left in syringe after filtering of biochar-PFCA solution. Total mass CWC is 0.1000 ± 0.004 g.

	Mass (g)	$\bar{x}$	SDEV	CV
		0.0488	0.003	8 %
1	0.0429			
2	0.0413			
3	0.0484			
4	0.0428			
5	0.0485			

C.3 Uncertainties in the preparation of batch tests

All pipettes used for spiking the PFCA batch tests were calibrated, and all values were below the permitted values specific to the coefficient of variation (CV = 0.3, 0.5, and 2 % corresponding respectively to each sample, details in Appendix C). The dilutions for each batch test was prepared by pipetting the standards into the sample tubes, and diluting with water to the 50 mL mark. Measurement error was quantified by weighing the water added to the 50 mL mark in 10 pre-weighed sample tubes containing 0.1 g biochar. The results from weighing show that the weights of the ten 50 mL measurements were not 100% precise. However all samples were prepared within an acceptable range, even though each sample's volume may have deviated from 50 mL by ± 2 mL (Appendix C Table C.6). Preparation of cocktail spikes was done in two different ways: some by individually pipetting each standard compound, and some (the majority) by spiking with a prepared standard cocktail.

Table C.3: Pipette calibration for 2-10 mL pipette. PASS is given if CV $\leq$ 1.0 % and the average volume dispensed is within 1.8400 - 2.1600 mL.

Operator: Thermo Fishcer Scientific
Serial number: EJ08813
Date: 04.10.2021

Test volume (mL)		Weight of dispensed volume (g)	Corrected volume (g)	Average volume (mL)	SDEV	CV	PASS/FAIL
2				2.0868	0.006	0.3 %	
	1	2.0804	2.0842				
	2	2.0923	2.0961				
	3	2.0902	2.0940				
	4	2.0861	2.0899				
	5	2.0817	2.0855				
	6	2.0852	2.0890				
	7	2.0807	2.0845				
	8	2.0829	2.0867				
	9	2.0778	2.0815				
	10	2.0727	2.0764				
							PASS

Table C.4: Pipette calibration for 200-1000 µL pipette. PASS is given if CV $\leq$ 1.0 % and the average volume dispensed is within 992 - 1008 µL.

Operator: Thermo Fischer Scientific
Serial Number: EH23798 4500
Date: 04.10.2021

Test volume (µL)		Weight of dispensed volume (g)	Corrected volume (µL)	Average volume (µL)	SDEV	CV	PASS/FAIL
1000				994.2	5	0.5 %	
	1	997.0	998.8				
	2	999.4	1001.2				
	3	990.4	992.2				
	4	992.3	994.1				
	5	990.5	992.3				
	6	990.9	992.7				
	7	983.8	985.6				
	8	990.9	992.7				
	9	990.5	992.3				
	10	998.4	1000.2				
							PASS

Table C.5: Pipette calibration for 5 - 50 µL pipette. PASS is given if CV $\leq$ 2.5 % and the average volume dispensed is within 19.8 - 20.2 µL.

Operator: Thermo Fischer Scientific
Serial Number: EH94947 4500
Date: 04.10.2021

Test volume (µL)		Weight of dispensed volume (g)	Corrected volume (mL)	Average volume (mL)	SDEV	CV	PASS/FAIL
20				19.8	0.4	2 %	
	1	19.8	19.8				
	2	19.5	19.5				
	3	19.8	19.8				
	4	20.8	20.8				
	5	19.9	19.9				
	6	19.6	19.6				
	7	19.7	19.7				
	8	19.5	19.5				
	9	19.2	19.2				
	10	19.9	19.9				
							PASS

C.4 Volume calibration for 50 mL batch tests

Table C.6: Volume calibration for 50 mL Falcon high-clarity polypropylene (PP) conical centrifuge tube. PASS is given if CV $\leq$ and the average volume filled is within 49.0 - 51.0 mL.

					Date: 26.10.2021			
Test volume (mL)		**Initial weight (g)**	**Final weight (g)**	**Net weight (g)**	**Average volume (mL)**	**SDEV**	**CV**	**PASS/FAIL**
50					48.4756	0.2	0.4 %	
	1	13.0354	61.3521	48.3167				
	2	13.0572	61.3498	48.2926				
	3	13.0154	61.1161	48.1007				
	4	13.0857	61.8386	48.7529				
	5	13.0658	61.6241	48.5583				
	6	12.9908	61.6972	48.7064				
	7	13.0073	61.4474	48.4401				
	8	13.0699	61.7248	48.6549				
	9	12.7855	61.3788	48.5933				
	10	12.9962	61.3365	48.3403				
								FAIL

Appendix D

Element analysis soil and biochar

Table D.1: Total element composition of the biochars.

		CWC		ULS		DSL	
		Mean	Std.dev	Mean	Std.dev	Mean	Std.dev
Main elements							
C	%	91.4	2.5	29.6	0.5	13.5	0.2
N	%	0.69	0.02	1.13	0.04	0.82	0.02
H	%	1.01	0.14	1.24	0.05	1.05	0.16
O*	%	5.50		57.1		61.4	
Ca	g/kg	8.03	0.15	21.0		26.0	
Fe	g/kg	0.125	0.039	23.0		180	
K	g/kg	4.03	0.06	6.80		3.73	0.06
Mg	g/kg	0.907	0.023	5.30		4.70	0.17
Na	g/kg	0.052	0.001	2.40		1.83	0.06
P	g/kg	0.410	0.010	45.0		8.03	0.49
S	g/kg	0.089	0.004	2.90		7.23	0.68
Si	g/kg	0.167	0.015	1.70		0.620	0.079
Trace elements							
As	mg/kg	0.011	0.003	3.00		3.13	0.21
Ba	mg/kg	217	6	310		177	6
Cd	mg/kg	0.0004	-	0.008		0.029	0.003
Co	mg/kg	0.300	0.026	7.10		10.0	0.1
Cr	mg/kg	1.69	1.22	56		53.3	1.5
Cu	mg/kg	5.17	0.60	220		277	6
Mo	mg/kg	0.06	0.02	7.10		19	
Ni	mg/kg	1.77	0.64	41		34.7	0.6
Pb	mg/kg	0.08	0.02	13		25.3	4.0
Sr	mg/kg	36.3	2.1	87		120	
V	mg/kg	00.096	0.016	34		54	1
Zn	mg/kg	3.20	0.56	480		0.797	0.006

* Calculated as by subtraction of all other elements listed.

Table D.2: Total concentration, exchangeable ions and summary parameters for the soil used in the batch leaching tests. Total concentrations are in mg/kg d.w.

Main parameters		Mean	Std. dev
pH (H_2O)		5.38	0.02
pH (0.01 M $CaCl_2$)		4.36	0.01
C-org	%	1.32	0.03
N-tot	%	0.11	0.003
Exchangeable ions			
Al^{3+}	meqv/100g	0.87	0.01
H^+	meqv/100g	0.09	0.03
Mg^{2+}	meqv/100g	0.07	0.00
Ca^{2+}	meqv/100g	1.53	0.03
Na^+	meqv/100g	0.01	0.00
K^+	meqv/100g	0.05	0.00
CEC	meqv/100g	2.63	0.06
Total concentrations			
Ba	mg/kg	11.0	0.3
Be	mg/kg	0.269	0.003
Cd	mg/kg	0.195	0.063
Co	mg/kg	2.07	0.08
Cr	mg/kg	6.13	0.43
Cu	mg/kg	9.10	1.1
Fe	mg/kg	6740	445
Hg	mg/kg	<1	
Mn	mg/kg	124	7
Ni	mg/kg	3.09	0.20
P	mg/kg	525	29
Pb	mg/kg	8.45	0.53
Sr	mg/kg	6.80	0.67
V	mg/kg	12.7	0.9
Zn	mg/kg	22.2	1.3

Appendix E

Sorption

E.1 Alternative sorption mechanism explanation

The following is a discussion on potential sorption mechanisms between the sewage sludge biochars and PFAS. These ideas were developed and written during the initial stages of the discussion for this thesis. At a later stage it was decided that a more simple explanation for the sewage sludge char sorption mechanisms could be provided with the same outcome. Therefore, this section was removed from the main thesis, but added to the appendix to show the evolution of ideas developed in this work.
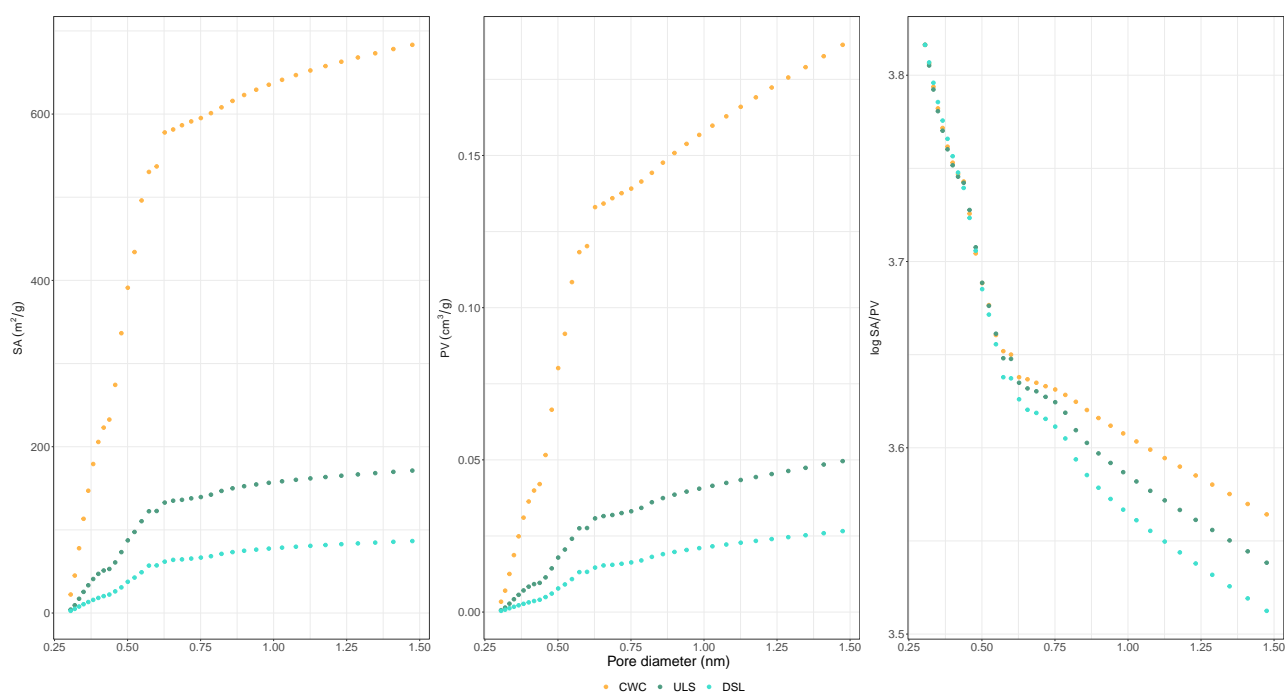
Figure E.1: Cumulative pore size distribution for pores 0.4-1.5 nm using DFT with (a) surface area (SA), (b) pore volume (PV), and (c) SA/PV ratio.

The surface area to pore volume ratio (SA/PV) can be used to more accurately represent available sorption sites, where a lower ratio indicates higher porosity (Presser et al., 2011). Since PV increases by increasing pore diameter (Figure E.1), the relative increase in PV will
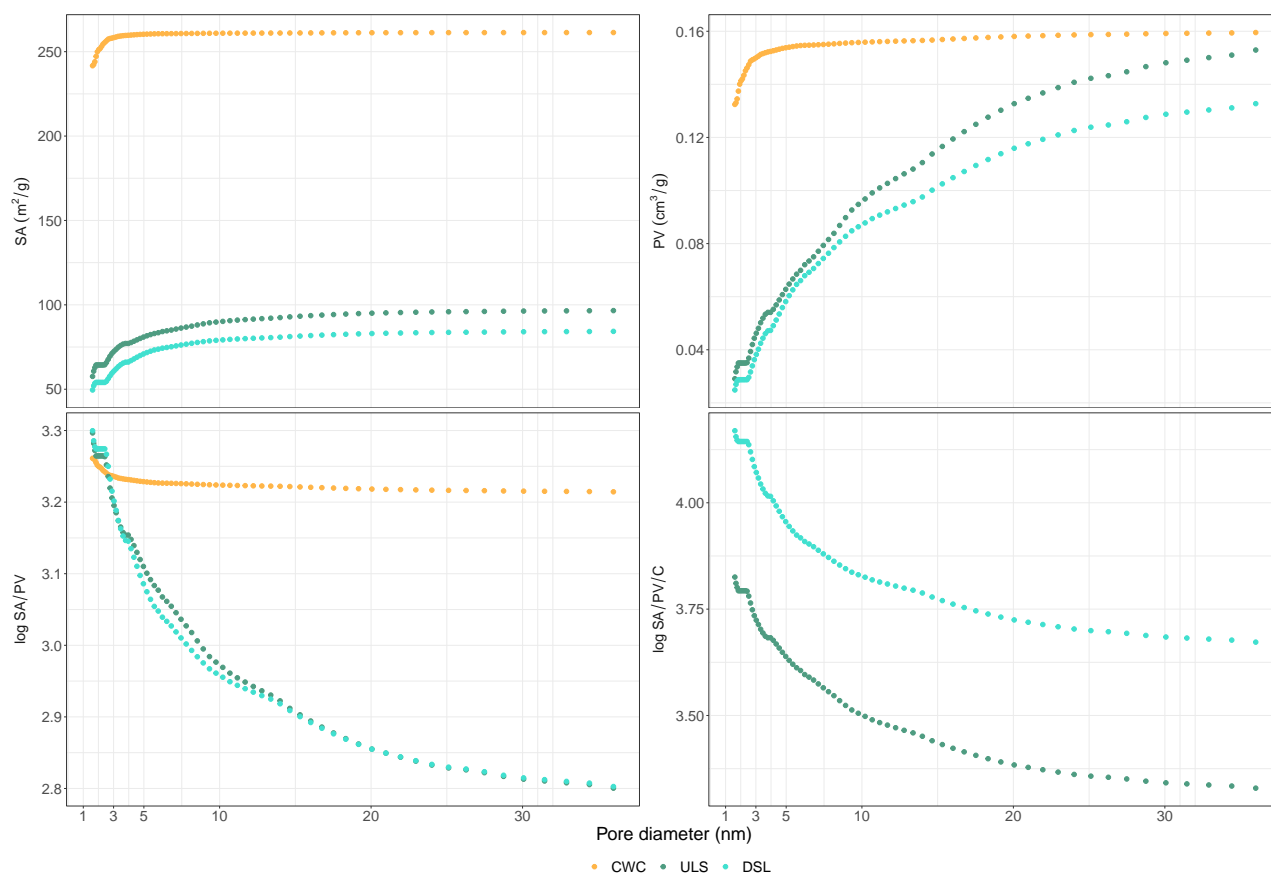
Figure E.2: Cumulative pore size distribution for pores > 1.5 nm using DFT theory with (a) surface area (SA) and (b) pore volume (PV), (c) log SA/PV, (d) log SA/PV/C (carbon).

be higher than the relative increase in SA. This means that the SA/PV ratio is expected to decrease more rapidly for biochar with higher pore volumes. This expectation is confirmed in Figure 4.4 where the SA/PV ratios for ULS and DSL are nearly equivalent to CWC, despite the fact that SA and PV are significantly different from CWC taken separately. This is reflected in the cumulative SA/PV ratios (Table 4.2) which are similar: 3 674, 3 502, and 3 206 m^2 cm^{-3} for CWC, ULS, and DSL respectively. This means that despite CWC being more numerous in micropores than ULS and DSL, its porosity is similar, and is predominantly allocated within the ultra micropore fraction.

Similar to the trend for small pores, CWC also had the largest cumulative SA but the lowest PV for pores >1.5 nm (323 m^2 g^{-1} versus 110 and 128 m^2 g^{-1} for DSL and ULS, respectively).

Table E.1: Surface area (SA), pore volume (PV), elemental content (C, O, H, N) and ratios for the biochars produced for the batch tests.

Biochar sorbent	N$_2$ sorption (pores >1.5 nm)				CO$_2$ sorption (pores 0.4-1.5 nm)			Elemental content				Elemental ratio		
	BET SA (m^2 g^{-1})	BJH PV (cm^3 g^{-1})	log SA/PV (m^2cm^{-3})	log SA/PV/C ($m^2cm^{-3}g^{-1}$)	DFT SA (m^2 g^{-1})	DFT PV (cm^3 g^{-1})	log SA/PV (m^2cm^{-3})	C (%)	O (%)	H (%)	N (%)	O/C	H/C	N/C
CWC	323	0.017	4.28	2.32	683	0.186	3.54	91.4	5.50	1.01	0.69	0.06	0.01	0.008
ULS	128	0.126	3.01	1.54	165	0.047	3.57	29.6	57.1	1.24	1.13	1.9	0.04	0.04
DSL	110	0.111	3.00	1.87	87	0.027	3.51	13.5	61.4	1.05	0.82	4.6	0.08	0.06

Figure E.2a shows that the highest proportion of SA is allocated to pores between 1.5-3 nm for CWC and 1.5-5 nm for ULS and DSL. Cumulative PV is highest for ULS (0.126 cm^3 g^{-1}), where PV for CWC was one order of magnitude lower (0.017 cm^3 g^{-1}). Furthermore, the development of PV with pore diameter in Figure 4.6b shows a clear distinction between CWC and the two sewage sludge biochars. CWC has most of its PV in pores <3 nm, whereas PV for ULS and DSL steadily increase up to the maximum pore size of 35 nm. This difference becomes important for the SA/PV ratio seen in Figure 4.6c. Here, ULS and DSL have low and equivalent cumulative log SA/PV ratios of 2.8 compared to the higher ratio of 3.2 for CWC (Table 4.2). Previous studies have consistently concluded that a large internal surface area and pore volume of adsorbents are the two most important parameters for achieving high sorption capacity of PFAS (Du et al., 2014; Sørmo et al., 2021; Hale et al., 2016; Ahmed et al., 2020). Similarly, the results of this study provide clear indications that a low SA/PV ratio can be considered a proxy for good PFAS sorption. The most plausible explanation for why CWC is the weakest sorbent among the three samples in this study is that CWC consists almost exclusively of micropores, whereas ULS and DSL also have pores in the mesopore range (2-50 nm). The shift observed by comparing SA and PV together demonstrates the importance of considering both pore size *and* surface area when evaluating available sorption sites on biochar.

Since ULS and DSL had nearly equivalent SA/PV ratios, an additional parameter is needed to explain why ULS is a better sorbent than DSL (Figure 4.6c). Apart from SA and PV, carbon content has, in previous literature, been a good predictor of sorption affinity to PFAS (Hale et al., 2016; Cornelissen et al., 2005). ULS contains 29.6 % carbon whereas DSL contains 13.5 %. This means that high porosity and sufficiently large pores are the two most important parameters that regulate high sorption capacity, and that the pore wall composition further contributes to enhanced sorption.

Figure E.3 shows the relationship between each of carbon content (log C), log SA/PV and log $SA/PV/C$, now as a function of log K_d (normalized to 1 $\mu g\ L^{-1}$). This figure shows that a linear relationship exists between log K_d and log $SA/PV/C$, and that no such relationship is present for carbon content and the SA/PV ratio individually.

Table E.2: Freundlich sorption coefficients and standard errors for isotherms. $log\ K_F$ for the soil samples are the collective partition coefficients for soil and biochar because. All K_F data are in units of $(\mu g/kg)/(\mu g/L)^{n_F}$.

Compound	Biochar	type	$log\ K_F$	se $log\ K_F$	n_F	se n_F	r^2	p
PFPeA	CWC	BC_S_mix						
PFHxA	CWC	BC_S_mix	3.05	0.95	0.61	0.39	0.38	>0.05
PFHpA	CWC	BC_S_mix	3.30	0.23	0.46	0.14	0.73	*
PFOA	CWC	BC_S_mix	3.25	0.48	0.77	0.18	0.82	*
PFNA	CWC	BC_S_mix	3.84	0.28	0.60	0.10	0.89	*
PFDA	CWC	BC_S_mix	4.31	0.18	0.57	0.06	0.95	**
PFOA	CWC	BC_S_sing	3.45	0.21	0.88	0.09	0.96	**
PFPeA	CWC	BC_sing	3.98	0.36	0.56	0.33	0.30	>0.05
PFHxA	CWC	BC_sing	4.59	0.50	-0.14	0.26	0.04	>0.05
PFHpA	CWC	BC_sing	4.44	0.05	0.59	0.11	0.80	**
PFOA	CWC	BC_sing	5.06	0.08	0.39	0.05	0.90	***
PFNA	CWC	BC_sing	4.88	0.04	0.65	0.04	0.98	***
PFDA	CWC	BC_sing	5.22	0.07	0.45	0.04	0.94	***
PFPeA	DSL	BC_S_mix						
PFHxA	DSL	BC_S_mix	4.54	0.30	0.18	0.15	0.33	>0.05
PFHpA	DSL	BC_S_mix	4.10	0.19	0.09	0.15	0.10	>0.05
PFOA	DSL	BC_S_mix	4.91	0.06	0.39	0.03	0.97	***
PFNA	DSL	BC_S_mix	5.10	0.06	0.35	0.03	0.97	***
PFDA	DSL	BC_S_mix	5.48	0.04	0.35	0.03	0.98	***
PFOA	DSL	BC_S_sing	5.08	0.10	0.46	0.08	0.90	*
PFPeA	DSL	BC_sing	4.25	0.74	0.14	0.38	0.06	>0.05
PFHxA	DSL	BC_sing	3.30	0.15	1.12	0.11	0.93	***
PFHpA	DSL	BC_sing	4.67	0.06	0.57	0.09	0.86	***
PFOA	DSL	BC_sing	5.12	0.02	0.60	0.02	0.99	***
PFNA	DSL	BC_sing	5.33	0.03	0.80	0.07	0.94	***
PFDA	DSL	BC_sing	5.61	0.02	0.61	0.02	0.99	***
PFPeA	ULS	BC_S_mix						
PFHxA	ULS	BC_S_mix	4.39	0.13	0.32	0.06	0.86	**
PFHpA	ULS	BC_S_mix	4.12	0.13	0.14	0.10	0.35	>0.05
PFOA	ULS	BC_S_mix	5.00	0.05	0.39	0.03	0.98	***
PFNA	ULS	BC_S_mix	5.22	0.04	0.37	0.03	0.97	***
PFDA	ULS	BC_S_mix	5.62	0.04	0.37	0.03	0.97	***
PFOA	ULS	BC_S_sing	5.16	0.03	0.62	0.03	0.99	***
PFPeA	ULS	BC_sing	4.10	0.13	0.67	0.16	0.74	**
PFHxA	ULS	BC_sing	4.80	0.06	0.34	0.09	0.72	**
PFHpA	ULS	BC_sing	5.98	0.17	1.08	0.11	0.93	***
PFOA	ULS	BC_sing	5.73	0.02	0.65	0.05	0.95	***
PFNA	ULS	BC_sing	5.89	0.02	0.71	0.03	0.99	***
PFDA	ULS	BC_sing	6.00	0.04	0.35	0.05	0.86	***

Significant codes: *** $\sim$ 0.001, ** $\sim$ 0.01, * $\sim$ 0.05
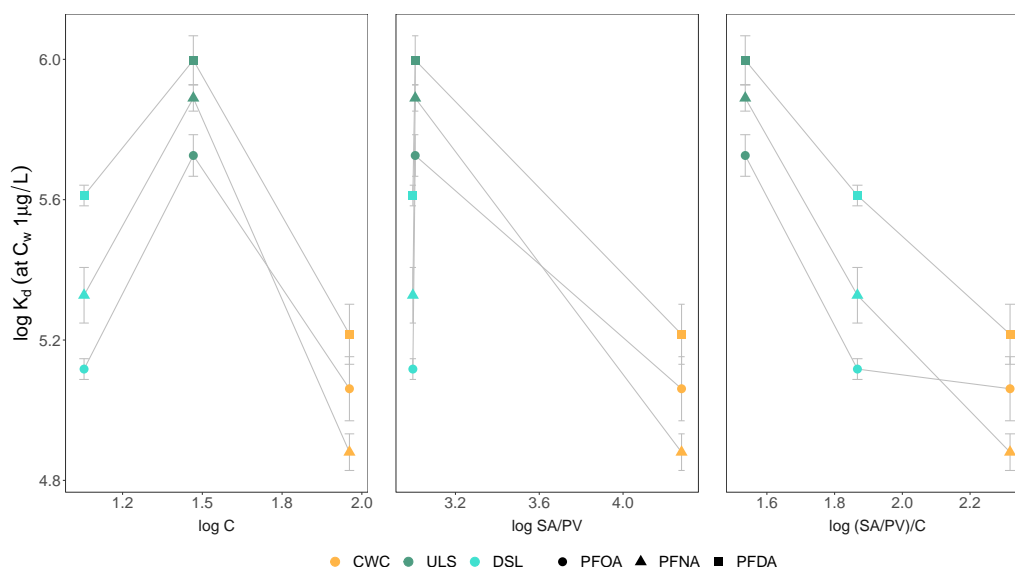
Figure E.3: The correlation of log K_d vs. (a) log C (b) log SA/PV (c) log (SA/PV)/C using BET for SA and BJH for PV by biomass feedstock. The points are discrete measurements, and the lines have been added to indicate trends. Error bars are the propagated standard error of log K_F and n.

E.2 Determination of $K_d s$ for calculating attenuation

Although not according to standard procedure, K_d values were calculated based on the point where the same mass PFCA was added to the system, not at the equilibrium concentration. This was because not all batch test categories were prepared as isotherms. K_ds for the BC soil samples have not been corrected for the amount sorbed by soil itself due to inconsistent results for the K_d in soil (Table E.3). Therefore, K_d for BC soil single, BC soil mixed and BC mixed represent the collective partitioning coefficients for biochar and soil. However, the sandy soil used has low sorption strength, with a mean log K_d value of 2.47, over 1000 times lower than for, e.g., singly-spiked PFDA to ULS-water (6.06). Therefore, biochar is by far the dominant sorbent in the system. Attenuation of PFPeA, PFHxA and PFHpA have not been presented due to lack of consistent results.

Table E.3: *log K_d* for the soil (S) used in the batch shaking tests with a PFCA cocktail and single-spiked PFOA, n=3.

Compound	type	log K_d
PFPeA	S cocktail	
PFHxA	S cocktail	2.34 ± 3.29
PFHpA	S cocktail	2.17 ± 3.00
PFOA	S cocktail	2.72 ± 4.35
PFNA	S cocktail	2.57 ± 4.63
PFDA	S cocktail	2.55 ± 5.19
PFOA	S single	2.82 ± 3.90
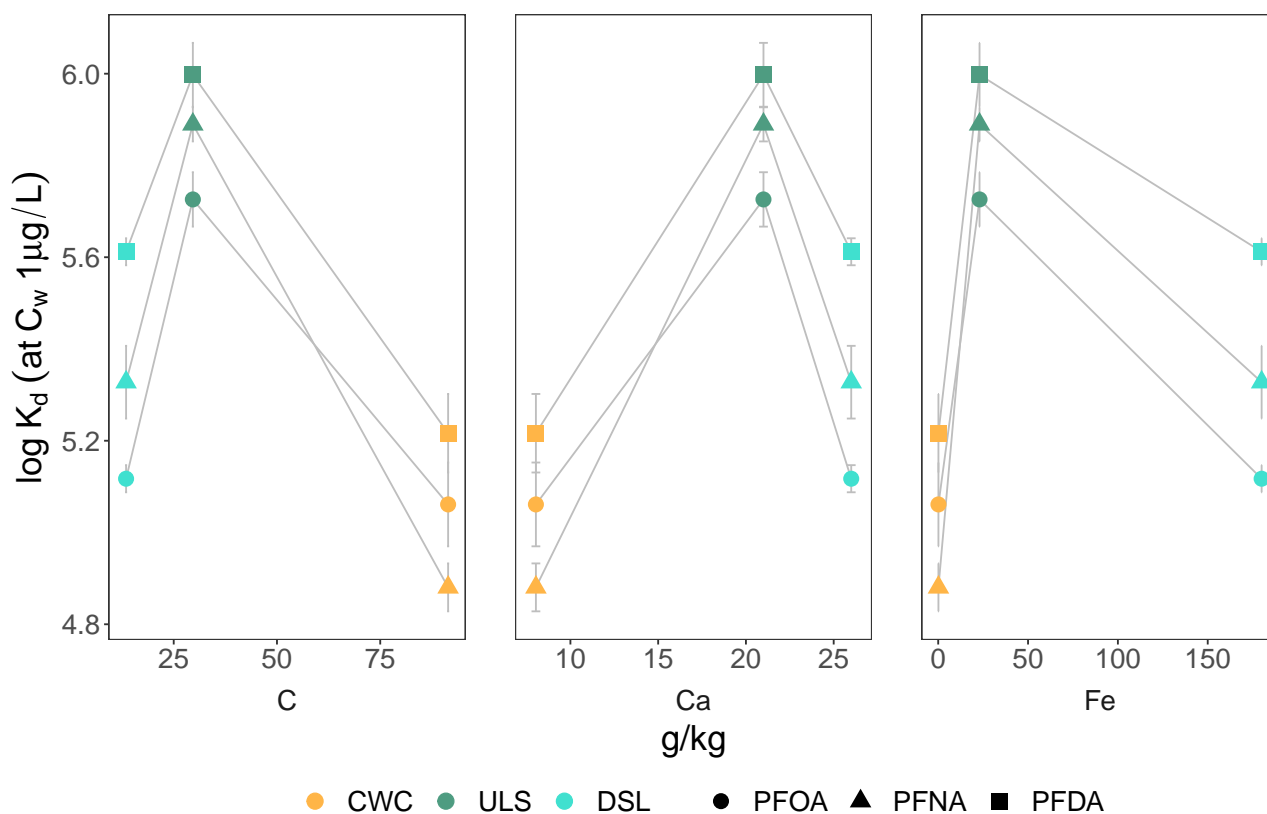
Figure E.4: The correlation between *log* K_d at 1 $\mu g/L$, and carbon (C), calcium (Ca), and iron (Fe) contents of the biochars. Lines are added to indicate trends. Error bars are the propagated standard error.

Appendix F

PFAS concentrations of batch test filtrates

Table F.1: Raw data for measured PFAS concentrations in the filtrate from the biochar water batch test experiments. Initial concentration (C_i) and equilibrium aqueous concentration (C_w) in μg/L and sorbed concentration (C_s) in μg/kg. 100 mg biochar was used.

Conc. point	C_i	C_w	C_s	Compound	Biochar	type
1	0.02	0.1	-37	PFPeA	CWC	BC_sing
2	20.7	7.5	6623	PFPeA	CWC	BC_sing
3	43.0	2.1	20478	PFPeA	CWC	BC_sing
4	63.8	12.3	25721	PFPeA	CWC	BC_sing
5	86.1	17.1	34478	PFPeA	CWC	BC_sing
6	106.8	10.8	48027	PFPeA	CWC	BC_sing
7	127.5	12.0	57770	PFPeA	CWC	BC_sing
8	149.9	11.0	69418	PFPeA	CWC	BC_sing
9	170.6	14.6	77973	PFPeA	CWC	BC_sing
10	191.3	40.4	75479	PFPeA	CWC	BC_sing
1	0.03	0.01	11	PFHxA	CWC	BC_sing
2	37.2	6.4	15390	PFHxA	CWC	BC_sing
3	72.9	14.9	28998	PFHxA	CWC	BC_sing
4	110.1	100.5	4797	PFHxA	CWC	BC_sing
5	145.9	21.5	62187	PFHxA	CWC	BC_sing
6	184.4	103.0	40704	PFHxA	CWC	BC_sing
7	220.2	112.3	53944	PFHxA	CWC	BC_sing
8	256.0	234.5	10735	PFHxA	CWC	BC_sing
9	291.7	276.5	7625	PFHxA	CWC	BC_sing
10	330.3	225.6	52341	PFHxA	CWC	BC_sing
1	0.01	0.001	6	PFHpA	CWC	BC_sing
2	11.3	0.1	5568	PFHpA	CWC	BC_sing
3	24.8	0.3	12222	PFHpA	CWC	BC_sing
4	38.3	0.3	18986	PFHpA	CWC	BC_sing
5	51.8	0.5	25652	PFHpA	CWC	BC_sing

Conc. point	C_i	C_w	C_s	Compound	Biochar	type
6	65.3	2.7	31306	PFHpA	CWC	BC_sing
7	78.8	2.6	38100	PFHpA	CWC	BC_sing
8	92.4	2.3	45031	PFHpA	CWC	BC_sing
9	105.9	2.4	51758	PFHpA	CWC	BC_sing
10	117.1	1.4	57858	PFHpA	CWC	BC_sing
1	0.20	0.004	96	PFOA	CWC	BC_sing
2	215.7	1.7	107002	PFOA	CWC	BC_sing
3	435.4	6.6	214414	PFOA	CWC	BC_sing
4	651.1	7.9	321615	PFOA	CWC	BC_sing
5	870.8	15.7	427596	PFOA	CWC	BC_sing
6	1086.5	79.6	503439	PFOA	CWC	BC_sing
7	1302.2	42.3	629925	PFOA	CWC	BC_sing
8	1521.9	88.7	716640	PFOA	CWC	BC_sing
9	1741.7	225.9	757874	PFOA	CWC	BC_sing
10	1953.3	198.7	877300	PFOA	CWC	BC_sing
1	0.1	0.001	70	PFNA	CWC	BC_sing
2	156.3	1.2	77580	PFNA	CWC	BC_sing
3	312.7	3.2	154745	PFNA	CWC	BC_sing
4	471.2	4.6	233294	PFNA	CWC	BC_sing
5	625.3	8.4	308466	PFNA	CWC	BC_sing
6	783.9	10.6	386655	PFNA	CWC	BC_sing
7	942.4	22.4	460023	PFNA	CWC	BC_sing
8	1096.6	21.8	537354	PFNA	CWC	BC_sing
9	1255.1	23.1	616006	PFNA	CWC	BC_sing
10	1409.2	29.8	689699	PFNA	CWC	BC_sing
1	0.4	0.01	187	PFDA	CWC	BC_sing
2	425.1	2.3	211406	PFDA	CWC	BC_sing
3	850.2	10.0	420131	PFDA	CWC	BC_sing
4	1275.4	14.2	630566	PFDA	CWC	BC_sing
5	1700.5	36.3	832080	PFDA	CWC	BC_sing
6	2125.6	98.7	1013444	PFDA	CWC	BC_sing
7	2550.7	44.4	1253152	PFDA	CWC	BC_sing
8	2975.8	101.8	1437011	PFDA	CWC	BC_sing
9	3400.9	211.4	1594770	PFDA	CWC	BC_sing
10	3829.9	216.2	1806844	PFDA	CWC	BC_sing
10	191.3	156.2	17559	PFPeA	CWC	BC_mix
10	191.3	349.7	-79168	PFPeA	CWC	BC_mix
10	191.3	137.7	26785	PFPeA	CWC	BC_mix
10	330.3	642.2	-155971	PFHxA	CWC	BC_mix
10	330.3	613.1	-141419	PFHxA	CWC	BC_mix
10	330.3	646.6	-158156	PFHxA	CWC	BC_mix
10	117.1	124.0	-3439	PFHpA	CWC	BC_mix
10	117.1	124.7	-3794	PFHpA	CWC	BC_mix
10	117.1	119.2	-1028	PFHpA	CWC	BC_mix
10	1953.3	821.6	565842	PFOA	CWC	BC_mix

Conc. point	C_i	C_w	C_s	Compound	Biochar	type
10	1953.3	832.4	560448	PFOA	CWC	BC_mix
10	1953.3	792.0	580669	PFOA	CWC	BC_mix
10	1409.2	1003.3	202964	PFNA	CWC	BC_mix
10	1409.2	1001.9	203656	PFNA	CWC	BC_mix
10	1409.2	962.2	223488	PFNA	CWC	BC_mix
10	3829.9	1536.6	1146648	PFDA	CWC	BC_mix
10	3829.9	1386.4	1221731	PFDA	CWC	BC_mix
10	3829.9	1249.3	1290271	PFDA	CWC	BC_mix
1	0.02	0.1	-33	PFPeA	ULS	BC_sing
2	20.7	1.4	9642	PFPeA	ULS	BC_sing
3	43.0	1.5	20795	PFPeA	ULS	BC_sing
4	63.8	3.8	29978	PFPeA	ULS	BC_sing
5	86.1	5.2	40451	PFPeA	ULS	BC_sing
6	106.8	9.4	48704	PFPeA	ULS	BC_sing
7	127.5	14.1	56732	PFPeA	ULS	BC_sing
8	149.9	4.8	72531	PFPeA	ULS	BC_sing
9	170.6	13.6	78495	PFPeA	ULS	BC_sing
10	191.3		95658	PFPeA	ULS	BC_sing
1	0.03	0.01	11	PFHxA	ULS	BC_sing
2	37.2		18578	PFHxA	ULS	BC_sing
3	72.9	1.0	35962	PFHxA	ULS	BC_sing
4	110.1	0.2	54923	PFHxA	ULS	BC_sing
5	145.9	1.5	72208	PFHxA	ULS	BC_sing
6	184.4	3.9	90247	PFHxA	ULS	BC_sing
7	220.2	5.9	107141	PFHxA	ULS	BC_sing
8	256.0	5.6	125173	PFHxA	ULS	BC_sing
9	291.7	6.5	142649	PFHxA	ULS	BC_sing
10	330.3	11.7	159314	PFHxA	ULS	BC_sing
1	0.01	0.001	6	PFHpA	ULS	BC_sing
2	11.3	0.01	5626	PFHpA	ULS	BC_sing
3	24.8	0.02	12382	PFHpA	ULS	BC_sing
4	38.3	0.02	19139	PFHpA	ULS	BC_sing
5	51.8	0.03	25892	PFHpA	ULS	BC_sing
6	65.3	0.0	32646	PFHpA	ULS	BC_sing
7	78.8	0.1	39395	PFHpA	ULS	BC_sing
8	92.4	0.1	46154	PFHpA	ULS	BC_sing
9	105.9	0.1	52903	PFHpA	ULS	BC_sing
10	117.1	0.1	58533	PFHpA	ULS	BC_sing
1	0.2	0.002	97	PFOA	ULS	BC_sing
2	215.7	0.1	107780	PFOA	ULS	BC_sing
3	435.4	0.2	217588	PFOA	ULS	BC_sing
4	651.1	0.5	325312	PFOA	ULS	BC_sing
5	870.8	0.5	435188	PFOA	ULS	BC_sing
6	1086.5	0.8	542840	PFOA	ULS	BC_sing
7	1302.2	1.7	650259	PFOA	ULS	BC_sing

Conc. point	C_i	C_w	C_s	Compound	Biochar	type
8	1521.9	1.6	760177	PFOA	ULS	BC_sing
9	1741.7	2.8	869462	PFOA	ULS	BC_sing
10	1953.3	2.4	975427	PFOA	ULS	BC_sing
1	0.1	0.001	70	PFNA	ULS	BC_sing
2	156.3	0.04	78146	PFNA	ULS	BC_sing
3	312.7	0.1	156290	PFNA	ULS	BC_sing
4	471.2	0.2	235518	PFNA	ULS	BC_sing
5	625.3	0.3	312518	PFNA	ULS	BC_sing
6	783.9	0.5	391711	PFNA	ULS	BC_sing
7	942.4	0.4	470985	PFNA	ULS	BC_sing
8	1096.6	0.6	547982	PFNA	ULS	BC_sing
9	1255.1	0.7	627218	PFNA	ULS	BC_sing
10	1409.2	0.9	704141	PFNA	ULS	BC_sing
1	0.4	0.001	191	PFDA	ULS	BC_sing
2	425.1	0.01	212555	PFDA	ULS	BC_sing
3	850.2	0.4	424917	PFDA	ULS	BC_sing
4	1275.4	0.4	637483	PFDA	ULS	BC_sing
5	1700.5	1.0	849757	PFDA	ULS	BC_sing
6	2125.6	0.8	1062400	PFDA	ULS	BC_sing
7	2550.7	2.5	1274125	PFDA	ULS	BC_sing
8	2975.8	3.4	1486234	PFDA	ULS	BC_sing
9	3400.9	3.6	1698684	PFDA	ULS	BC_sing
10	3829.9	1.7	1914101	PFDA	ULS	BC_sing
10	191.3	399.0	-103842	PFPeA	ULS	BC_mix
10	191.3	796.4	-302542	PFPeA	ULS	BC_mix
10	191.3	250.2	-29442	PFPeA	ULS	BC_mix
10	330.3	204.7	62767	PFHxA	ULS	BC_mix
10	330.3	229.3	50505	PFHxA	ULS	BC_mix
10	330.3	178.4	75946	PFHxA	ULS	BC_mix
10	117.1	34.1	41499	PFHpA	ULS	BC_mix
10	117.1	37.6	39764	PFHpA	ULS	BC_mix
10	117.1	24.7	46218	PFHpA	ULS	BC_mix
10	1953.3	75.2	939051	PFOA	ULS	BC_mix
10	1953.3	81.2	936062	PFOA	ULS	BC_mix
10	1953.3	56.4	948435	PFOA	ULS	BC_mix
10	1409.2	34.1	687557	PFNA	ULS	BC_mix
10	1409.2	25.2	691993	PFNA	ULS	BC_mix
10	1409.2	24.2	692487	PFNA	ULS	BC_mix
10	3829.9	23.7	1903104	PFDA	ULS	BC_mix
10	3829.9	11.2	1909347	PFDA	ULS	BC_mix
10	3829.9	15.7	1907112	PFDA	ULS	BC_mix
1	0.02	0.4	-173	PFPeA	DSL	BC_sing
2	20.7	53.9	-16563	PFPeA	DSL	BC_sing
3	43.0	83.1	-20039	PFPeA	DSL	BC_sing
4	63.8	87.5	-11872	PFPeA	DSL	BC_sing

Conc. point	C_i	C_w	C_s	Compound	Biochar	type
5	86.1	140.1	-27008	PFPeA	DSL	BC_sing
6	106.8	152.5	-22842	PFPeA	DSL	BC_sing
7	127.5	63.6	31961	PFPeA	DSL	BC_sing
8	149.9	94.3	27775	PFPeA	DSL	BC_sing
9	170.6	92.7	38940	PFPeA	DSL	BC_sing
10	191.3	120.3	35511	PFPeA	DSL	BC_sing
1	0.03	0.02	9	PFHxA	DSL	BC_sing
2	37.2	5.8	15667	PFHxA	DSL	BC_sing
3	72.9	12.1	30407	PFHxA	DSL	BC_sing
4	110.1	19.8	45156	PFHxA	DSL	BC_sing
5	145.9	24.2	60854	PFHxA	DSL	BC_sing
6	184.4	30.1	77137	PFHxA	DSL	BC_sing
7	220.2	29.0	95617	PFHxA	DSL	BC_sing
8	256.0	26.6	114703	PFHxA	DSL	BC_sing
9	291.7	36.7	127504	PFHxA	DSL	BC_sing
10	330.3	47.8	141228	PFHxA	DSL	BC_sing
1	0.01	0.001	5	PFHpA	DSL	BC_sing
2	11.3	0.02	5621	PFHpA	DSL	BC_sing
3	24.8	0.2	12287	PFHpA	DSL	BC_sing
4	38.3	0.2	19056	PFHpA	DSL	BC_sing
5	51.8	0.6	25591	PFHpA	DSL	BC_sing
6	65.3	0.7	32316	PFHpA	DSL	BC_sing
7	78.8	0.3	39279	PFHpA	DSL	BC_sing
8	92.4	0.7	45836	PFHpA	DSL	BC_sing
9	105.9	1.0	52441	PFHpA	DSL	BC_sing
10	117.1	1.3	57921	PFHpA	DSL	BC_sing
1	0.2	0.01	95	PFOA	DSL	BC_sing
2	215.7	0.8	107444	PFOA	DSL	BC_sing
3	435.4	2.2	216600	PFOA	DSL	BC_sing
4	651.1	5.1	323003	PFOA	DSL	BC_sing
5	870.8	6.4	432224	PFOA	DSL	BC_sing
6	1086.5	9.4	538585	PFOA	DSL	BC_sing
7	1302.2	13.2	644477	PFOA	DSL	BC_sing
8	1521.9	19.9	751006	PFOA	DSL	BC_sing
9	1741.7	27.0	857323	PFOA	DSL	BC_sing
10	1953.3	28.7	962274	PFOA	DSL	BC_sing
1	0.1	0.001	70	PFNA	DSL	BC_sing
2	156.3	0.4	77982	PFNA	DSL	BC_sing
3	312.7	0.7	155968	PFNA	DSL	BC_sing
4	471.2	0.7	235260	PFNA	DSL	BC_sing
5	625.3	1.9	311745	PFNA	DSL	BC_sing
6	783.9	2.1	390886	PFNA	DSL	BC_sing
7	942.4	2.9	469747	PFNA	DSL	BC_sing
8	1096.6	3.1	546728	PFNA	DSL	BC_sing
9	1255.1	3.7	625673	PFNA	DSL	BC_sing

Conc. point	C_i	C_w	C_s	Compound	Biochar	type
10	1409.2	4.6	702290	PFNA	DSL	BC_sing
1	0.4		191	PFDA	DSL	BC_sing
2	425.1	0.4	212357	PFDA	DSL	BC_sing
3	850.2	1.0	424622	PFDA	DSL	BC_sing
4	1275.4	2.0	636678	PFDA	DSL	BC_sing
5	1700.5	3.1	848681	PFDA	DSL	BC_sing
6	2125.6	3.9	1060848	PFDA	DSL	BC_sing
7	2550.7	6.6	1272065	PFDA	DSL	BC_sing
8	2975.8	8.1	1483856	PFDA	DSL	BC_sing
9	3400.9	9.8	1695557	PFDA	DSL	BC_sing
10	3829.9	15.0	1907436	PFDA	DSL	BC_sing
10	191.3	1772.9	-790776	PFPeA	DSL	BC_mix
10	191.3	886.1	-347389	PFPeA	DSL	BC_mix
10	191.3	1486.8	-647736	PFPeA	DSL	BC_mix
10	330.3	1553.9	-611806	PFHxA	DSL	BC_mix
10	330.3	645.5	-157602	PFHxA	DSL	BC_mix
10	330.3	1394.1	-531909	PFHxA	DSL	BC_mix
10	117.1	379.2	-131042	PFHpA	DSL	BC_mix
10	117.1	141.2	-12024	PFHpA	DSL	BC_mix
10	117.1	343.2	-113022	PFHpA	DSL	BC_mix
10	1953.3	749.4	601936	PFOA	DSL	BC_mix
10	1953.3	308.6	822341	PFOA	DSL	BC_mix
10	1953.3	676.6	638342	PFOA	DSL	BC_mix
10	1409.2	715.5	346863	PFNA	DSL	BC_mix
10	1409.2	260.6	574307	PFNA	DSL	BC_mix
10	1409.2	666.8	371202	PFNA	DSL	BC_mix
10	3829.9	1309.0	1260465	PFDA	DSL	BC_mix
10	3829.9	184.1	1822918	PFDA	DSL	BC_mix
10	3829.9	1191.0	1319443	PFDA	DSL	BC_mix

Table F.2: Raw data for measured PFAS concentrations in the filtrate from the soil biochar water batch test experiments. Initial concentration (C_i) and equilibrium aqueous concentration (C_w) in μg/L and sorbed concentration (C_s) in μg/kg. 100 mg biochar and 5 g soil was used.

Conc. point	C_i	C_w	C_s	Compound	Biochar	type
10	283	3145	-1431209	PFPeA	no	S_mix
10	283	2741	-1229440	PFPeA	no	S_mix
10	283	688	-202492	PFPeA	no	S_mix
10	836	578	128917	PFHxA	no	S_mix
10	836	580	128057	PFHxA	no	S_mix
10	836	590	122707	PFHxA	no	S_mix
10	153	116	18568	PFHpA	no	S_mix
10	153	117	18318	PFHpA	no	S_mix
10	153	122	15468	PFHpA	no	S_mix

Conc. point	C_i	C_w	C_s	Compound	Biochar	type
10	1974	914	530152	PFOA	no	S_mix
10	1974	937	518852	PFOA	no	S_mix
10	1974	1058	458302	PFOA	no	S_mix
10	2310	1198	556119	PFNA	no	S_mix
10	2310	1303	503819	PFNA	no	S_mix
10	2310	1489	410869	PFNA	no	S_mix
10	5288	2849	1219244	PFDA	no	S_mix
10	5288	2833	1227594	PFDA	no	S_mix
10	5288	3770	758844	PFDA	no	S_mix
10	1953	863	545221	PFOA	no	S_sing
10	1953	840	556671	PFOA	no	S_sing
10	1953	807	572871	PFOA	no	S_sing
2	31	319	-143820	PFPeA	CWC	BC_S_mix
3	63	450	-193751	PFPeA	CWC	BC_S_mix
5	126	1391	-632893	PFPeA	CWC	BC_S_mix
6	157	1517	-679934	PFPeA	CWC	BC_S_mix
8	220	1062	-420924	PFPeA	CWC	BC_S_mix
10	283	372	-44606	PFPeA	CWC	BC_S_mix
2	92	56	17668	PFHxA	CWC	BC_S_mix
3	185	150	17760	PFHxA	CWC	BC_S_mix
5	372	349	11311	PFHxA	CWC	BC_S_mix
6	465	321	71739	PFHxA	CWC	BC_S_mix
8	651	540	55207	PFHxA	CWC	BC_S_mix
10	836	639	98418	PFHxA	CWC	BC_S_mix
2	17	7	4751	PFHpA	CWC	BC_S_mix
3	34	18	8039	PFHpA	CWC	BC_S_mix
5	68	53	7764	PFHpA	CWC	BC_S_mix
6	85	48	18611	PFHpA	CWC	BC_S_mix
8	119	89	15093	PFHpA	CWC	BC_S_mix
10	153	116	18749	PFHpA	CWC	BC_S_mix
2	217	86	65403	PFOA	CWC	BC_S_mix
3	438	238	99606	PFOA	CWC	BC_S_mix
5	878	599	139413	PFOA	CWC	BC_S_mix
6	1 098	546	276274	PFOA	CWC	BC_S_mix
8	1 538	875	331207	PFOA	CWC	BC_S_mix
10	1 974	953	510758	PFOA	CWC	BC_S_mix
2	254	67	93360	PFNA	CWC	BC_S_mix
3	512	208	151814	PFNA	CWC	BC_S_mix
5	1 027	600	213397	PFNA	CWC	BC_S_mix
6	1 285	541	372365	PFNA	CWC	BC_S_mix
8	1 799	965	416893	PFNA	CWC	BC_S_mix
10	2 310	1181	564562	PFNA	CWC	BC_S_mix
2	581	77	251726	PFDA	CWC	BC_S_mix
3	1 172	253	459139	PFDA	CWC	BC_S_mix
5	2 351	879	735997	PFDA	CWC	BC_S_mix

Conc. point	C_i	C_w	C_s	Compound	Biochar	type
6	2 941	775	1083442	PFDA	CWC	BC_S_mix
8	4 118	1459	1329567	PFDA	CWC	BC_S_mix
10	5 288	2016	1636139	PFDA	CWC	BC_S_mix
2	31	7	12130	PFPeA	ULS	BC_S_mix
3	63	65	-1153	PFPeA	ULS	BC_S_mix
5	126	138	-6235	PFPeA	ULS	BC_S_mix
6	157	438	-140193	PFPeA	ULS	BC_S_mix
8	220	228	-3957	PFPeA	ULS	BC_S_mix
10	283	1275	-496190	PFPeA	ULS	BC_S_mix
2	92	10	41041	PFHxA	ULS	BC_S_mix
3	185	26	79675	PFHxA	ULS	BC_S_mix
5	372	114	128607	PFHxA	ULS	BC_S_mix
6	465	168	148356	PFHxA	ULS	BC_S_mix
8	651	312	169458	PFHxA	ULS	BC_S_mix
10	836	557	139481	PFHxA	ULS	BC_S_mix
2	17	1	8132	PFHpA	ULS	BC_S_mix
3	34	2	16203	PFHpA	ULS	BC_S_mix
5	68	14	26822	PFHpA	ULS	BC_S_mix
6	85	25	30301	PFHpA	ULS	BC_S_mix
8	119	64	27445	PFHpA	ULS	BC_S_mix
10	153	125	13968	PFHpA	ULS	BC_S_mix
2	217	2	107502	PFOA	ULS	BC_S_mix
3	438	5	216323	PFOA	ULS	BC_S_mix
5	878	36	420691	PFOA	ULS	BC_S_mix
6	1 098	59	519450	PFOA	ULS	BC_S_mix
8	1 538	159	689436	PFOA	ULS	BC_S_mix
10	1 974	284	844988	PFOA	ULS	BC_S_mix
2	254	1	126445	PFNA	ULS	BC_S_mix
3	512	2	254991	PFNA	ULS	BC_S_mix
5	1 027	17	505151	PFNA	ULS	BC_S_mix
6	1 285	32	626611	PFNA	ULS	BC_S_mix
8	1 799	87	856259	PFNA	ULS	BC_S_mix
10	2 310	195	1057599	PFNA	ULS	BC_S_mix
2	581	1	290006	PFDA	ULS	BC_S_mix
3	1 172	2	585027	PFDA	ULS	BC_S_mix
5	2 351	11	1169792	PFDA	ULS	BC_S_mix
6	2 941	24	1458812	PFDA	ULS	BC_S_mix
8	4 118	81	2018342	PFDA	ULS	BC_S_mix
10	5 288	175	2556197	PFDA	ULS	BC_S_mix
2	31	179	-74083	PFPeA	DSL	BC_S_mix
3	63	328	-132507	PFPeA	DSL	BC_S_mix
5	126	271	-72557	PFPeA	DSL	BC_S_mix
6	157	1461	-651719	PFPeA	DSL	BC_S_mix
8	220	5681	-2730615	PFPeA	DSL	BC_S_mix
10	283	2219	-968326	PFPeA	DSL	BC_S_mix

Conc. point	C_i	C_w	C_s	Compound	Biochar	type
2	92	11	40450	PFHxA	DSL	BC_S_mix
3	185	35	75169	PFHxA	DSL	BC_S_mix
5	372	141	115145	PFHxA	DSL	BC_S_mix
6	465	202	131551	PFHxA	DSL	BC_S_mix
8	651	523	63799	PFHxA	DSL	BC_S_mix
10	836	945	-54579	PFHxA	DSL	BC_S_mix
2	17	1	8088	PFHpA	DSL	BC_S_mix
3	34	2	15765	PFHpA	DSL	BC_S_mix
5	68	17	25417	PFHpA	DSL	BC_S_mix
6	85	29	27967	PFHpA	DSL	BC_S_mix
8	119	101	9204	PFHpA	DSL	BC_S_mix
10	153	209	-28164	PFHpA	DSL	BC_S_mix
2	217	3	106989	PFOA	DSL	BC_S_mix
3	438	11	213137	PFOA	DSL	BC_S_mix
5	878	54	411715	PFOA	DSL	BC_S_mix
6	1 098	75	511717	PFOA	DSL	BC_S_mix
8	1 538	269	634206	PFOA	DSL	BC_S_mix
10	1 974	442	766281	PFOA	DSL	BC_S_mix
2	254	1	126116	PFNA	DSL	BC_S_mix
3	512	6	252834	PFNA	DSL	BC_S_mix
5	1 027	32	497349	PFNA	DSL	BC_S_mix
6	1 285	54	615505	PFNA	DSL	BC_S_mix
8	1 799	207	796125	PFNA	DSL	BC_S_mix
10	2 310	438	936083	PFNA	DSL	BC_S_mix
2	581	1	289761	PFDA	DSL	BC_S_mix
3	1 172	7	582440	PFDA	DSL	BC_S_mix
5	2 351	32	1159274	PFDA	DSL	BC_S_mix
6	2 941	55	1443460	PFDA	DSL	BC_S_mix
8	4 118	223	1947439	PFDA	DSL	BC_S_mix
10	5 288	512	2387956	PFDA	DSL	BC_S_mix
2	216	41	87137	PFOA	CWC	BC_S_sing
3	435	128	153933	PFOA	CWC	BC_S_sing
5	871	220	325533	PFOA	CWC	BC_S_sing
6	1 087	309	388613	PFOA	CWC	BC_S_sing
8	1 522	384	568858	PFOA	CWC	BC_S_sing
10	1 953	477	738208	PFOA	CWC	BC_S_sing
2	216	1	107513	PFOA	ULS	BC_S_sing
3	435	2	216838	PFOA	ULS	BC_S_sing
5	871	7	432158	PFOA	ULS	BC_S_sing
6	1 087	8	539505	PFOA	ULS	BC_S_sing
8	1 522	12	754951	PFOA	ULS	BC_S_sing
10	1 953	24	964821	PFOA	ULS	BC_S_sing
2	216	1	107159	PFOA	DSL	BC_S_sing
3	435	4	215723	PFOA	DSL	BC_S_sing
5	871	10	430279	PFOA	DSL	BC_S_sing

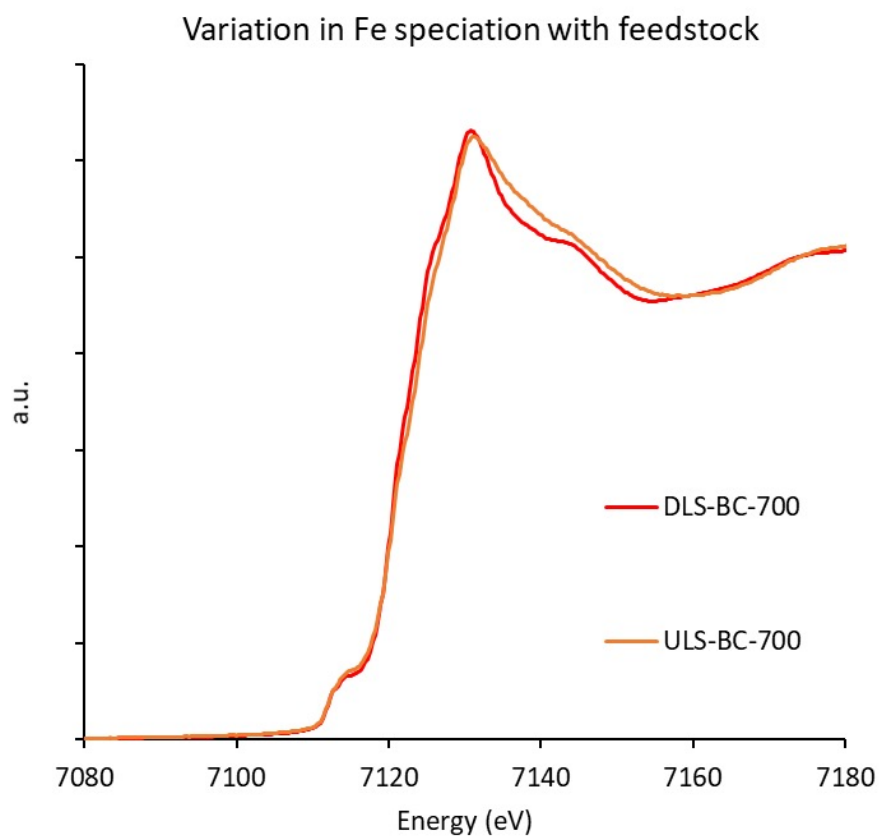| Conc. point	C_i	C_w	C_s	Compound	Biochar	type
6	1 087	11	537631	PFOA	DSL	BC_S_sing
8	1 522	83	719368	PFOA	DSL	BC_S_sing
10	1 953	97	928096	PFOA	DSL	BC_S_sing

Appendix G

Iron speciation

Figure G.1: Fe K-edge XANES (X-ray absorption near edge structure) spectra for ULS and DSL analyzed and processed by research partners at the Norwegian Geotechnical Institute..
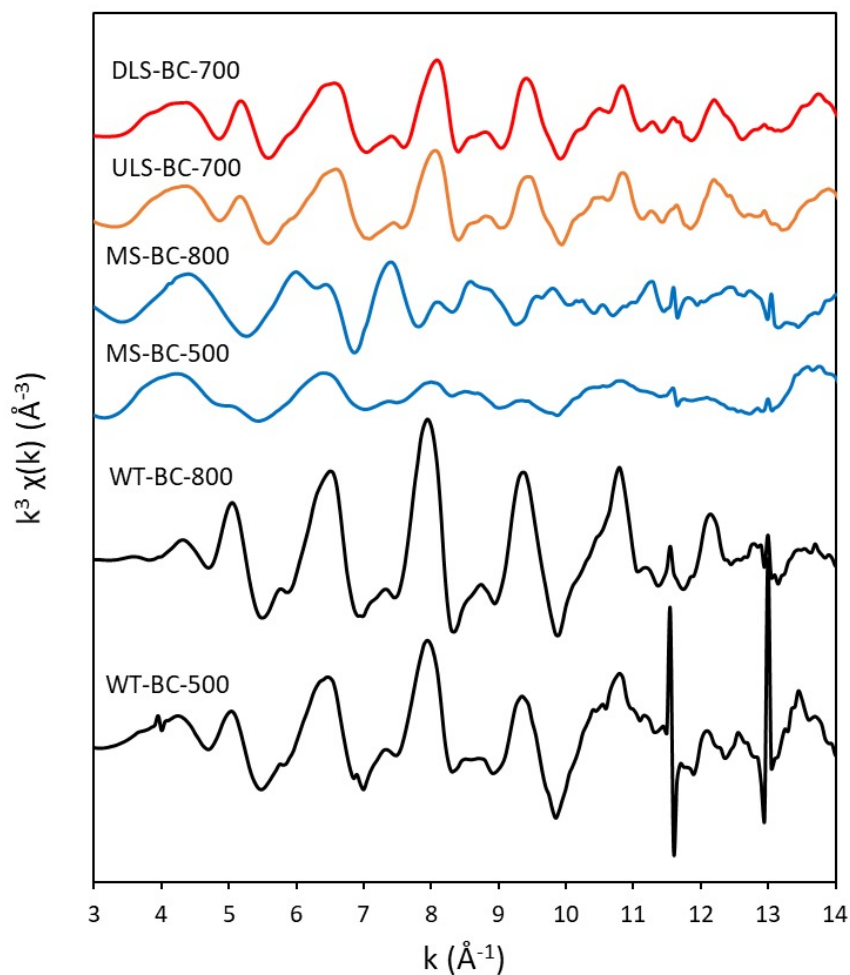
Figure G.2: Fe K-edge EXAFS (extended X-ray absorption fine structure) spectra for ULS, DSL and other feedstocks analyzed and processed by research partners at the Norwegian Geotechnical Institute.

Appendix H

Poster

The poster below is a summary of the work conducted in this thesis and was presented at the Society of Environmental Toxicology and Chemistry (SETAC) Europe's 32nd annual conference in Copenhagen, Denmark in May 2022.

Promising potentials for the application of sewage-sludge-based biochars as sorbents for PFAS

Katinka M. Krahn[1,2], Erlend Sørmo[1,2], Hans Peter Arp[2,3], Gabriela C. Varela[3], Gerard Cornelissen[2]

[1]Norwegian University of Life Sciences (NMBU), 1430 Ås, Norway, [2]Norwegian Geotechnical Institute (NGI), 0484 Oslo, Norway,
[3]Norwegian University of Science and Technology (NTNU), 7024 Trondheim, Norway

✉ katinka.muri.krahn@nmbu.no

Objectives

- Compare the relative abilities of sewage sludge biochars and clean wood chips to sorb perfluorinated carboxylic acids (PFCA)

- Identify possible sorption mechanisms of PFCA for the different biochar feedstocks

- Study the effects of increasing perfluorinated carbon chain-length, competing sorbates, and the presence of soil on sorption

Figure 1: Biochar collection from the ETIA pyrolysis unit at Lindum AS, Norway.

Figure 2: Raw sewage sludge pellets (left) and sewage sludge biochar (right).

Methods

Biochar samples (pyrolysis T = 700°C):
- **ULS**: raw sewage sludge from Ullensaker WWTP (29% carbon)
- **DSL**: digested sewage sludge (13% carbon)
- **CWC**: clean wood chips (91% carbon)

Batch shaking tests with C5-C10 PFCA:
- 100 mg biochar
- 50 mL water
- Spiked with individual PFCAs at 10 concentrations over four orders of magnitude
- Shaken end-over-end for >14 days
- Filtered through 0.45 μm regenerated cellulose filter

- Solid Phase Extraction (SPE) of filtrate
- Analyte quantification with LC-MS/MS at the Norwegian University of Science and Technology (NTNU), Trondheim, Norway
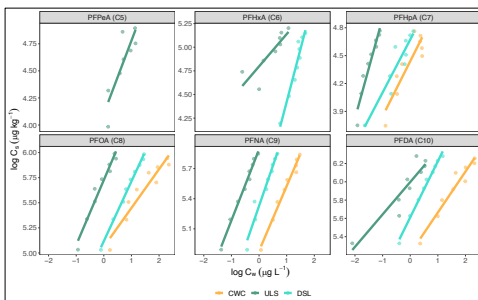
Results

Figure 3: Freundlich sorption isotherms for the ULS, DSL, and CWC biochars. Log C_w is the equilibrium aqueous concentration and log C_s is the equilibrium sorbed concentration
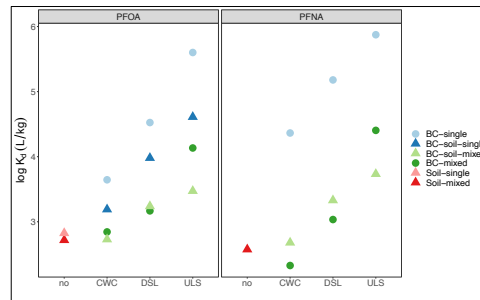

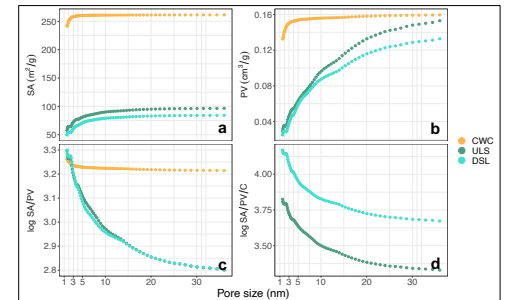**Figure 4**: Sorption attenuation in the presence of other PFCAs and soil

Figure 5: Pore size distribution >1.5 nm by **(a)** surface area (SA), **(b)** pore volume (PV), **(c)** log SA/PV, and **(d)** log (SA/PV)/C (C = carbon)

- Sorption increased from CWC < DSL < ULS, and with increasing perfluorinated chain-length (**Fig. 3**). The Freundlich sorption coefficients (log K_F) found in this study are equivalent to, or higher than, log K_F values for activated carbon reported in previous literature[1,2,3]

- Sorption was attenuated by factors 6-140 in the presence of a cocktail and 8-138 in the presence of soil and a cocktail for PFOA, PFNA, and PFDA (**Fig. 4**)

- Stronger sorption of PFCA to sewage sludge biochars is likely due to a higher fraction of mesopores (2-50 nm, **Fig. 5c**)

- A higher carbon-fraction in the pore wall matrix (lower log SA/PV/C ratio) of ULS biochar is hypothesized to explain why PFCA sorb stronger to ULS than to DSL (**Fig. 5d** and **Fig. 6**)
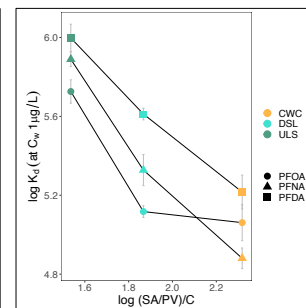

Figure 6: Relationship between log (SA/PV)/C (C = carbon) ratio and log K_d for PFOA, PFNA and PFDA across biochar samples.

Conclusion

- The strong sorption of PFCA found to sewage sludge biochars is promising for their incorporation in a circular economy, for example their use as fertilizers, sorbents in wastewater treatment plants, or as amendments to PFAS-contaminated soil

- Future work should aim at further investigating the ratios between surface area, pore volume, carbon, and minerals (mainly Ca and Fe) in determining the sorption affinity of PFAS and other organic contaminants to sewage sludge biochars

References:
[1] Kupryianchyk et al., 2016. Chemosphere. 142:35-40
[2] Silvani et al., 2019. Sci. of the Tot. Env. 694:133693
[3] Hansen et al., 2010). Jour. of Soil and Sed. 10(2):179-185

This research concludes the master thesis of Katinka Muri Krahn at the Norwegian University of Life Sciences, (NMBU), May 15, 2022